Polarizability of the Nucleon and Compton Scattering

Martin Schumacher*
Zweites Physikalisches Institut der Universität Göttingen
Friedrich-Hund-Platz 1, D-37077 Göttingen

February 2, 2008

Abstract

One of the central challenges of hadron physics in the regime of strong (non-perturbative) QCD is to identify the relevant degrees of freedom of the nucleon and to quantitatively explain experimental data in terms of these degrees of freedom. Among the processes studied so far Compton scattering plays a prominent role because of the well understood properties of the electromagnetic interaction. Different approaches to describe Compton scattering have been discussed up to now. It will be shown that the most appropriate ones are provided by nonsubtracted dispersion theories of the fixed-t and fixed-θ types, where the properties of these two versions are complementary so that advantage can be taken from both of them. In the frame of fixed-t dispersion theory it was possible to precisely reproduce experimental differential cross sections obtained for the proton in a wide angular range and for energies up to 1 GeV. At energies of the first resonance region and below, precise values for the electromagnetic polarizabilities and spin-polarizabilities have been determined for the proton and the neutron. As a summary we give the following *recommended* experimental values for the electromagnetic polarizabilities and backward spin-polarizabilities of the nucleon: $\alpha_p = 12.0 \pm 0.6$, $\beta_p = 1.9 \mp 0.6$, $\alpha_n = 12.5 \pm 1.7$, $\beta_n = 2.7 \mp 1.8$, in units of $10^{-4}\mathrm{fm}^3$ and $\gamma_\pi^{(p)} = -38.7 \pm 1.8$, $\gamma_\pi^{(n)} = 58.6 \pm 4.0$ in units of $10^{-4}\mathrm{fm}^4$. These data show that diamagnetism is a prominent property of nucleon structure. It will be shown that the largest part of diamagnetism, or equivalently $(\alpha - \beta)$, is not related to the conventional isobar-meson structure of the nucleon as showing up in meson photo-production. Rather, the underlying mechanism is a t-channel σ-meson exchange, with the constituent-quark-meson configuration remaining in its ground state. The same is true for the backward spin-polarizability γ_π where the relevant meson is the π^0. Making the reasonable assumption that the quantities $(\alpha - \beta)$ and γ_π are related to the structure of the nucleon, we come to the conclusion that the σ and π^0 intermediate states are part of the structure of the nucleon. It is a challenge for further research to integrate these degrees of freedom into a consistent description of the structure of the nucleon.

*Supported by Deutsche Forschungsgemeinschaft SPP(1034) and projects SCHU222 and 436RUS 113/510. Email address: mschuma3@gwdg.de (Martin Schumacher)

1 Introduction

The idea to apply the coherent elastic scattering of photons (Compton scattering) to an investigation of the internal structure of the nucleon dates back to the early 1950's. From these early days up to the present the following questions have been investigated:

- What are the appropriate degrees of freedom of the nucleon if we probe it with (quasi-static) electromagnetic fields?
- What are the appropriate theoretical tools to relate the experimental observables to the presumed degrees of freedom of the nucleon?
- How can one measure differential cross sections for Compton scattering very precisely in view of the extremely small size of these quantities at energies below π photoproduction threshold and in view of the tremendously large background of photons due to photoproduction of neutral pions with their subsequent decay into two photons at energies above π photoproduction threshold?

Though large progress has been made in these fields the work is not complete. The aim of this article, therefore, cannot be to give final answers. Instead it may be considered as some intermediate status report written in a way that future researchers are given an easy access to the field. This work is facilitated by the fact that there are two other excellent recent reviews (i) the publication of Drechsel, Pasquini and Vanderhaeghen "Dispersion relations in real and virtual Compton scattering" [1] and the work of Wissmann "Compton Scattering: Investigating the structure of the nucleon with real photons" [2]. The work of Drechsel et al. [1] emphasizes recent progress made in dispersion theories, the work of Wissmann [2] is concerned with experimental methods and recent experimental results and their evaluation and interpretation in terms of the nonsubtracted fixed-t dispersion theory. Furthermore, the review articles of A.I. L'vov "Theoretical aspects of the polarizability of the nucleon" [3] and of V.A. Petrun'kin "Electric and magnetic polarizability of hadrons" [4] may be studied in parallel.

Using hydrogen and deuterium targets, Compton scattering by the proton and neutron has recently been studied at the tagged photon beam of the MAMI (Mainz) accelerator using different experimental setups. Due to these investigations there are precise experimental differential cross sections available for the proton in a large angular range at energies below the π photoproduction threshold and for the first and second resonance region. For the neutron, Compton differential cross sections have been measured in the first resonance region using the method of quasi-free Compton scattering by the neutron bound in the deuteron. When combined with an accurate theoretical description of the quasi-free process these experiments are expected to provide differential cross sections for Compton scattering by the free neutron. The basic achievements of these experiments will be described in this article.

The large improvement on the data base achieved through these recent experiments makes a reconsideration of dispersion theories advisable which serve as the tools for data analysis and interpretation. The appropriate versions of dispersion theories are nonsubtracted dispersion theories, either formulated for fixed scattering angle, θ, or for fixed momentum transfer squared, t. These two approaches have their technical advantages and disadvantages and to some extent are complementary. They have in common that the physics of subtractions inherent in the scattering amplitudes becomes an essential part of the theory. It will become apparent in the following that this is neither a shortcoming nor a disadvantage of the dispersive approach. On the contrary, the physics of subtractions is an essential part of the physics of polarizability and Compton scattering and leads to new insights into the relevant degrees of freedom of the nucleon.

1.1 The early history and basic ideas

The possibility that the polarizability of the "meson cloud" of a proton or neutron plays a role when the nucleon scatters a photon elastically or is scattered itself in a nuclear Coulomb field has been noted by several authors [5, 6] already in the 1950's. A phenomenological description of the effect of nucleon polarization on the processes

$$\gamma + p \to \gamma' + p', \tag{1}$$

$$\gamma^* + n \to \gamma^{*\prime} + n' \tag{2}$$

which are illustrated by the diagrams of Figure 1 is obtained by an extension of the low-energy theorem

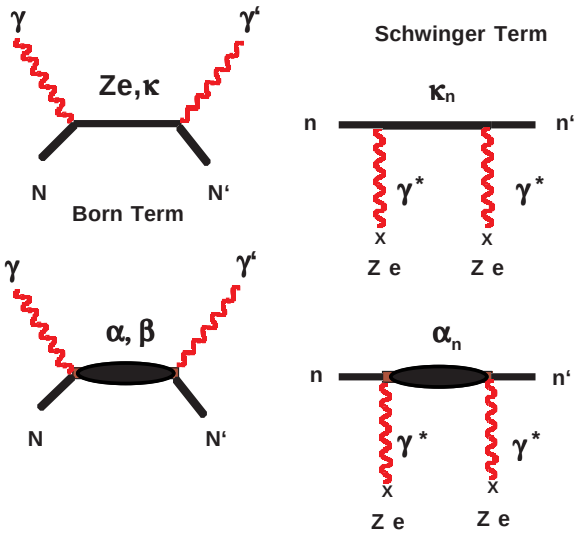

Figure 1: Left panel: Born term (upper part) and polarizability diagram (lower part) for Compton scattering by the nucleon. Ze, κ: electric charge and anomalous magnetic moment of the nucleon. α, β: electric and magnetic polarizability. Right panel: Schwinger term describing double Schwinger scattering due to electric fields acting on the magnetic moment (upper part) and polarizability diagram for electromagnetic scattering of a neutron in a Coulomb field (lower part). κ_n: anomalous magnetic moment of the neutron. Ze: electric charge of the scattering nucleus. γ^*: virtual photon. The crossed diagrams are not shown (see also [3]).

of Low, Gell-Mann and Goldberger [7, 8] for scattering amplitudes to quadratic terms in the photon energy ω. It was shown [9–14] that allowance for the ω^2-dependent terms in the amplitude for Compton scattering by the proton requires the introduction of two new constants in addition to the charge e, mass M and anomalous magnetic moment κ (for spin 1/2) of the target particle. By analogy with the nonrelativistic theory of photon scattering by a complex system (atom or nucleus) they have been named the electric and magnetic polarizabilities, α and β, respectively.

The first experimental data on electromagnetic polarizabilities analyzed from differential cross sections for Compton scattering by the proton were obtained by Gol'danskii et al. in 1960 [15]. The later experiment of Baranov et al. [16] arrived at a good precision for the electric polarizability. These two experiments were re-evaluated recently [17] and also other experiments of the 1950's – 1990's were given consideration. The results of this re-evaluation are listed in Table 1.

It should be noted that the data listed in Table 1 have been obtained without the tagging technique by which quasi-monochromatic photons are obtained and without including the constraint of the Baldin

Table 1: Summary of results obtained in the 1950's – 1970's for the electromagnetic polarizabilities of the proton [17] given without constraint of the Baldin sum rule [10]. The data are obtained [17] through a re-evaluation of the differential cross sections available for energies below pion photoproduction threshold. The unit is 10^{-4}fm^3.

Experiment	α_p	β_p	$\alpha_p + \beta_p$
Oxley(58)	17.0± 8.1	-6.7±3.7	10.2±9.2
Hyman(59)	13.9± 5.6	-4.7±7.2	9.2±6.1
Goldansky(60)	10.1± 7.8	9.0±5.0	19.1±10.2
Bernardini(61)	11.4± 2.9	2.6±2.9	–
Frish(67)	14.2±4.0	5.6± 4.2	19.8±4.3
Baranov(74)	11.4± 1.4	-4.7±2.5	6.7±3.3
average	12.8±1.1	-0.3±1.6	12.5±2.2

sum rule [10] which allows to calculate $\alpha + \beta$ from the total photo-absorption cross section. In view of this, the data have to be considered as remarkably precise. Nevertheless the important question remains unanswered whether the magnetic polarizability is positive or negative, i.e. the nucleon mainly behaves as a paramagnetic or diamagnetic system. This question has been answered by modern experiments described in Section 5.

Experiments on Compton scattering by the neutron appeared to be impossible in these early days. Therefore, the electromagnetic scattering of neutrons in a Coulomb field of heavy nuclei exploited in narrow-beam neutron transmission experiments was given preference. Due to the absence of a magnetic field component at low neutron velocities, only the electric polarizability is measured in these experiments. The early history of these studies is summarized in [18]. The experimental results obtained in the 1980's are summarized in Table 2. The data in Table 2 show that the errors obtained

Table 2: Summary of results obtained in the 1980's for the electric polarizability of the neutron using the method of electromagnetic scattering of neutrons in the Coulomb field of heavy nuclei. The unit is 10^{-4}fm^3.

Experiment	α_n
Alexandrov(86) [19]	15 ± 33
Koester(86) [20]	30 ± 40
Schmiedmayer(88) [21]	12 ± 10
Koester(88) [22]	8 ± 10

for the electric polarizability of the neutron are of the order of 100%. This means that the electric polarizability of the neutron remained uncertain in these early experiments. Improvements on the technique of electromagnetic scattering of neutrons in the Coulomb field of heavy nuclei have been made recently. This will be described in Section 5.3.1.

1.2 Polarizabilities defined for real and quasi-real photons

We include this subsection for the sake of completeness and because there are uncertainties about the definition of polarizabilities in the literature up to recent times[1].

The electric (α) and magnetic (β) polarizabilities are defined through the second-order effective Hamiltonian $H^{(2)}$. Standard text books prefer the Gauss unit system [25] whereas modern particle physics prefers the Heaviside system. Furthermore, the Particle Data Group (PDG) [24] promotes the SI system. A definition which is independent of the unit system reads

$$H^{(2)} = -4\pi\alpha\rho_{\rm el} - 4\pi\beta\rho_{\rm mag} \tag{3}$$

where $\rho_{\rm el}$ is the energy density due to the electric field, $\rho_{\rm mag}$ the energy density due to the magnetic field and $H^{(2)}$ the energy change. The factor 4π indicates that the electromagnetic polarizabilities have originally been defined in the Gauss unit system. Induced electric and magnetic dipole moments are given by the variational derivatives

$$\mathbf{d} = -\frac{\delta H^{(2)}}{\delta \mathbf{E}}, \quad \mathbf{m} = -\frac{\delta H^{(2)}}{\delta \mathbf{H}}, \tag{4}$$

for the Gauss and the Heaviside system and by

$$\mathbf{d} = -\frac{\delta H^{(2)}}{\delta \mathbf{E}}, \quad \mathbf{m} = -\frac{\delta H^{(2)}}{\delta \mathbf{B}}, \tag{5}$$

for the SI system.

Table 3 contains the relevant relations valid for static electric and magnetic fields, given in the three unit systems. The corresponding $\mathcal{O}(\omega^2)$ Compton differential cross section for a particle with charge

Table 3: The electromagnetic polarizabilities α, β defined in the Gauss unit system ($\hbar = c = 1$) and their relations to electromagnetic field strengths expressed in different unit systems. $\mathbf{E}$, $\mathbf{H}$ are the electric and magnetic field strength in the respective unit system. In the SI system we also have $\mathbf{D} = \epsilon_0\mathbf{E}$, $\mathbf{B} = \mu_0\mathbf{H}$. $\mathbf{d}$ and $\mathbf{m}$ are induced electric and magnetic dipole moments, respectively.

System	$H^{(2)}$	$\mathbf{d}$	$\mathbf{m}$	$\alpha_e = 1/137.04$
Gauss	$-\frac{1}{2}\,\alpha\,\mathbf{E}^2 - \frac{1}{2}\,\beta\,\mathbf{H}^2$	$\alpha\mathbf{E}$	$\beta\mathbf{H}$	e^2
Heaviside	$-\frac{1}{2}4\pi\,\alpha\,\mathbf{E}^2 - \frac{1}{2}4\pi\,\beta\,\mathbf{H}^2$	$4\pi\alpha\mathbf{E}$	$4\pi\beta\mathbf{H}$	$e^2/4\pi$
SI	$-\frac{1}{2}4\pi\,\alpha\,\mathbf{E}\cdot\mathbf{D} - \frac{1}{2}4\pi\,\beta\,\mathbf{H}\cdot\mathbf{B}$	$4\pi\alpha\mathbf{D}$	$4\pi\beta\mathbf{H}$	$e^2/4\pi\epsilon_0\hbar c$

Ze but without spin becomes

$$\begin{aligned}
&\frac{d\sigma}{d\Omega} = (\omega'/\omega)^2 |T^{(2)}|^2, \\
&T^{(2)} = \boldsymbol{\epsilon}\cdot\boldsymbol{\epsilon}'\left(\frac{-Z^2e^2}{M} + \omega\omega'\bar{\alpha}\right) + (\boldsymbol{\epsilon}\times\hat{\mathbf{k}})\cdot(\boldsymbol{\epsilon}'\times\hat{\mathbf{k}}')\;\omega\omega'\bar{\beta} + \mathcal{O}(\omega^4)
\end{aligned} \tag{6}$$

if we use the Gauss system and if we denote – for a temporary distinction – the electromagnetic polarizabilities by $\bar{\alpha}$ and $\bar{\beta}$. In the Heaviside system $\bar{\alpha}$ and $\bar{\beta}$ carry a factor 4π and correspondingly

[1] E.g., the Review of Particle Physics of 2002 [23] considers a difference between the Compton polarizabilities $\bar{\alpha}_p$ and $\bar{\beta}_p$ on the one hand and the polarizabilities measured via static fields α_n and β_n on the other, whereas the Review of Particle Physics of 2004 [24] consistently uses α and β.

$|T^{(2)}|^2$ a factor $(1/4\pi)^2$. As far as necessary we will make a statement about the unit system. The general expression for the amplitude of Compton scattering by a spin-$\frac{1}{2}$ particle up to the ω^2 terms has been derived by Petrun'kin [4].

The "dynamic" (Compton) electromagnetic polarizabilities, $\bar{\alpha}$ and $\bar{\beta}$, measured in Compton scattering experiments, and the "static" electromagnetic polarizabilities, α and β, measured with static fields or with quasi-real ($Q^2 \to 0$) virtual photons are identical quantities. This is easily seen by calculating the electric and magnetic field strengths provided by a real photon. Simplifying the quantum-electrodynamic notation [25] we write the vector potential of a real photon in the form

$$\mathbf{A}(\mathbf{r},t) = \boldsymbol{\epsilon} N e^{-i\omega t} e^{i\mathbf{k}\cdot\mathbf{r}} + c.c. \tag{7}$$

where $\boldsymbol{\epsilon}$ denotes the polarization vector of the photon, N a factor normalizing the integrated energy density to the energy ω of one photon and $c.c.$ stands for the complex conjugate term. Using

$$\mathbf{E}(\mathbf{r},t) = -\frac{\partial}{\partial t}\mathbf{A}(\mathbf{r},t), \qquad \mathbf{H}(\mathbf{r},t) = \nabla \times \mathbf{A}(\mathbf{r},t), \tag{8}$$

we arrive at the conclusion that the factors $(\omega\boldsymbol{\epsilon})\cdot(\omega'\boldsymbol{\epsilon}')$ and $(\omega\,\hat{\mathbf{k}}\times\boldsymbol{\epsilon})\cdot(\omega'\,\hat{\mathbf{k}}'\times\boldsymbol{\epsilon}')$ entering into (6) may be interpreted as products $\mathbf{E}\cdot\mathbf{E}'$ and $\mathbf{H}\cdot\mathbf{H}'$ of electric and magnetic fields, respectively.

Static electric fields $\mathbf{E}$ are provided with sufficient strength by heavy nuclei. Therefore, use may be made of the differential cross section for electromagnetic scattering of slow neutrons in the Coulomb field of heavy nuclei [3]

$$\frac{\mathrm{d}\sigma_{\mathrm{pol}}}{\mathrm{d}\Omega} = \pi M p (Ze)^2 \mathrm{Re} a \left\{ \alpha_n \sin\frac{\theta}{2} - \frac{e^2\kappa_n^2}{2M^3}\left(1 - \sin\frac{\theta}{2}\right)\right\} \tag{9}$$

applied in its solid-angle integrated form

$$\sigma_{\mathrm{pol}} = \frac{8}{3}\pi^2 M p (Ze)^2 \mathrm{Re} a \left\{ \alpha_n - \frac{e^2\kappa_n^2}{4M^3}\right\} \tag{10}$$

to determine the neutron electric polarizability α_n. In (9) and (10) p is the neutron momentum and $-a$ the amplitude for hadronic scattering by the nucleus. The second term in the braces is due to the Schwinger term, *i.e.* the term describing neutron scattering in the Coulomb field due to the magnetic moment of the neutron only. As outlined above the two different definitions of electromagnetic polarizabilities are equivalent. This means that the polarizabilities measured by quasi-static electromagnetic fields, *i.e.*, either by using real photons to measure amplitudes for Compton scattering up to $\mathcal{O}(\omega^2)$ or by using virtual photons in the initial state at the limit $Q^2 \to 0$ lead to the same result. As explained above, the magnetic polarizability cannot be measured by electromagnetic scattering of slow neutrons in a Coulomb field.

1.3 Calculations of electromagnetic polarizabilities from models of the nucleon

The electromagnetic polarizabilities of the nucleon have attracted a great number of researchers to calculate these quantities from nucleon models. These are the MIT bag model [26], the nonrelativistic quark model [27] the chiral quark model [28], the chiral soliton model [29] and the Skyrme model [30]. In addition, model calculations for the charged pion have been carried out [31].

The majority of these calculations apply the concept of internal coordinates of the nucleon which are well defined in a nonrelativistic approach. In this nonrelativistic approach second-order perturbation theory leads to the expressions [12, 32, 33]

$$\alpha = 2\sum_{n\neq 0}\frac{|\langle n^{(i)}|D_z|0\rangle|^2}{E_n^{(i)}-E_0^{(i)}} + Z^2\frac{e^2\langle r_E^2\rangle}{3M}, \tag{11}$$

$$\beta = 2\sum_{n\neq 0}\frac{|\langle n^{(i)}|M_z|0\rangle|^2}{E_n^{(i)}-E_0^{(i)}} - e^2\sum_i\frac{q_i^2}{6m_i}\langle 0|\rho_i^2|0\rangle - \frac{\langle 0|\mathbf{D}^2|0\rangle}{2M}. \tag{12}$$

These equations contain the retardation correction $\Delta\alpha = Z^2e^2\langle r_E^2\rangle/3M$ of the electric polarizability and the diamagnetic susceptibility $\beta_{\rm dia} = -e^2\sum_i(q_i^2/6m_i)\langle 0|\rho_i^2|0\rangle - \langle 0|\mathbf{D}^2|0\rangle/2M$ in addition to the leading terms coming from second-order perturbation theory in the long wave-length limit. In (11) and (12) Z and M are the charge number and total mass, respectively, of the hadron and r_E^2 the square of the quadratic charge radius. The quantity $\mathbf{D}$ is the electric dipole moment and D_z and M_z the z-components of the electric and magnetic dipole moments, respectively. The quantities q_i, m_i and ρ_i are the charge fraction, the mass and the internal coordinate of the constituents inside the hadron. Recently, it has been shown that these relations contain large uncertainties, especially in the r_E^2 dependent retardation correction because there are other relativistic terms of at least the same order [34]. This will be outlined in more detail in Section 1.4.

A simple argument may be first discussed here. One of several equivalent derivations of (11) makes use of the separation of the Compton amplitude into a Thomson amplitude calculated classically for an extended charged sphere and an internal amplitude which – in the long wavelength limit – is given by the first term on r.h.s. of (11). The classical treatment of Thomson scattering of photons by an extended charged sphere leads to

$$T^{\rm cl} = T^0F_E(\mathbf{k})F_E(\mathbf{k}') = T^0\left(1-\frac{1}{3}\langle r_E^2\rangle\omega\omega' + \mathcal{O}(\omega^4)\right) \tag{13}$$

where T^0 is the scattering amplitude of a point-like particle and

$$F_E(\mathbf{k}) = \frac{1}{e}\int d^3r\rho(\mathbf{r})e^{i\mathbf{k}\cdot\mathbf{r}} \tag{14}$$

is the form-factor with respect to the wave vector $\mathbf{k}$ of the photon. Then the second term in the parentheses of (13) may be considered as part of the electric polarizability so that the expression on the r.h.s. of (11) is obtained. It can be shown [35, 36] that the amplitude $T^0F_E^2(\mathbf{k})$ is not in agreement with forward-direction dispersion theory, i.e. it violates causality. As a consequence we conclude that when using the expression of (11) it is necessary to take into account relativistic corrections, because they substantionally modify the prediction. An equivalent conclusion has previously been discussed by L'vov [3]. A possible extension of the expressions given in (11) which includes relativistic corrections will be discussed in Section 1.4.

1.4 Effects of the Breit Hamiltonian and of the relativistic center-of-mass variable

The difficulties discussed in the foregoing find an explanation in the fact that the retardation correction $\Delta\alpha$ is only one of several relativistic corrections.

In order to take into account these further relativistic corrections for the most simple case of two charged point particles, we write the two-particle Hamiltonian with Coulomb interaction [34] in the form

$$\tilde{H}[\mathbf{A}] = \tilde{H}_{\rm nr}[\mathbf{A}] + \tilde{H}_{\rm B}[\mathbf{A}] + \delta\tilde{H}[\mathbf{A}] \tag{15}$$

where $\mathbf{A}$ is the vector potential with the Coulomb field as its time component, $\tilde{H}_{\rm nr}[\mathbf{A}]$ the nonrelativistic Hamiltonian, $\tilde{H}_{\rm B}[\mathbf{A}]$ the Breit Hamiltonian and $\delta\tilde{H}[\mathbf{A}]$ a spin dependent correction to both, the nonrelativistic Hamiltonian and the Breit Hamiltonian. For a two-particle system the nonrelativistic Hamiltonian has the form

$$\tilde{H}_{\rm nr}[\mathbf{A}] = \frac{{\boldsymbol{\pi}_1}^2}{2m_1} + \frac{{\boldsymbol{\pi}_2}^2}{2m_2} - \frac{g}{|\mathbf{r_1} - \mathbf{r_2}|} \tag{16}$$

where $\boldsymbol{\pi}_i = \mathbf{p}_i - e_i\mathbf{A}(\mathbf{r}_i)$ and g the coupling constant which, for two particles with electric charges e_1 and e_2, is given by $g = -e_1e_2 > 0$. This means that the unit system $e^2 = 1/137.04$, $\hbar = c = 1$ is used. The Breit Hamiltonian takes into account relativistic corrections in lowest order. These are corrections to the kinetic energies of the particles and corrections to the Coulomb field which has to be supplemented by the space component of the vector potential. This latter correction frequently is termed "magnetic quanta exchange". For two particles the Breit Hamiltonian may be written in the form [37]

$$\tilde{H}_{\rm B}[\mathbf{A}] = -\frac{(\boldsymbol{\pi}_1^2)^2}{8m_1^3} - \frac{(\boldsymbol{\pi}_2^2)^2}{8m_2^3} + \frac{g}{2m_1m_2}\left(\frac{\delta^{ij}}{r} + \frac{r^ir^j}{r^3}\right)\pi_1^i\pi_2^j. \tag{17}$$

The spin dependent correction $\delta\tilde{H}[\mathbf{A}]$ takes into account the effects of the magnetic moments of the two particles coming into play because of the non-vanishing space component of the vector potential. As discussed in detail in [34] also the internal dipole moment

$$D = e_1\mathbf{r}_1 + e_2\mathbf{r}_2 - (e_1 + e_2)\mathbf{R}_{\rm cm} \tag{18}$$

needs a relativistic correction because of the center-of-mass vector $\mathbf{R}_{\rm cm}$ which has to be defined to satisfy the relations

$$[\mathbf{R}_{\rm cm}, \mathbf{P}] = i, \quad i[H_{\rm tot}, \mathbf{R}_{\rm cm}] = \frac{\mathbf{P}}{H_{\rm tot}}. \tag{19}$$

Here, $H_{\rm tot}$ is the total relativistic Hamiltonian of the system and $\mathbf{P}$ the total momentum. This leads to the center of mass operator

$$\mathbf{R}_{\rm cm} = \mathbf{R} + \frac{(m_2 - m_1)}{2M^2}\left(\{\mathbf{r}, H_{\rm nr}\} + g\frac{\mathbf{r}}{r}\right) \tag{20}$$

with $\mathbf{r}_1 = \mathbf{R} + \frac{m_2}{M}\mathbf{r}$, $\mathbf{r}_2 = \mathbf{R} - \frac{m_1}{M}\mathbf{r}$, $M = m_1 + m_2$ and the notation $\{a, b\} = ab + ba$.

For a two-particle system with charges e_1 and e_2 the following results are obtained

$$\alpha_{0\rm nr} = \frac{9}{2\mu g^4}\left(\frac{e_1}{m_1} - \frac{e_2}{m_2}\right)^2, \tag{21}$$

$$\Delta\alpha = \frac{e_1 + e_2}{Mg^2}\left(\frac{e_1}{m_1^2} + \frac{e_2}{m_2^2}\right), \tag{22}$$

$$\alpha_{0\rm B} = -\frac{1}{g^2}\left(\frac{e_1}{m_1} - \frac{e_2}{m_2}\right)^2\left(\frac{121}{6\mu} - \frac{113}{4M}\right) - \frac{e_1 + e_2}{Mg^2}\left(\frac{e_1}{m_1} - \frac{e_2}{m_2}\right)\frac{m_1 - m_2}{2m_1m_2}, \tag{23}$$

where $\mu = m_1m_2/(m_1 + m_2)$. The first term (21) corresponds to the nonrelativistic result of second-order perturbation theory, the second (22) to the retardation correction and the third (23) to the Breit correction. The correction due to spins has not been given consideration here.

Applying these formulae to a hydrogen-like atom with charge number Z and mass M we arrive at the following results

$$\begin{aligned}
\alpha_{0\mathrm{nr}} &= \frac{9}{2}\frac{1}{Z^4}\, a_{\mathrm{H}}^3, \\
\Delta\alpha &= -\frac{m_e}{M}\frac{Z-1}{Z^2}\alpha_e^2\, a_{\mathrm{H}}^3, \\
\alpha_{0\mathrm{B}} &= -\frac{1}{Z^2}\frac{121}{6}\alpha_e^2\, a_{\mathrm{H}}^3,
\end{aligned} \tag{24}$$

where m_e is the electron mass and a_{H} the Bohr radius of the hydrogen atom. The negative $\Delta\alpha$ is a consequence of the negative electron charge. These formulae show that the retardation correction $\Delta\alpha$ is much smaller than the Breit correction $\alpha_{0\mathrm{B}}$ for any charge number Z. For $Z = 1$ $\alpha_{0\mathrm{nr}}$ provides the by far largest contribution to the electric polarizability. With increasing Z the Breit correction leads to a large negative contribution. Due to the cancellation between $\alpha_{0\mathrm{nr}}$ and $\alpha_{0\mathrm{B}}$ the calculated electric polarizability becomes small and even becomes equal to zero for $Z = 65$ or $Z\alpha = 0.47$. We interpret this result as a consequence of the fact that the Breit correction is valid for $Z\alpha \ll 1$ only.

Summary: Electric polarizabilities evaluated from experiments using static electric fields were occasionally assumed to be identical with the "true" electric polarizability α_0, a quantity given by the first term on r.h.s. of (11). The error contained in this identification has already been discussed and corrected by L'vov [3]. This quantity merely is an incomplete nonrelativistic decription of the electric polarizability but not a physical observable. Furthermore, also the inclusion of the second term on the r.h.s. of (11) does not lead to a reasonable expression because of missing relativistic corrections. Finally, the polarizabilities α and β measured – or at least defined – by static electromagnetic fields are identical to the polarizabilties $\bar{\alpha}$ and $\bar{\beta}$ measured by Compton scattering.

1.5 Chiral perturbation theory

Electromagnetic polarizabilities have been calculated in chiral perturbation theory (χPT) in a series of papers [38]. In a leading-order relativistic χPT calculation, it was obtained

$$\begin{aligned}
\alpha_p &= \frac{e^2 g_{\pi N}^2}{192\pi^3 M^3}\left\{\frac{5\pi}{2\mu} + 18\ln\mu + \frac{33}{2} + \mathcal{O}(\mu)\right\} = \ 7.4, \\
\beta_p &= \frac{e^2 g_{\pi N}^2}{192\pi^3 M^3}\left\{\frac{\pi}{4\mu} + 18\ln\mu + \frac{63}{2} + \mathcal{O}(\mu)\right\} = -2.0, \\
\alpha_n &= \frac{e^2 g_{\pi N}^2}{192\pi^3 M^3}\left\{\frac{5\pi}{2\mu} + 6\ln\mu - \frac{3}{2} + \mathcal{O}(\mu)\right\} = 10.1, \\
\beta_n &= \frac{e^2 g_{\pi N}^2}{192\pi^3 M^3}\left\{\frac{\pi}{4\mu} + 6\ln\mu + \frac{5}{2} + \mathcal{O}(\mu)\right\} = -1.2,
\end{aligned} \tag{25}$$

where $\mu = m_\pi/M$ is the pion-nucleon mass ratio. In (25) the numerical values correspond to the full calculation whereas the first three terms in the braces represent a semi-relativistic expansion up to and including next-to-leading order terms. This finding was explained [39] by using dispersion relations. The analog to chiral perturbation theory as underlying the results given in (25) is to carry out a calculation in terms of a dispersion theory where recoil corrections are included and the meson photoproduction amplitudes are used in the Born approximation. The results obtained in this way from dispersion theory are $\alpha_p = 7.3$, $\beta_p = -1.8$, $\alpha_n = 9.8$, $\beta_n = -0.9$ in reasonable agreement with the numbers in (25).

To leading order the results given in (25) have been summarized (see e.g. [1, 40, 41]) in the form

$$\alpha_p = \alpha_n = 10\beta_p = 10\beta_n = \frac{5}{96\pi}\left(\frac{g_A}{f_\pi}\right)^2 \frac{\alpha_e}{m_\pi} \simeq 12.6 \cdot 10^{-4}\mathrm{fm}^3 \tag{26}$$

where use has been made of the Goldberger-Treiman relation $g_{\pi N} f_\pi = g_A M$, with g_A being the axial coupling of the nucleon and f_π the pion-decay constant. The relation given in (26) was found to be exactly identical to the result of a calculation in heavy baryon χPT (HBχPT) [42]. The calculation carried out in HBχPT was extended beyond the one-loop approach [43] yielding $\alpha_p = 10.5 \pm 2.0$, $\beta_p = 3.5 \pm 3.6$, $\alpha_n = 13.4 \pm 1.5$ and $\beta_n = 7.8 \pm 3.6$. All terms up to order $\mathcal{O}(q^4)$ were included. At this order counter terms enter which were determined by several different procedures.

Subsequent attempts to overcome the shortcoming of the missing Δ contribution in terms of a "small scale expansion" (SSE) [44] led to $\alpha_p = 16.4$ and $\beta_p = 9.1$ where both numbers are much larger than the experimental results. Attempts to reproduce the predictions of Baldin's sum rule [10] for $\alpha + \beta$ have been published in [45], emphasizing the need for relativistic chiral EFT calculations. Recent calculations on differential cross sections for Compton scattering by the nucleon [46, 47] have in common that free parameters are introduced, corresponding to counter-terms of unnatural size [46]. A counter-term of unnatural size signals the fact that the theory fails because of physics beyond the theory [46]. It remains to be a challenge for the χPT community to find out what this missing physics is[2]

1.6 Diagrammatic description of Compton scattering and dispersion theories

The foregoing approaches have in common that they start from a given set of degrees of freedom of the nucleon and calculate the electromagnetic polarizabilities in theoretical frameworks which in general contain further approximations. A more satisfactory approach of course would be to start from a phenomenological description of the structure of the nucleon and to relate the information obtained to polarizability and Compton scattering without further approximations. The appropriate tools for this latter approach are provided by dispersion theories.

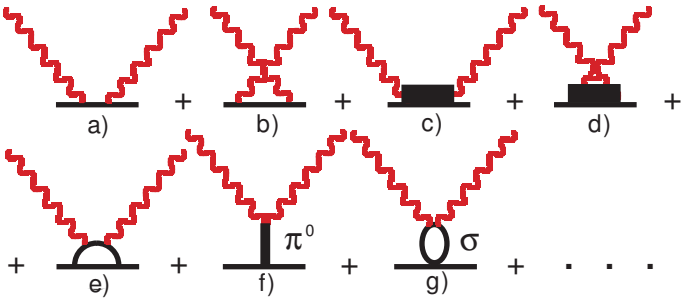

Figure 2: a) and b): Born terms, c) and d): scattering through isobar excitation, e) scattering through excitation of the pion cloud, f) scattering via exchanges of pseudoscalar mesons in the t-channel, g) scattering via exchanges of scalar mesons in the t-channel.

In a diagrammatic approach Compton scattering by the nucleon is described by a series of graphs which give an overview over the processes related to Compton scattering. An example is given in Figure

[2]Among other aspects it is of importance to know that χPT includes the graph f) of Figure 2 but does not explicitly include the graph g).

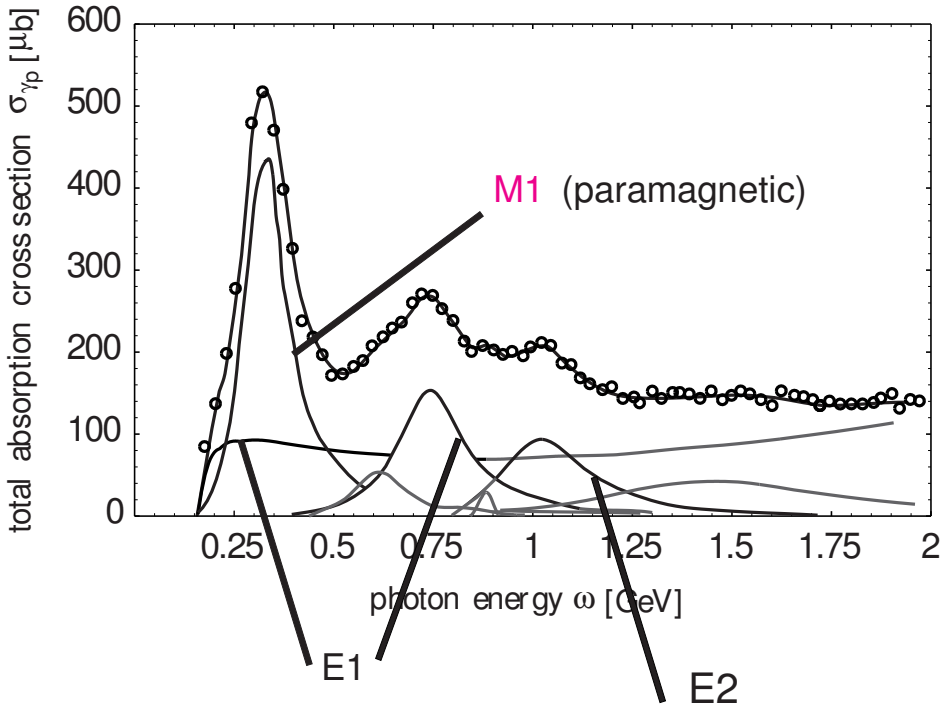

Figure 3: Total photo-absorption cross section of the proton disentangled into multipole components.

2 containing the selection of graphs given by Drechsel et al. [1]. These graphs denote the Born term a) and its crossing partner b), the scattering through the excitation of isobars c) and the crossing partner d), and the scattering through the meson cloud e). This latter graph is one example of a larger number of graphs as discussed in chiral perturbation theory. The graphs f) and g) depict scattering through exchanges of pseudoscalar and scalar mesons in the t-channel, respectively.

The Born terms a) and b) involve the scattering through the electric charge and magnetic moment of the nucleon without excitation of the internal structure. This process may be viewed as classical Thomson scattering, approximating a high-energy process where the virtual creation and annihilation of a nucleon-antinucleon pair in the field of the scattering nucleon is involved.

The physical meaning of graphs c) to e) is illustrated in Figures 3 and 4. The M1-strength leading to a strong source of paramagnetism is provided by the $P_{33}(1232)$ or Δ resonance. The $E1$-strength has a nonresonant component due to single-pion photoproduction, supplemented by a high-energy tail of double- and many-pion photoproduction which presumably is also mainly of $E1$ multipolarity. The nonresonant single-pion component may be identified with the meson-cloud contribution to the electric polarizability, illustrating the common supposition that the electric polarizability is mainly generated by the meson cloud. A further smaller amount of $E1$-strength is provided by the $D_{13}(1520)$ resonance. The $E2$-strength of the $F_{15}(1680)$-resonance makes contributions to the electric as well as the magnetic polarizability.

Graph f) in Figure 2 represents the so-called pion pole term as introduced by Low in 1958 [48]. The idea is that not the isobar-meson structure of the nucleon is excited as discussed above. Instead, a π^0 meson is created in the intermediate state which then couples to the incoming and outgoing photon on the one side and to the nucleon on the other. Because of the small widths of the π^0 meson resonance, this contribution to the Compton scattering process can be described by a pole located at positive $t = m_\pi^2$ in the Mandelstam plane (t-channel).

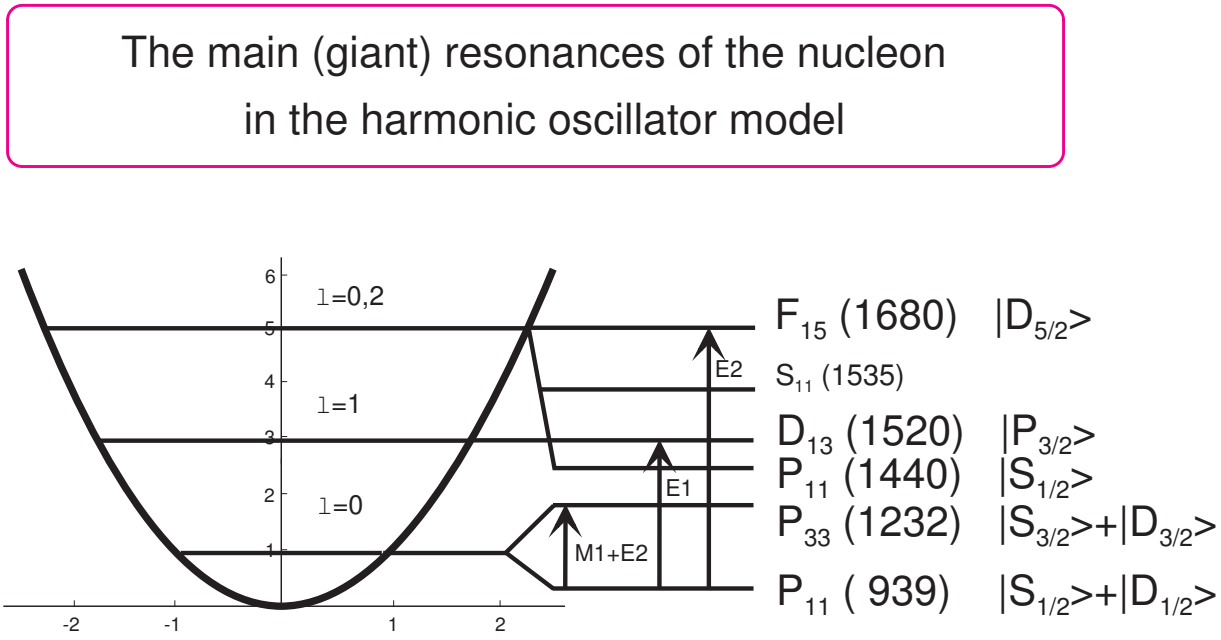

Figure 4: The main (giant) resonances of the nucleon in a diquark-quark harmonic oscillator model. The lines inside the parabola denote the harmonic oscillator states. The lines on the right side indicate the centers of the resonant states. The observed widths of these states are generated through emission and reabsorption of pions by the constituent quarks.

The scalar analogue of the pseudoscalar π^0 pole term depicted in g) has first been discussed by Hearn and Leader in 1962 [49]. These authors pointed out that in addition to the pion pole a continuum of two-pion states should make a contribution to Compton scattering. Since these two-pion states do not form a particle with a narrow width, the mathematical tools necessary for the description of this contribution have to be somewhat different. Nevertheless, it was discussed very early (see e.g. [50]) that these two-pion states possibly may form some kind of a broad resonance with an energy of about 600 MeV. Nowadays this resonance is identified with the pole-structure seen in π-π phase-analyses of data obtained in $\pi N \to N\pi\pi$ scattering experiments. It appears possible that the meaning of graph g) in Figure 2 goes beyond the physics suggested by this graph. As will be explained in more detail later, the interpretation of the graph g) of Figure 2 in terms of correlated π pairs is incomplete. Only part of the strength seems to be exhausted by the $|\pi\pi\rangle$ component whereas an other part correspond to a "core" component of probably $|q\bar{q}\rangle$ structure [51]. This important finding will be worked out and substantiated in more detail in our ongoing work [52].

2 Forward and backward Compton scattering and related phenomena

The physics of polarizability and Compton scattering can be understood best when considering the extreme forward and extreme backward directions. Indeed, the relevant phenomena show up very transparently in these two cases whereas for experimental purposes, of course, intermediate angles have to be used. Our concept, therefore, is to first consider forward and backward scattering and then to develop the tools to cover also intermediate angles.

The differential cross section for Compton scattering

$$\gamma N \to \gamma' N' \tag{27}$$

may be written in the form [54]

$$\frac{d\sigma}{d\Omega} = \Phi^2 |T_{fi}|^2 \tag{28}$$

with $\Phi = \frac{1}{8\pi M}\frac{\omega'}{\omega}$ in the lab frame and $\Phi = \frac{1}{8\pi\sqrt{s}}$ in the c.m. frame ($\sqrt{s}$ = total energy). For the following discussion it is convenient to use the lab frame and to consider special cases for the amplitude T_{fi}. These special cases are the extreme forward ($\theta = 0$) and extreme backward ($\theta = \pi$) direction where the amplitudes for Compton scattering may be written in the form [54]

$$\frac{1}{8\pi M}[T_{fi}]_{\theta=0} = f_0(\omega)\boldsymbol{\epsilon}'^{*} \cdot \boldsymbol{\epsilon} + g_0(\omega)\,\mathrm{i}\,\boldsymbol{\sigma} \cdot (\boldsymbol{\epsilon}'^{*} \times \boldsymbol{\epsilon}), \tag{29}$$

$$\frac{1}{8\pi M}[T_{fi}]_{\theta=\pi} = f_\pi(\omega)\boldsymbol{\epsilon}'^{*} \cdot \boldsymbol{\epsilon} + g_\pi(\omega)\,\mathrm{i}\,\boldsymbol{\sigma} \cdot (\boldsymbol{\epsilon}'^{*} \times \boldsymbol{\epsilon}). \tag{30}$$

For circularly polarized photons the polarization vectors $\boldsymbol{\epsilon}$ may be represented in terms of a linearly polarized basis $\hat{\mathbf{e}}_x$ and $\hat{\mathbf{e}}_y$. The most frequently used form of this representation is

$$\boldsymbol{\epsilon}_\lambda = \frac{1}{\sqrt{2}}(-\lambda\hat{\mathbf{e}}_x - i\hat{\mathbf{e}}_y), \qquad \lambda = \pm 1, \tag{31}$$

where λ is the photon helicity [55]. Linearly polarized photons with electric vectors perpendicular or parallel to the x-z reaction plane have polarization vectors $\boldsymbol{\epsilon}_\perp$ and $\boldsymbol{\epsilon}_\parallel$, respectively, where

$$\begin{aligned} \boldsymbol{\epsilon}_\perp &= \hat{\mathbf{e}}_y = \frac{i}{\sqrt{2}}(\boldsymbol{\epsilon}_+ + \boldsymbol{\epsilon}_-), \\ \boldsymbol{\epsilon}_\parallel &= \hat{\mathbf{e}}_x = -\frac{1}{\sqrt{2}}(\boldsymbol{\epsilon}_+ - \boldsymbol{\epsilon}_-). \end{aligned} \tag{32}$$

For linearly polarized photons the relations (29) and (30) remain valid if we interpret $\boldsymbol{\epsilon}$ and $\boldsymbol{\epsilon}'$ as polarization vectors for linear polarization.

The process described in (29) is the transmission of linearly polarized photons through a medium as provided by a proton with spin vector $\boldsymbol{\sigma}$ parallel or antiparallel to the direction of the incident photon with rotation of the direction of linear polarization [56]. The amplitudes f_0 and g_0 correspond to the polarization components of the outgoing photon parallel and perpendicular to the direction of linear polarization of the incoming photon. The interpretation of (30) is the same as that of (29) except for the fact that the photon is reflected. In case of forward scattering (29) the origin of the rotation of the direction of linear polarization may be related to the alignment of the internal magnetic dipole moments of the nucleon and in this sense the process may be considered as a Faraday effect. In case of backward scattering (30) a large portion of the relevant phenomenon is of a completely different origin which will be studied in detail in the following. It is important to realize that in contrast to frequent belief there is no flip of any spin in the two cases of Compton scattering. The factor $\boldsymbol{\sigma}$ in the second terms of the two equations may be interpreted as a spin dependence of scattering in the sense that the direction of rotation of the electric vector changes sign (from *e.g.* clock-wise to anti clock-wise) when the spin of the target nucleon is reversed.

The two scattering processes may also be related to the two states of circular polarization, i.e. helicity amplitudes for forward and backward Compton scattering. Here, we first restrict the discussion to the well known case of forward scattering [56]. The equally important case of backward scattering

is more complicated and will be considered later. If the photon and nucleon spins are parallel (photon helicity $\lambda_\gamma = +1$, nucleon helicity $\lambda_N = -\frac{1}{2}$, and net helicity in the photon direction $\lambda = \lambda_\gamma - \lambda_N = \frac{3}{2}$) then the amplitude is

$$f_0^{3/2}(\omega) = f_0(\omega) - g_0(\omega), \tag{33}$$

while for the spins being anti-parallel (photon helicity $\lambda_\gamma = +1$, nucleon helicity $\lambda_N = +\frac{1}{2}$, and net helicity along the photon direction $\lambda = \lambda_\gamma - \lambda_N = +\frac{1}{2}$) the amplitude is

$$f_0^{1/2}(\omega) = f_0(\omega) + g_0(\omega). \tag{34}$$

The amplitudes $f_0^{3/2}$ and $f_0^{1/2}$ are related by the optical theorem to the total cross sections $\sigma_{3/2}$ and $\sigma_{1/2}$ for the reaction

$$\gamma + N \to N^* \to N + \text{mesons} + \text{radiative decay of N}^*$$

(see Section 4.1) when the photon spin is parallel or anti-parallel to the nucleon spin:

$$\mathrm{Im} f_0^{3/2}(\omega) = \frac{\omega}{4\pi}\sigma_{3/2}(\omega), \tag{35}$$

$$\mathrm{Im} f_0^{1/2}(\omega) = \frac{\omega}{4\pi}\sigma_{1/2}(\omega). \tag{36}$$

Therefore,

$$\mathrm{Im}\, f_0(\omega) = \frac{\omega}{4\pi}\,\frac{\sigma_{1/2}(\omega) + \sigma_{3/2}(\omega)}{2} = \frac{\omega}{4\pi}\sigma_{\mathrm{tot}}(\omega), \tag{37}$$

$$\mathrm{Im}\, g_0(\omega) = \frac{\omega}{4\pi}\frac{\sigma_{1/2}(\omega) - \sigma_{3/2}(\omega)}{2} = \frac{\omega}{8\pi}\,\Delta\sigma(\omega), \tag{38}$$

where $\sigma_{\mathrm{tot}}(\omega) = (\sigma_{1/2} + \sigma_{3/2})/2$ is the spin averaged total cross section and $\Delta\sigma = \sigma_{1/2} - \sigma_{3/2}$.

2.1 Definition of polarizabilities

Following Babusci et al. [54] the equations (29) and (30) can be used to define the electromagnetic polarizabilities and spin-polarizabilities as the lowest-order coefficients in an ω-dependent development of the nucleon-structure dependent parts of the scattering amplitudes:

$$f_0(\omega) = -(e^2/4\pi M)q^2 + \omega^2(\alpha+\beta) + \mathcal{O}(\omega^4) \tag{39}$$

$$g_0(\omega) = \omega\left[-(e^2/8\pi M^2)\,\kappa^2 + \omega^2\gamma_0 + \mathcal{O}(\omega^4)\right] \tag{40}$$

$$f_\pi(\omega) = \left(1 + (\omega'\omega/M^2)\right)^{1/2}\left[-(e^2/4\pi M)q^2 + \omega\omega'(\alpha-\beta) + \mathcal{O}(\omega^2\omega'^2)\right] \tag{41}$$

$$g_\pi(\omega) = \sqrt{\omega\omega'}[(e^2/8\pi M^2)(\kappa^2 + 4q\kappa + 2q^2) + \omega\omega'\gamma_\pi + \mathcal{O}(\omega^2\omega'^2)] \tag{42}$$

where qe is the electric charge ($e^2/4\pi = 1/137.04$), κ the anomalous magnetic moment of the nucleon and $\omega' = \omega/(1 + \frac{2\omega}{M})$.

In the relations for $f_0(\omega)$ and $f_\pi(\omega)$ the first nucleon structure dependent coefficients are the photon-helicity non-flip $(\alpha+\beta)$ and photon-helicity flip $(\alpha-\beta)$ linear combinations of the electromagnetic polarizabilities α and β. In the relations for $g_0(\omega)$ and $g_\pi(\omega)$ the corresponding coefficients are the spin polarizabilities γ_0 and γ_π, respectively.

In principle it is possible to define polarizabilities related to higher orders in ω. We do not consider these higher-order polarizabilities is this paper. For a discussion of these higher-order polarizabilities we refer to [1, 2, 53, 54] and references therein.

2.2 Sum-rules for the forward direction

Sum-rules for the forward direction are derived from Cauchy's theorem which may be formulated in the form [57, 58]

$$\mathrm{Re}F(\omega) = \frac{1}{\pi}\mathcal{P}\int_{-\infty}^{+\infty}\frac{\mathrm{Im}F(\omega')}{\omega'-\omega}d\omega' + C(\infty), \tag{43}$$

where the principal value integral runs along the real ω axis and is closed by a contour contribution $C(\infty)$ which in general is nonzero. However, for the present consideration we make the assumption that this contour (or asymptotic) contribution is equal to zero, i.e. we apply the no-subtraction hypothesis $C(|\omega| \to \infty) \to 0$. In case this hypothesis is valid, (43) may be written in the form

$$\mathrm{Re}F(\omega) = \frac{1}{\pi}\int_0^{\infty}\frac{-\mathrm{Im}F(-\omega')}{\omega'+\omega}d\omega' + \frac{1}{\pi}\mathcal{P}\int_0^{\infty}\frac{\mathrm{Im}F(\omega')}{\omega'-\omega}d\omega'. \tag{44}$$

Crossing symmetry [57]

$$F(-\omega) = F^*(\omega). \tag{45}$$

implies that

$$\mathrm{Im}F(-\omega) = -\mathrm{Im}F(\omega). \tag{46}$$

Inserting (46) into (44) we arrive at

$$\mathrm{Re}F(\omega) = \frac{2}{\pi}\mathcal{P}\int_0^{\infty}\frac{\omega'\,\mathrm{Im}F(\omega')}{\omega'^2-\omega^2}d\omega' = \frac{1}{2\pi^2}\mathcal{P}\int_{\omega_0}^{\infty}\frac{\omega'^2\sigma_{\mathrm{tot}}(\omega')}{\omega'^2-\omega^2}d\omega', \tag{47}$$

where ω_0 is the threshold energy below which the total photo-absorption cross section is equal to zero. Applying the same procedure to the function $F_1(\omega)$ defined through

$$\omega^2 F_1(\omega) = f_0(\omega) + (e^2/4\pi M)q^2 = \omega^2(\alpha+\beta) + \mathcal{O}(\omega^4) \tag{48}$$

and also make use of the crossing symmetry (45) for $F_1(\omega)$, we arrive at

$$\mathrm{Re}f_0(\omega) + (e^2/4\pi M)q^2 = \frac{\omega^2}{2\pi^2}\mathcal{P}\int_{\omega_0}^{\infty}\frac{\sigma_{\mathrm{tot}}(\omega')}{\omega'^2-\omega^2}d\omega' \tag{49}$$

and

$$\alpha+\beta = \frac{1}{2\pi^2}\int_{\omega_0}^{\infty}\frac{\sigma_{\mathrm{tot}}(\omega')}{\omega'^2}d\omega'. \tag{50}$$

Similarly, for the function $F_2(\omega)$ defined through

$$\omega F_2(\omega) = g_0(\omega) = -\omega\frac{e^2\kappa^2}{8\pi M^2} + \mathcal{O}(\omega^3) \tag{51}$$

we arrive at

$$\mathrm{Re}\,g_0(\omega) = \frac{\omega}{4\pi^2}\mathcal{P}\int_{\omega_0}^{\infty}\frac{\omega'\Delta\sigma(\omega')}{\omega'^2-\omega^2}d\omega' \tag{52}$$

and

$$\frac{2\pi^2\alpha_e\kappa^2}{M^2} = \int_{\omega_0}^{\infty}\frac{\sigma_{3/2}(\omega)-\sigma_{1/2}(\omega)}{\omega}d\omega; \quad \alpha_e = 1/137.04. \tag{53}$$

Applying a Taylor expansion to (52) and making use of (40) we arrive at

$$\gamma_0 = -\frac{1}{4\pi^2}\int_{\omega_0}^{\infty}\frac{\sigma_{3/2}(\omega)-\sigma_{1/2}(\omega)}{\omega^3}d\omega. \tag{54}$$

It should be noted that in (48) to (54) the no-subtraction hypothesis applies to the function $F_1(\omega)$ and $F_2(\omega)$.

The sum rule given in (50) was first derived by Baldin [10] and later discussed in more detail by Lapidus [59]. It, therefore, appears justified [3] to call it the "BL" sum rule. The sum rule (53) has independently been derived by Gerasimov [60] and Drell and Hearn [61]. A further independent derivation in terms of current algebra has been given by Hosada [62]. It has become customary to call it the "GDH" sum rule.

2.3 Properties of amplitudes for the backward direction

In order to arrive at general properties of scattering amplitudes for the backward direction we make use of the fact that in the forward and backward directions Compton scattering takes place via photon-helicity non-flip and photon-helicity flip amplitudes, respectively. Denoting the corresponding scattering amplitudes by $T_{1,1}$ and $T_{1,-1}$, respectively, we apply the usual partial wave expansion of the helicity amplitudes [36, 63, 64]

$$T_{1,\pm1}(\omega,\theta) = \sum_{L=1}^{\infty} T^L_{1,\pm1}(\omega) d^L_{1,\pm1}(\theta) \tag{55}$$

with $d^L_{1,\pm1}(\theta)$ being the d-functions, having the special values

$$d^L_{1,+1}(\theta=0) = 1, \tag{56}$$

$$d^L_{1,-1}(\theta=\pi) = (-1)^{L-1}. \tag{57}$$

The partial waves $T^L_{1,\pm1}(\omega)$ contain electric (T^{EL}) and magnetic (T^{ML}) multipoles:

$$T^L_{1,\pm1}(\omega) = T^{EL}(\omega) \pm T^{ML}(\omega). \tag{58}$$

This leads to the equations

$$T_{1,+1}(\omega,\theta=0) = \sum_{L=1}^{\infty} \left[T^{EL}(\omega) + T^{ML}(\omega)\right], \tag{59}$$

$$\begin{aligned} T_{1,-1}(\omega,\theta=\pi) &= \sum_{L=1}^{\infty} (-1)^{L-1} \left[T^{EL}(\omega) - T^{ML}(\omega)\right], \\ &= T^{\Delta P=\text{yes}}(\omega) - T^{\Delta P=\text{no}}(\omega), \end{aligned} \tag{60}$$

where $\Delta P = \text{yes}$ and $\Delta P = \text{no}$ denote excitation processes with parity change ($\Delta P = \text{yes} : E1, M2, E3, \cdots$) and parity nonchange ($\Delta P = \text{no} : M1, E2, M3, \cdots$), respectively. Applying the optical theorem in the generic form[3] $\text{Im}F(\omega) = (\omega/4\pi)\sigma(\omega)$ these properties can be used to supplement the relations (37) and (38) by

$$\text{Im}f_\pi(\omega) = \frac{\omega}{4\pi}\left[\sigma(\omega,\Delta P=\text{yes}) - \sigma(\omega,\Delta P=\text{no})\right], \tag{61}$$

$$\begin{aligned} \text{Im}g_\pi(\omega) &= \frac{\omega}{8\pi}\left[\Delta\sigma(\omega,\Delta P=\text{yes}) - \Delta\sigma(\omega,\Delta P=\text{no})\right], \\ &\equiv \frac{\omega}{8\pi}\{[\sigma_{1/2}(\omega,\Delta P=\text{yes}) - \sigma_{1/2}(\omega,\Delta P=\text{no})], \\ &\quad -[\sigma_{3/2}(\omega,\Delta P=\text{yes}) - \sigma_{3/2}(\omega,\Delta P=\text{no})],\} \\ &\equiv \frac{\omega}{8\pi}\sum_n P_n[\sigma^n_{3/2}(\omega) - \sigma^n_{1/2}(\omega)] \end{aligned} \tag{62}$$

[3]This is a formal use of the optical theorem. In a physical sense the optical theorem is only valid in the forward direction.

with $P_n = +1$ for $\Delta P =$ no and $P_n = +1$ for $\Delta P =$ yes. Eq. (61) has been used to derive a sum rule for $\alpha - \beta$. Its first formulation was published by Bernabeu, Ericson and Ferro Fontan [65], its final form was first given by Bernabeu and Tarrach [66]. It, therefore, appears justified to call it the "BEFT" sum rule. Eq. (62) was used by L'vov and Nathan [67] to derive a sum rule for γ_π, which may be called the "LN" sum rule.

We will see later that these four sum rules, e.g. "BL", "GDH", "BEFT", and "LN", contain very important information for an understanding of the polarizability of the nucleon. The following parts of this section will be devoted to a description of phenomena which are essential for these sum rules. For the derivation of the "BEFT", and "LN" sum rules dispersion theories for nonzero angle are needed which will be discussed in Section 3.

2.4 Mandelstam variables

The conservation of energy and momentum in nucleon Compton scattering

$$\gamma(k,\lambda) + N(p) \to \gamma'(k',\lambda') + N'(p') \tag{63}$$

is given by

$$k + p = k' + p' \tag{64}$$

where the four-momenta may be expressed through the energies and three-momenta in the form $k = (\omega, \mathbf{k})$, $k' = (\omega', \mathbf{k}')$, $p = (E, \mathbf{p})$ and $p' = (E', \mathbf{p}')$. The metric is chosen such that $k^2 = \omega^2 - \mathbf{k}^2 = 0$, $p^2 = E^2 - \mathbf{p}^2 = M^2$ which analogous expressions for the final states.

Let us introduce the three Mandelstam variables

$$s = (k+p)^2 = (k'+p')^2, \tag{65}$$
$$t = (k-k')^2 = (p'-p)^2, \tag{66}$$
$$u = (k-p')^2 = (k'-p)^2. \tag{67}$$

They are constrained by the relation

$$s + t + u = 2M^2. \tag{68}$$

which follows from the energy-momentum relations given above.

It is useful to introduce one other variable

$$\nu = \frac{s-u}{4M} \tag{69}$$

which may replace s and u via

$$\nu = \frac{s - M^2 + t/2}{2M}, \tag{70}$$
$$-\nu = \frac{u - M^2 + t/2}{2M}. \tag{71}$$

Furthermore, we have

$$\nu = E_\gamma + \frac{t}{4M} = \frac{1}{2}(E_\gamma + E_{\gamma'}), \tag{72}$$
$$\sin^2\frac{\theta_s}{2} = -\frac{st}{(s-M^2)^2} \tag{73}$$

where E_γ and $E_{\gamma'}$ are the energies of the initial and final photon in the laboratory and θ_s the c.m. scattering angle of Compton scattering (s-channel). The definition of θ_s is illustrated in the left panel of Figure 5. It should be noted that the definition given in (73) may lead to scattering angles outside the "physical range" $-1 \leq \cos\theta_s \leq +1$ [68]. Unphysical ranges may be of importance for the completeness of dispersion integrals and the definition given in (73) provides the tool for the analytical continuation.

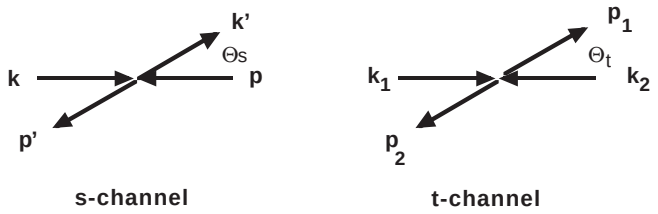

Figure 5: Left panel: Definition of the c.m. scattering angle of Compton scattering (s-channel). Right panel: Definition of the c.m. scattering angle of a two-photon fusion process (t-channel). The quantities $\mathbf{k}$ are three-momenta of photons, the quantities $\mathbf{p}$ three-momenta of nucleons.

The t-channel corresponds to the fusion of two photons with four-momenta k_1 and k_2 and helicities λ_1 and λ_2 to form a t-channel intermediate state $|t\rangle$ from which – in a second step – a proton-antiproton pair is created. The corresponding reaction may be formulated in the form

$$\gamma(k_1,\lambda_1) + \gamma(k_2,\lambda_2) \to \bar{N}(p_1) + N(p_2). \tag{74}$$

For Compton scattering the related $N\bar{N}$ pair creation-process is only virtual, i.e. the energy is too low to put the proton-antiproton pair on the mass shell. This means that we have to treat the process described in (74) in the unphysical region. The s-channel to t-channel transition may be summarized as follows

$$k \to k_1 \qquad \boldsymbol{\epsilon} \to \boldsymbol{\epsilon}_1, \tag{75}$$
$$k' \to -k_2 \quad \boldsymbol{\epsilon}'^{*} \to \boldsymbol{\epsilon}_2, \tag{76}$$
$$p \to -p_1 \qquad u(p) \to v(p_1), \tag{77}$$
$$p' \to p_2 \qquad u(p') \to u(p_2), \tag{78}$$

where $u(p)$, $u(p')$ and $u(p_2)$ denote nucleon states and $v(p_1)$ an antinucleon state. The sign changes in (76) and (77) mean that instead of an outgoing photon γ' there is a second incoming photon γ_2 and instead of an incoming nucleon N there is an outgoing antinucleon $\bar{N}$.

The sign change in (76) when replacing the four-momentum of the outgoing scattered photon by the four-momentum of a second incoming photon leads to the following relations between photon-helicities

$$\lambda \to \lambda_1, \tag{79}$$
$$\lambda' \to -\lambda_2, \tag{80}$$
$$\Delta\lambda^s_{\gamma\gamma} \equiv |\lambda - \lambda'| = 0 \to \Delta\lambda^t_{\gamma\gamma} \equiv |\lambda_1 - \lambda_2| = 2, \tag{81}$$
$$\Delta\lambda^s_{\gamma\gamma} \equiv |\lambda - \lambda'| = 2 \to \Delta\lambda^t_{\gamma\gamma} \equiv |\lambda_1 - \lambda_2| = 0. \tag{82}$$

The case described in (81) is given in forward Compton scattering ($\theta_s = 0$) , the case described in (82) in backward Compton scattering ($\theta_s = \pi$). Forward Compton scattering may be related to a two-photon fusion process where the helicity difference of the two photons is equal to 2. Backward

Compton scattering, on the other hand, may be related with a two-photon fusion process where the helicity difference of the two photons is 0. For sake of completeness we give the following relation for the t-channel scattering angle

$$\cos\theta_t = \frac{s + \frac{1}{2}t - M^2}{\frac{1}{2}\sqrt{t(t-4M^2)}} \equiv \frac{4M\nu}{\sqrt{t(t-4M^2)}}. \tag{83}$$

For $\theta_s = \pi$ we have $16M^2\nu^2 = t(t-4M^2)$ and, therefore[4], $\cos\theta_t = -1$. As in case of $\cos\theta_s$ also $\cos\theta_t$ is the essential variable for analytical continuations. In the c.m. system of the two photons k_1 and k_2 the quantity t has the meaning of a total energy squared:

$$t = (k_1 + k_2)^2 = (\omega_1 + \omega_2)^2 = (W^t)^2. \tag{84}$$

2.5 Selection rules and photon-polarization correlations of t-channel intermediate states

For the discussion of properties of the t-channel it is useful to study the selection rules for spins, parities and photon-polarization correlations of mesons decaying into two photons.

Following early work of Landau [69] the problem of selection rules and photon-polarization correlation was treated by C.N. Yang [70] in its general form. In [70] two-photon decay of $J^{PC} = 3^{++}, 5^{++}, \cdots$ mesons was discussed without a definite statement about the correlation of linear polarizations. The necessary completion was possible using the formulae given in [70]. The results obtained in this way are summarized in the following.

The polarization correlation can be formulated in terms circular and linear polarization. In terms of circular polarization the states are denoted by ψ^{RR} ,ψ^{LL}, ψ^{RL} and ψ^{LR}, where, e.g., RR means that the two photons going into $+z$ and $-z$ direction, respectively, both are righthanded circular, i.e. they have positive helicity. The linear combinations ψ_1 to ψ_4 of these states describe two-photon states with definite linear polarization-correlation, where symmetric linear combinations correspond to parallel linear polarization of the two photons and antimetric linear combinations to perpendicular linear polarization. It is easy to see that $\psi_2 = \psi^{RR} - \psi^{LL}$ has negative parity whereas the other states, ψ_1, ψ_3 and ψ_4 have positive parity. The states ψ^{RR} and ψ^{LL} correspond to t-channel helicity differences of $\Delta\lambda^t_{\gamma\gamma} = 0$, the states ψ^{RL} and ψ^{LR} to $\Delta\lambda^t_{\gamma\gamma} = 2$. Furthermore, two-photon decay implies that the C-parity quantum number is $C = +1$. Collecting all pieces of information we arrive at Table 4.

Table 4: Selection rules and photon-polarization correlations of meson decaying into two photons.

$\gamma\gamma$-state	$\gamma\gamma$-polarization	$\Delta\lambda^t_{\gamma\gamma}$	$\Delta\lambda^s_{\gamma\gamma}$	quantum numbers	
$\psi_1 = \psi^{RR} + \psi^{LL}$	parallel	0	2	$J^{PC} = 0^{++}, 2^{++}, 4^{++}, \cdots$	f_π
$\psi_2 = \psi^{RR} - \psi^{LL}$	perpendicular	0	2	$J^{PC} = 0^{-+}, 2^{-+}, 4^{-+}, \cdots$	g_π
$\psi_3 = \psi^{RL} + \psi^{LR}$	parallel	2	0	$J^{PC} = 2^{++}, 4^{++}, 6^{++}, \cdots$	f_0
$\psi_4 = \psi^{RL} - \psi^{LR}$	perpendicular	2	0	$J^{PC} = 3^{++}, 5^{++}, 7^{++}, \cdots$	g_0

[4]There should be a $\pm$ sign in front of $\cos\theta_t$ indicating that the photons γ_1 and γ_2 are indistinguishable so that θ_t and $\pi - \theta_t$ are physically equivalent. We will follow the convention to use the $-$ sign.

The helicity differences $\Delta^t_{\gamma\gamma}$ and $\Delta^s_{\gamma\gamma}$ (Eqs. (81) and (82)) and the $\gamma\gamma$-polarization correlations corresponding to the four states $\Psi^1, .., \Psi^4$ coincide with the properties of the four scattering amplitudes f_π, g_π, f_0, g_0, respectively. This means that the respective quantum numbers J^{PC} (J=spin, P=parity, $C = C$-parity) given in Table 4 may be attributed to the t-channel intermediate states of these amplitudes. Making use of the reasonable assumption that the lowest spin quantum number J is the most relevant one we arrive at the t-channel intermediate states given in Table 5.

Table 5: t-channel intermediate states.

	J^{PC}	exchanged particles
$f_\pi(\omega)$	0^{++}	$\sigma(600), f_0(980), a_0(980)$
$g_\pi(\omega)$	0^{-+}	$\pi^0(135)$, $\eta(547)$, $\eta'(958)$
$f_0(\omega)$	2^{++}	Pomeron P, $f_2(1270)$, $a_2(1320)$
$g_0(\omega)$:	3^{++}	mesons not known

2.6 Properties of scalar mesons

It may be expected that the dominating t-channel contributions to the amplitudes f_π and g_π result from the mesons with lowest angular momenta, i.e. $J^{PC} = 0^{++}$ and $J^{PC} = 0^{-+}$, respectively, as shown in Table 5. In contrast to the pseudoscalar mesons π^0, η, η' which have comparatively small widths, the scalar counterparts $f_0(600), a_0(980)$ and $f_0(980)$ have open two-particle hadronic channels and, therefore, have large widths. For the pseudoscalar mesons the $|q\bar{q}\rangle$ structure in the $^1S_0$ spectroscopic state is the generally adopted description of the internal structure. For the scalar mesons the $^3P_0$ $|q\bar{q}\rangle$ content of the wave-function may be of minor importance, whereas the major part of the wave-function may be due to the two-meson configurations, also showing up in the decay-channel and the two-meson configurations with thresholds above the resonance energies.

An up-to-date description of the properties of scalar mesons is given by the Particle Data Group [24]. In connection with the interpretation of Compton scattering the $f_0(600)$ meson is the most relevant one in the scalar sector. We, therefore, restrict the following discussion to the $f_0(600)$ meson.

2.6.1 Historical introduction to the $f_0(600)$ or σ

The iso-singlet (isoscalar $I = 0$) scalar ($J = 0$) σ meson was introduced theoretically by Schwinger in 1957 [71] as a supplement of the π meson. The σ meson was predicted [71] to have strong interactions and, therefore, should immediately disintegrate into two π mesons thus making the experimental observation difficult. This difficulty was considered as the explanation for the fact that the σ meson had not been found in experiments. On the other hand the theoretical arguments were considered firm enough to be convinced that this particle should exist. Extending the arguments of Schwinger, Gell-Mann and Levi [72] developed the σ model in its linear and nonlinear versions.

Later, the existence of the σ meson was suggested in the one-boson-exchange potential model of nuclear forces [73], where it was introduced to supply the attraction between nucleons at intermediate distances. Fits of the NN partial-wave phase-shift led to a mass of $m_\sigma \approx 500 - 600$ MeV.

The σ meson was also introduced in relation [74] with the dynamical symmetry breaking of QCD based on the Nambu-Jona-Lasinio model, making a prediction for the σ mass of $m_\sigma \approx 600 - 700$ MeV.

In spite of the very strong demands on the side of the theory for the existence of the σ meson the experimental verification was considered uncertain for a long time, mainly based on negative results [75] of $\pi\pi$ scattering phase-shift analyses. This failure was explained later [76] to be a consequence of not considering the cancellation mechanism between the resonant (Breit-Wigner type) part of the σ meson $\pi\pi$ phase-shift δ_0^0 and a nonresonant (repulsive core type) $\pi\pi$ phase-shift, also contributing to δ_0^0. This will be discussed in more detail in Section 2.6.2.

In the 2002 edition, the PDG group [23] has given the σ meson the status of a particle, $f_0(600)$, with a mass assignment[5]. This mass assignment may be understood as a nominal value, the meaning of which will be explained in Sections 2.6.2. and 2.6.3. Of the large number of the experimental aspects of the σ meson we only discuss those which are of importance for our purposes.

2.6.2 The $f_0(600)$ or σ in the $\pi + N \to N\pi\pi$ reaction

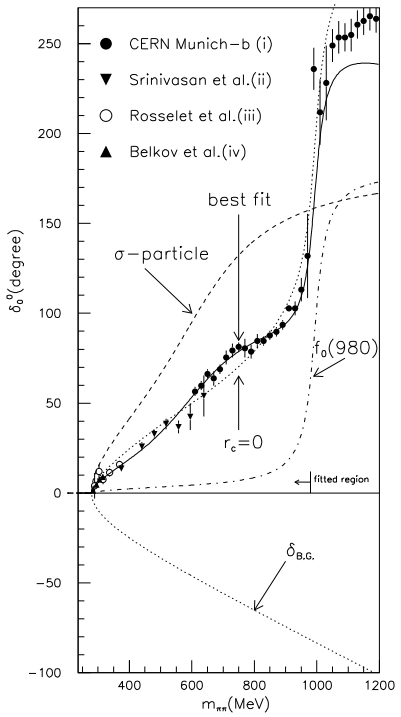

Figure 6: Fit to $I = 0$ S-wave $\pi\pi$ scattering phase-shift δ_0^0 according to Ishida [79]. The fit takes into account a hard-core (seagull type) component $\delta_{\rm BG}$ shown as a dotted curve in the lower part of the figure and a resonant (Breit-Wigner type) component shown in the upper part of the figure as a dashed curve labeled σ-particle

Of the more recent analyses [77] of the reaction $\pi + N \to N\pi\pi$ in terms of $\pi\pi$ scattering we want to inspect the ones given in [78] and [79] in more detail. In [78] the analysis of the $\pi\pi$ scattering amplitude is based on chiral perturbation theory starting from the observation that chiral symmetry determines the low energy behavior of the $\pi\pi$ scattering amplitude to within very small uncertainties. According to this analysis the σ meson $\pi\pi$ phase-shift δ_0^0 consists of a superposition of a resonant (pole) part and a nonresonant part stemming from a repulsive core. The destructive interference of the two parts leads to a 90° crossing of the scalar phase at (844 ± 13) MeV. This result is summarized in the second line of Table 6.

[5]In the foregoing editions only a mass range, *viz.* 400–1200 MeV, was given.

Table 6: Position of the $\sigma(600)$ pole, and 90° crossing of the scalar phase. Supplement a) is an estimate provided by the present author.

$\sqrt{s}(\text{pole})[MeV]$	$\sqrt{s}(\delta_S = 90°)$	reference
$(470 \pm 30) - i(295 \pm 20)$	844 ± 13 MeV	[78]
$(585 \pm 20) - i(193 \pm 35)$	∼900 MeV	[79]
PDG summary[a)]		*recommended*
$(500 \pm 40) - i(250 \pm 40)$		average [24]

a) supplemented by estimated errors.

In the second approach [79] the analysis of the phase-shift δ_0^0 of the $\pi\pi$ scattering amplitude is based on the Interfering Amplitude method, where the total phase-shift δ_0^0 below $m_{\pi\pi} \simeq 1$ GeV is represented by the sum of the component phase-shifts,

$$\delta_0^0 = \delta_\sigma + \delta_{\rm BG} + \delta_{f_0}. \tag{85}$$

This analysis is shown in Figure 6. The term δ_σ is from the attractive resonant (Breit-Wigner type) part of the $\pi\pi$ scattering amplitude of the σ meson and $\delta_{\rm BG}$ from the background non-resonant repulsive $\pi\pi$ amplitude which is taken phenomenologically to be of the hard-core type. The term δ_{f_0} is from the $f_0(980)$ Breit-Wigner amplitude with comparatively narrow width. This part has to be separately determined and eliminated by subtraction. The combined phase-shift $\delta_\sigma + \delta_{\rm BG}$ passes 90° at about ∼ 900 MeV as listed in the third line of Table 6.

2.6.3 The $f_0(600)$ or σ in the $\gamma + \gamma \to \pi^+\pi^-$ reaction

Figure 7 shows experimental data on the two-photon fusion reaction $\gamma + \gamma \to \pi^+ + \pi^-$ and their decomposition into components. At threshold the main part of the cross section is due to the Born term which may be viewed as the production of two uncorrelated point-like pions. The Born term is superimposed by a pion-structure dependent term which – at threshold – may be expressed through the polarizabilities of the pion. It should be noted that there is no clear indication of a bump-like structure at 600 MeV which could be attributed to a $f_0(600)$ particle. But there is a prominent bump at 1270 MeV corresponding to the tensor meson $f_2(1270)$. According to Tables 4 and 5 this tensor-meson may be related to the forward Compton scattering amplitude f_0 and its extension to larger angles. This will be discussed in Section 2.7.1.

2.6.4 The $f_0(600)$ or σ in the $\gamma\gamma \to \pi^0\pi^0$ reaction

Unknown parameters of the S-wave $\pi\pi$ interaction, represented as a broad Breit-Wigner resonance, have recently been determined [81] from fits to the experimental data [82] for the $\gamma\gamma \to \pi^0\pi^0$ process using dispersion relations. For the reaction $\gamma\gamma \to \pi^0\pi^0$ the Born term is equal to zero and the main contribution is determined by the S-wave of $\pi\pi$ interaction. For the fit to the experimental data there are five free parameters: the mass, the full width and the decay width of the σ meson into $\gamma\gamma$ and the sum and the difference of π^0 meson polarizabilities. The adopted set of parameters [83] obtained in this way are given in Table 7.

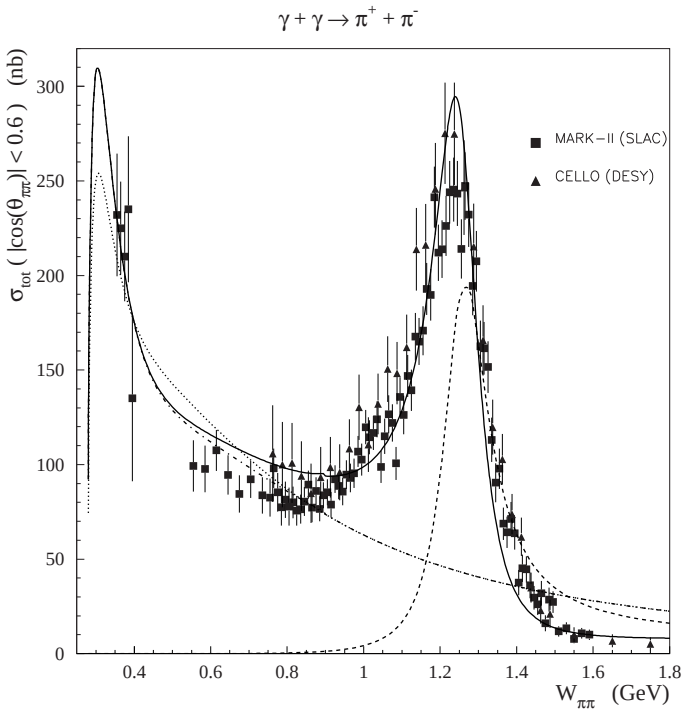

Figure 7: Total cross section for the $\gamma\gamma \to \pi^+\pi^-$ process as function of the c.m. energy and the analysis given by Drechsel et al. [80]: Born terms (dotted line), Born amplitude with unitarized s-wave (dashed-dotted line), $f_2(1270)$ resonance contribution (dashed line), and total cross section (full line).

Table 7: Parameters of the σ meson obtained from fits [81] to the experimental data [82] of the process $\gamma\gamma \to \pi^0\pi^0$

m_σ (MeV)	Γ_σ (MeV)	$\Gamma_{\sigma\to\gamma\gamma}$ (keV)	$(\alpha+\beta)_{\pi^0}$	$(\alpha-\beta)_{\pi^0}$
547± 45	1204 ± 362	0.62 ± 0.19	0.98±0.03	-1.6 ± 2.2

2.7 Regge phenomenology and Compton scattering

Regge phenomenology has been introduced in connection with hadronic reactions but is also widely used in connection with photo-absorption and Compton scattering. Though attempts have been made to replace Regge phenomenology by QCD, its apparent successes require a coverage of this topic in connection with the present review.

2.7.1 The $\rho - \omega$ and Pomeron trajectories

The left panel [84] of Figure 8 shows a) the Regge trajectories of the meson exchange reaction observed through

$$\pi^- + p \to \pi^0 + n, \tag{86}$$

and b) the Regge trajectory for an elastic scattering reaction, observed through

$$p + p \to p + p. \tag{87}$$

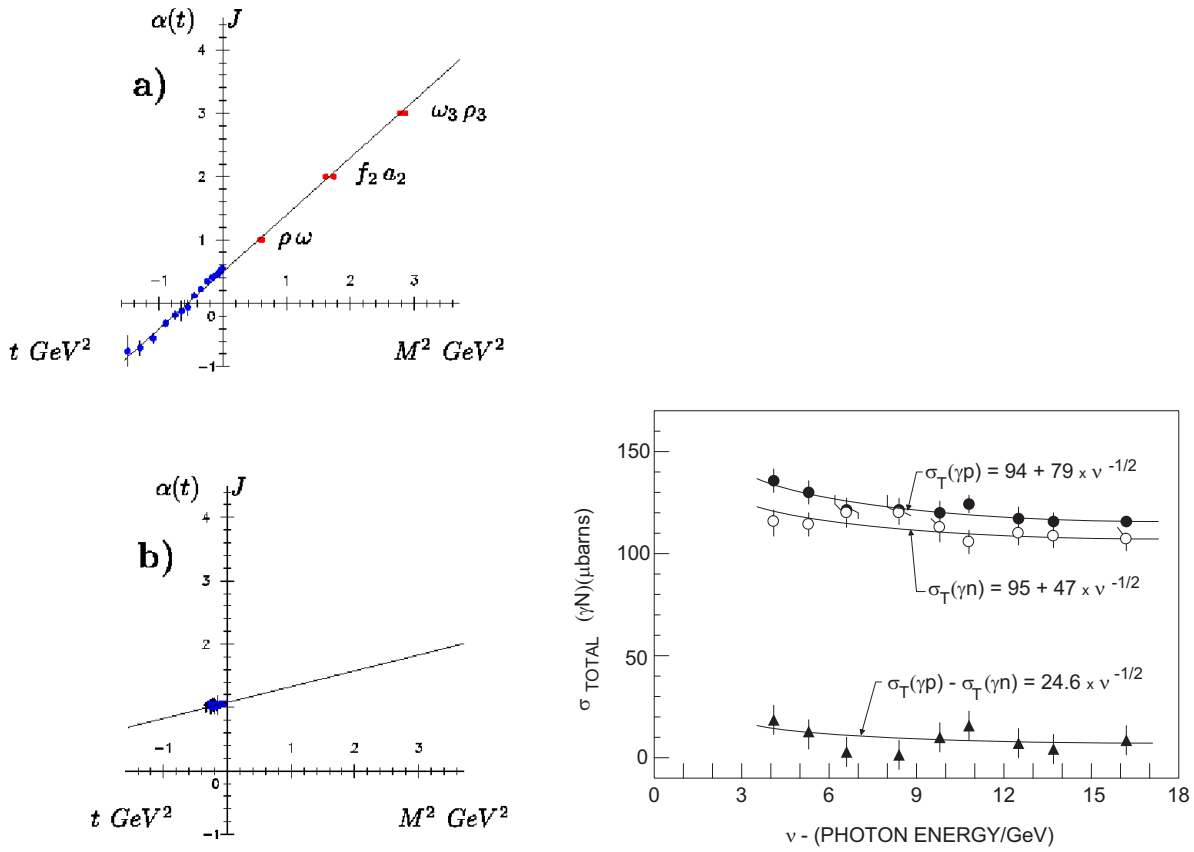

Figure 8: Left panel: Regge trajectory for the charge exchange a) and elastic scattering b) reaction [84]. Right panel: Comparison of the proton, neutron, and proton-neutron difference data of photo-absorption cross sections with ν-fits as given in [86].

Regge phenomenology says, that the differential cross-sections of these reactions are given by the function

$$\frac{d\sigma}{dt} \sim s^{2\alpha(t)-2}, \tag{88}$$

where s and t are the total energy and momentum transfer squared, respectively. The experimental data obtained for the meson-exchange reaction at negative t can be parameterized by a linear trajectory

$$\alpha(t) = \alpha(0) + \alpha' t. \tag{89}$$

The extrapolation of the trajectory to positive values $t \equiv M^2$ goes through the ρ point and through other resonances which belong to this trajectory including the $f_2(1270)$ and the $a_2(1320)$. The trajectory for the meson-exchange reaction may be represented by

$$\alpha_\rho(t) = 0.56 + 0.97\text{GeV}^{-2} t. \tag{90}$$

The trajectory for the elastic reaction has parameters which differ from those of the ρ-trajectory, namely an intercept $\alpha_{I\!P}(0) \approx 1.1$ and a slope $\alpha'_{I\!P} \approx 0.25\text{GeV}^{-2}$. This trajectory is called Pomeron trajectory and the object exchanged in the elastic reaction (87) is called Pomeron. It carries vacuum quantum numbers ($P = C = +1$) and is thought to be a composite system of gluons.

For diffractive processes where the scattering amplitude only has an imaginary part the optical theorem provides us with a total cross section in the form [85]

$$\sigma^{\text{tot}} \sim s^{\alpha(0)-1}. \tag{91}$$

The validity of this relation for the photo-absorption cross section has already shown in the 1970's where the total photo-absorption cross sections for the proton and the neutron in the 3 – 16 GeV range could be represented in the form [86]

$$\sigma^{\rm tot} = X + Y\nu^{-1/2}. \tag{92}$$

In (92) the variable s has been replaced by ν for convenience. The constant term corresponds to the Pomeron exchange where the approximation $\alpha_P(0) = 1$ has been used, whereas the $\nu^{-1/2}$ dependent term corresponds to $f_2(1270)$ and $a_2(1320)$ exchanges where the approximation $\alpha_\rho(0) = 0.5$ has been used. The decrease of the cross section with photon energy due to the second term in (92) and the isovector component due to $a_2(1320)$ exchange are clearly seen in the right panel of Figure 8.

The conclusion we can draw from this finding is that in the forward direction the $f_2(1270)$ and $a_2(1320)$ meson exchanges are part of the photo-absorption cross section. The reason for this is that these mesons interact with the photons via intermediate vector mesons thus making photo-absorption and Compton scattering effectively hadronic reactions. These hadronic reactions take place at the periphery of the nucleon and consequently can be observed in small-angle Compton scattering only. For larger Compton scattering angles the $f_2(1270)$ and the $a_2(1320)$ mesons undergo a direct coupling to the two photons and, therefore, have to be treated as genuine t-channel exchanges. This point will be discussed in Section 6.1 in more detail in connection with the validity of the Baldin sum rule.

2.7.2 The $f_1 - a_1$ trajectories

According to Table 4 the t-channel exchanges contributing to the spin independent amplitude f_0 are of natural parity whereas the t-channel exchanges contributing to the spin dependent amplitude g_0 are of unnatural parity. We, therefore, expect that the f_1 – a_1 trajectory is the relevant one for the spin-dependent amplitude g_0, where the meson $a_1(1260)$ has the quantum numbers $I^G(J^{PC}) = 1^-(1^{++})$ and the meson $f_1(1285)$ the quantum numbers $I^G(J^{PC}) = 0^+(1^{++})$. The first meson on the trajectory which is capable of coupling to two photons has the quantum number $J^{PC} = 3^{++}$. Such a meson is not known up to the present.

The f_1 and a_1 exchanges have been discussed [87] in connection with a parameterization of the cross section difference $\Delta\sigma = \sigma_{1/2} - \sigma_{3/2}$ investigated with virtual photons, leading to a nonresonant contribution to the GDH sum rule when extrapolated to the photon point ($Q^2 \to 0$). The isovector contribution to $\Delta\sigma$ is described by the $a_1(1260)$ meson trajectory, $\Delta\sigma_V \sim s^{\alpha^0_{a_1}-1}$, the isoscalar contribution to $\Delta\sigma$ by the $f_1(1285)$ meson trajectory, $\Delta\sigma_I \sim s^{\alpha^0_{f_1}-1}$. The trajectory slope is $\alpha' \simeq 0.8 - 0.9$ GeV^{-2} and the intercepts are $\alpha^0_{a_1} \approx -0.3$ and $\alpha^0_{f_1} = -0.4 \pm 0.1$, respectively. The intercept $\alpha^0_{a_1}$ shows a rather strong model dependence whereas the intercept $\alpha^0_{f_1}$ turns out to be more stable.

3 Scattering Amplitudes and Dispersion Relations

In the following we discuss the theoretical tools for the description of Compton scattering and the determination of polarizabilities. Two versions of dispersion theories are presented, the nonsubtracted fixed-t and fixed-θ dispersion theories. When applied appropriately, these versions are capable of providing predictions in the first and second resonance range of the nucleon, whereas the subtracted fixed-t dispersion theory has only been successful in the lower part of the Δ range [1, 80]. Though fixed-θ dispersion theory has the advantage of guaranteeing that the use of s- and t-channel contributions does not lead to problems like double counting of empirical input, it runs into technical difficulties [1]

when applied at small scattering angles. On the other hand fixed-t dispersion theory is constructed in formal analogy to forward-direction dispersion theory, where the s-channel contribution is replaced by the largely equivalent integral part [68] and the t-channel contribution by a contour integral, which already was discussed in Section 2.2 in connection with forward-direction dispersion theory. For the interpretation of the contour integral arguments were developed stemming from Regge theory [4, 17]. In this work we use arguments from Regge theory only in connection with forward-direction t-channel exchanges as discussed in Section 2.7.

3.1 S-matrix and invariant amplitudes

The amplitude T_{fi} for Compton scattering

$$\gamma(k)N(p) \to \gamma'(k')N(p') \tag{93}$$

is related to the S-matrix of the reaction through the relation

$$\langle f|S-1|i\rangle = i(2\pi)^4\delta^4(k+p-k'-p')T_{fi}. \tag{94}$$

The quantities $k=(\omega,\mathbf{k})$, $k'=(\omega',\mathbf{k}')$, $p=(E,\mathbf{p})$, $p'=(E',\mathbf{p}')$ are the four momenta of the photon and the nucleon in the initial and final states, respectively, related to the Mandelstam variables via (see also Section 2.4)

$$s=(k+p)^2, \quad t=(k-k')^2, \quad u=(k-p')^2. \tag{95}$$

The scattering amplitude T_{fi} may be expressed on an orthogonal basis suggested by Prange [88] by means of six invariant amplitudes $T_k(\nu,t)$ leading to the general form [68]

$$\begin{aligned} T_{fi} \;&= \bar{u'}e'^{*\mu}\Big[-\tfrac{P'_\mu P'_\nu}{P'^2}(T_1+(\gamma\cdot K)T_2)-\tfrac{N_\mu N_\nu}{N^2}(T_3+(\gamma\cdot K)T_4) \\ &\quad +i\tfrac{P'_\mu N_\nu - P'_\nu N_\mu}{P'^2K^2}\gamma_5 T_5 + i\tfrac{P'_\mu N_\nu + P'_\nu N_\mu}{P'^2K^2}\gamma_5(\gamma\cdot K)T_6\Big]e^\nu u. \end{aligned} \tag{96}$$

In (96) u' and u are the Dirac spinors of the final and the initial nucleon, e' and e are the polarization 4-vectors of the final and the initial photon, and $\gamma_5=-i\gamma_0\gamma_1\gamma_2\gamma_3$. The 4-vectors P', K and N together with the vector Q are orthogonal and are expressed in terms of the 4-momenta p', k' and p, k of the final and initial nucleon and photon, respectively, by

$$\begin{aligned} &K=\frac{1}{2}(k+k'), \quad P'=P-\frac{K(P\cdot K)}{K^2}, \quad N_\mu=\epsilon_{\mu\nu\lambda\sigma}P'^\nu Q^\lambda K^\sigma, \\ &P=\frac{1}{2}(p+p'), \quad Q=\frac{1}{2}(k'-k)=\frac{1}{2}(p-p') \end{aligned} \tag{97}$$

where $\epsilon_{\mu\nu\lambda\sigma}$ is the antisymmetric tensor with $\epsilon_{0123}=1$. The amplitudes T_k are functions of the two variables ν and t and M is the mass of the nucleon. The normalization of the amplitude T_{fi} is determined by

$$\bar{u}u=2M, \quad \frac{d\sigma}{d\Omega}=\frac{1}{64\pi^2 s}\sum_{\text{spins}}|T_{fi}|^2. \tag{98}$$

It follows from crossing symmetry of T_{fi}, that $T_{1,3,5,6}$ and $T_{2,4}$ are even and odd functions of ν, respectively.

The amplitudes $T_k(\nu,t)$ do not have kinematic singularities, but there are kinematic constraints, which arise from the vanishing of P'^2, N^2 and P'^2K^2 in the denominators of the decomposition (96) at

certain values of ν and t. The kinematic constraints can be removed by introducing linear combinations of the amplitudes $T_k(\nu,t)$. This problem has first been satisfactorily solved by Bardeen and Tung [89]. However, the Bardeen and Tung amplitudes contain the inconvenience that part of them are even functions of ν and part of them odd functions. This inconvenience has been removed by L'vov [90] so that these latter amplitudes now have become standard.

The linear combinations introduced by L'vov [90] are

$$\begin{aligned}
A_1 &= \frac{1}{t}[T_1 + T_3 + \nu(T_2 + T_4)],\\
A_2 &= \frac{1}{t}[2T_5 + \nu(T_2 + T_4)],\\
A_3 &= \frac{M^2}{M^4 - su}\left[T_1 - T_3 - \frac{t}{4\nu}(T_2 - T_4)\right],\\
A_4 &= \frac{M^2}{M^4 - su}\left[2MT_6 - \frac{t}{4\nu}(T_2 - T_4)\right],\\
A_5 &= \frac{1}{4\nu}[T_2 + T_4],\\
A_6 &= \frac{1}{4\nu}[T_2 - T_4].
\end{aligned} \tag{99}$$

The amplitudes $A_i(\nu,t)$ are even functions of ν and have no kinematic singularities or kinematic constraints. They have poles at zero energy because of contributions of the nucleon in the intermediate state. These poles are contained in two Born diagrams with the pole propagator $(\gamma\cdot p - M)^{-1}$ and on-shell vertices $\Gamma_\mu(p+k,p) = \gamma_\mu + [\gamma\cdot k, \gamma_\mu]\kappa/4M$, where $\kappa = 1.793q - 1.913(1-q)$ is the nucleon anomalous magnetic moment. Here the electric charge of the nucleon, $q = \frac{1}{2}(1+\tau_3) = 1$ or 0 is introduced. The Born contributions to the amplitudes A_i have a pure pole form

$$A_i^{\rm B}(\nu,t) = \frac{Me^2 r_i(t)}{(s-M^2)(u-M^2)}, \tag{100}$$

where e is the elementary electric charge ($e^2/4\pi = 1/137.04$) and

$$\begin{aligned}
&r_1 = -2q + (\kappa^2 + 2q\kappa)\frac{t}{4M^2}, \quad r_2 = 2q\kappa + 2q + (\kappa^2 + 2q\kappa)\frac{t}{4M^2},\\
&r_3 = r_5 = \kappa^2 + 2q\kappa, \quad r_4 = \kappa^2, \quad r_6 = -\kappa^2 - 2q\kappa - 2q^2.
\end{aligned} \tag{101}$$

3.2 Lorentz invariant definition of polarizabilities

The relations between the amplitudes f and g introduced in Section 2.1 and the invariant amplitudes A_i [54, 68] are

$$f_0(\omega) = -\frac{\omega^2}{2\pi}\left[A_3(\nu,t) + A_6(\nu,t)\right], \qquad g_0(\omega) = \frac{\omega^3}{2\pi M}A_4(\nu,t), \tag{102}$$

$$f_\pi(\omega) = -\frac{\omega\omega'}{2\pi}\left(1 + \frac{\omega\omega'}{M^2}\right)^{1/2}\left[A_1(\nu,t) - \frac{t}{4M^2}A_5(\nu,t)\right], \tag{103}$$

$$g_\pi(\omega) = -\frac{\omega\omega'}{2\pi M}\sqrt{\omega\omega'}\left[A_2(\nu,t) + \left(1 - \frac{t}{4M^2}\right)A_5(\nu,t)\right], \tag{104}$$

$$\omega'(\theta=\pi) = \frac{\omega}{1 + 2\frac{\omega}{M}},\ \nu = \frac{1}{2}(\omega+\omega'),\ t(\theta=0) = 0,\ t(\theta=\pi) = -4\omega\omega.' \tag{105}$$

For the electric, α, and magnetic, β, polarizabilities and the spin polarizabilities γ_0 and γ_π for the forward and backward directions, respectively, we obtain the relations

$$\alpha+\beta=-\frac{1}{2\pi}\left[A_3^{\rm nB}(0,0)+A_6^{\rm nB}(0,0)\right], \quad \alpha-\beta=-\frac{1}{2\pi}\left[A_1^{\rm nB}(0,0)\right],$$
$$\gamma_0=\frac{1}{2\pi M}\left[A_4^{\rm nB}(0,0)\right], \qquad \gamma_\pi=-\frac{1}{2\pi M}\left[A_2^{\rm nB}(0,0)+A_5^{\rm nB}(0,0)\right], \tag{106}$$

where $A_i^{\rm nB}$ are the non-Born parts of the invariant amplitudes.

According to Eqs. (102) to (106) the following linear combinations of invariant amplitudes are of special importance because they contain the physics of the four fundamental sum rules, *viz.* the BEFT, LN, BL and GDH sum rules, respectively:

$$\tilde{A}_1(\nu,t)\equiv A_1(\nu,t)-\frac{t}{4M^2}A_5(\nu,t), \tag{107}$$
$$\tilde{A}_2(\nu,t)\equiv A_2(\nu,t)+\left(1-\frac{t}{4M^2}\right)A_5(\nu,t), \tag{108}$$
$$\tilde{A}_3(\nu,t)\equiv A_{3+6}(\nu,t)\equiv A_3(\nu,t)+A_6(\nu,t), \tag{109}$$
$$\tilde{A}_4(\nu,t)\equiv A_4(\nu,t). \tag{110}$$

3.3 Properties of the s- and t-channel

For the general discussion of dispersion theories we shall consider the invariant amplitudes $A_i(s,t,\tilde{u})$ as functions of two *complex variables* (s and t) and establish their analytical properties in the "topological product" of the s- and t-planes [57]. For sake of completeness and for further applications we introduce the further variable u which is constrained by the two others, what frequently is denoted by the tilde [58], *i.e.*, in the present case $\tilde{u}$.

The amplitudes $A_i(s,t,\tilde{u})$ are chosen such that they do not have kinematical singularities or constraints. But there are *physical* singularities which are the basis for constructing the amplitudes. In the s-plane there are singularities on the real axis, a pole at $s=u=M^2$ and two cuts, representing the s- and the u-channel. This is illustrated in Figure 9. The pole at $s=u=M^2$ represents the Born term, i.e. Thomson scattering without excitation of internal degrees of freedom of the nucleon. The main singularities in the t-plane are poles on the positive real t axis corresponding to the pseudoscalar mesons π^0, η and η', and a cut starting $t=4m_\pi^2$. This cut consists of a $\pi\pi$ channel with a $\pi\pi$ phase-substructure which may be interpreted in terms of the scalar isoscalar $f_0(600)$ or σ particle (see Section 2.6.2). The singularities in the two planes are taken into account by imaginary parts of the amplitudes, i.e. $\mathrm{Im}_s A_i(s,t,\tilde{u})$ for the s-plane and $\mathrm{Im}_t A(s,t,\tilde{u})$ for the t-plane.

3.4 Properties of the Mandelstam plane

For illustration it is useful to merge the complex s and t planes into one plane by choosing the real axes as abscissa and ordinate. Furthermore, we may replace s by ν. This leads to the Mandelstam plane shown in Figure 10.

First we want to identify the region in the Mandelstam plane where Compton scattering may take place and will name that region the s-channel *physical region*. There are also physical regions for the u and t channel as shown in Figure 10. From a mathematical point of view the physical regions are of minor

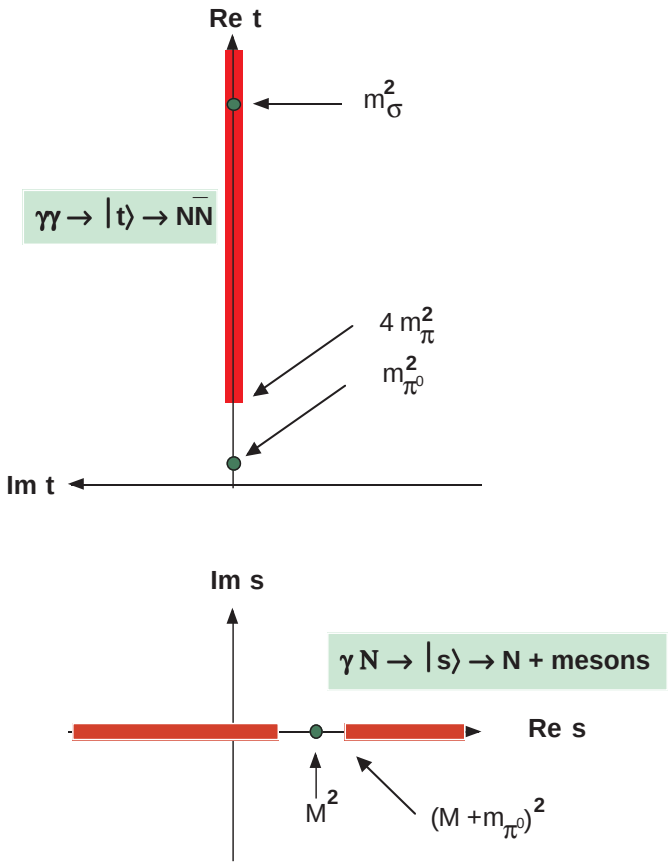

Figure 9: Singularities in the s and t planes. The s-plane contains the nucleon pole at $s = M^2$ and a right hand cut corresponding to the s-channel and a left-hand cut corresponding to the u-channel. The t-channel contains a pole at $t = m_{\pi_0}^2$ and a cut starting at $t_{\rm thr} = 4m_\pi^2$. In the range of the t-channel cut there are further poles at $t = m_\eta^2$ and $t = m_{\eta'}^2$. Furthermore, there is a pole-like phase substructure defining a "mass" at $t = m_\sigma^2$.

importance because the scattering amplitudes in principle are defined in the whole *topological product* of the complex s and t planes. As stated before, the appropriate tools for the analytical continuations are the generalized angles θ_s and θ_t given in Eqs. (73) and (83).

The boundary of the s-channel physical region (Figure 9) is defined through the threshold $s_0 = (M + m_\pi)^2$ for photo-absorption. In the Mandelstam plane (Figure 10) this physical region is given by the interval between $\theta = 0$ and $\theta = \pi$ of the *physical* scattering angle. The boundary $\theta = 0$ is equivalent with $t = 0$. The boundary corresponding to $\theta = \pi$ may be obtained through the following consideration. Let $s_\pi(t)$, $u_\pi(t)$ and $\nu_\pi(t)$ be the Mandelstam variables corresponding to $\theta = \pi$. Then with

$$\begin{aligned} &s_\pi(t)u_\pi(t) = M^4, \\ &s_\pi(t) + t + u_\pi(t) = 2M^2, \\ &\nu_\pi(t) = \left(s_\pi(t) - u_\pi(t)\right)/(4M), \end{aligned} \tag{111}$$

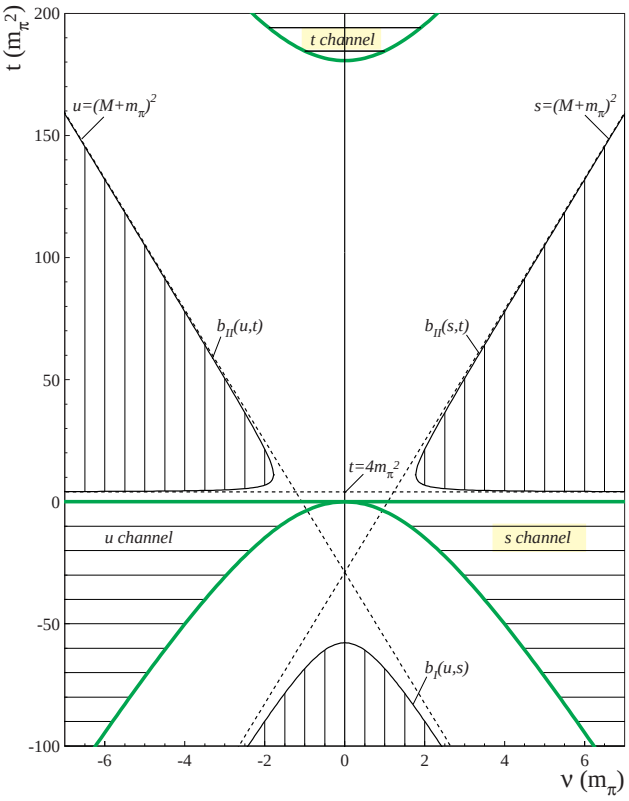

Figure 10: The Mandelstam plane for Compton scattering according to [1]. The physical regions are horizontally hatched. The spectral regions (with boundaries b_I and b_{II}) are vertically hatched.

we arrive at

$$s_\pi(t) = \frac{1}{2}\left(2M^2 - t + \sqrt{t(t-4M^2)}\right), \tag{112}$$

$$u_\pi(t) = \frac{1}{2}\left(2M^2 - t - \sqrt{t(t-4M^2)}\right), \tag{113}$$

$$\nu_\pi(t) = \frac{1}{4M}\sqrt{t(t-4M^2)}. \tag{114}$$

In Eqs. (112) to (114) the signs in front of the square roots have been chosen such that $\nu_\pi(t)$ is positive for negative t. In the Mandelstam plane of Figure 10, Eq. (114) describes the lower borderline of the physical region of the s-channel for positive ν and the lower borderline of the u-channel for negative ν if $t \leq 0$. For $t \geq 4M^2$ Eq. (114) describes the lower borderline of the physical region of the t-channel. The t-channel singularities of interest in connection with Compton scattering are positioned at $t = m_{\pi^0}^2$ and at $4M^2 \geq t \geq 4m_\pi^2$ i.e. outside the physical region of the t-channel for the reaction $\gamma\gamma \to N\bar{N}$. For the t-channel this means that the two photon fusion process $\gamma\gamma \to \pi\pi$ leading to the $|\pi\pi\rangle$ intermediate state or some other resonant or nonresonant intermediate state $|t\rangle$, takes place as a real (on-shell) process whereas the subsequent process $\pi\pi \to N\bar{N}$ takes place virtually, i.e. below threshold for $N\bar{N}$ pair production. This corresponds to low-energy Compton scattering processes proceeding through $|\pi^0\rangle$, $|\pi\pi\rangle$, etc. t-channel exchanges in the intermediate state with no excitation of the constituent-quark-meson structure of the nucleon.

In Figure 10 the vertically hatched areas are the regions of nonvanishing double spectral functions [1, 58, 80]. These spectral regions are those regions in the Mandelstam plane where two of the three variables s, t and u take on values that correspond with a physical (i.e., on-shell) intermediate state.

The boundaries of these regions follow from unitarity. The double spectral functions are of importance in connection with the foundation of dispersion theories [58]. No use is made of them in the following discussion of fixed-θ and fixed-t dispersion theories.

3.5 Discussion of Compton scattering in the complex s-plane

The $\theta = \pi$ constraint given in the first line of Eq. (111) may be generalized for other angles using the $s - u$ crossing symmetric hyperbolic integration paths [1, 58]

$$(s - a)(u - a) = b, \quad b = (a - M^2)^2, \tag{115}$$

where a is in one-to-one correspondence with the lab and c.m. scattering angles as:

$$a = -M^2 \frac{1 + \cos\theta_{\rm lab}}{1 - \cos\theta_{\rm lab}}, \qquad a = -s \frac{1 + \cos\theta_s}{1 - \cos\theta_s}, \tag{116}$$

where $\theta_{\rm lab}$ is the scattering angle in the laboratory system and θ_s the c.m. scattering angle in the s-channel. Eqs. (115) and (116) contain the main ingredients of the kinematics of fixed-θ dispersion theory.

The equations given above allow to project the t-channel singularities into the complex s-plane as first discussed by Hearn and Leader in 1962 [49] and later worked out in more detail by Köberle in 1968 [50]. The results of these considerations are very important because they prove that in fixed-θ

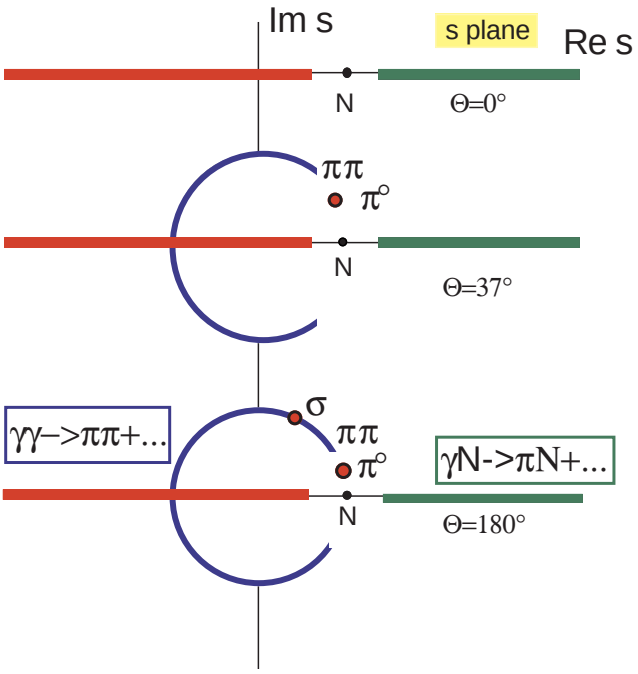

Figure 11: Singularities of Compton scattering amplitudes depicted in the complex s-plane according to Hearn and Leader [49]. The right thick line on the real axis corresponds to the s-channel, the circular line and π^0-pole to the "unphysical" part of the t-channel and the left thick line on the horizontal axis partly to the u-channel and partly to the "physical" part of the t-channel. For $\theta = 180°$ the lower limit of the u-channel cut is at $s = 0$.

dispersion theory double counting of physical input as coming from the s-channel and the t-channel is

avoided. Figure 11 reproduces the result obtained in [49], where the singularities contributing to the imaginary parts of the Compton scattering amplitudes are depicted for three scattering angles. The s-channel is represented by the right-hand cut on the real s-axis. The circular part contains the π^0 pole, the $\pi\pi$ cut and the other structures located in the unphysical region of the t-channel, i.e. below the $N\bar{N}$ threshold (see Figure 9). The left-hand cut on the real s-axis is shared by the u-channel and the physical part of the t-channel, i.e. the range above the $N\bar{N}$ threshold. It is of interest that the circular part corresponding to the "unphysical" part of the t-channel does only contribute when the scattering angle is nonzero and is most pronounced for $\theta = 180°$.

3.6 Fixed-θ dispersion relations

Along a path at fixed a defined in (115) and (116), one can write down [1, 58] a dispersion integral as

$$\begin{aligned} \mathrm{Re}A_i(s,t,a) &= A_i^{\mathrm{B}}(s,t,a) + A_i^{t-\mathrm{pole}}(s,t,a) \\ &+ \frac{1}{\pi}\int_{(M+m_\pi)^2}^{\infty} ds' \mathrm{Im}_s A_i(s',\tilde{t},a)\left[\frac{1}{s'-s}+\frac{1}{s'-u}-\frac{1}{s'-a}\right] \\ &+ \frac{1}{\pi}\int_{4m_\pi^2}^{\infty} dt' \frac{\mathrm{Im}_t A_i(\tilde{s},t',a)}{t'-t}, \end{aligned} \tag{117}$$

where $\mathrm{Im}_s A(s',\tilde{t},a)$ is evaluated along the hyperbola given by

$$(s'-a)(u'-a) = b, \quad s'+\tilde{t}+u' = 2M^2, \tag{118}$$

and $\mathrm{Im}_t A_i(\tilde{s},t',a)$ runs along the path defined by the hyperbola

$$(\tilde{s}-a)(\tilde{u}-a) = b, \quad \tilde{s}+t'+\tilde{u} = 2M^2. \tag{119}$$

The amplitude $A_i^{t-\mathrm{pole}}(s,t,a)$ entering into (117) describes the contribution of pseudoscalar mesons to the scattering amplitude and may be written in the form

$$A_2^{\pi^0+\eta+\eta'}(t) = \frac{g_{\pi^0 NN} F_{\pi^0\gamma\gamma}}{t-m_{\pi^0}^2}\tau_3 + \frac{g_{\eta NN} F_{\eta\gamma\gamma}}{t-m_\eta^2} + \frac{g_{\eta' NN} F_{\eta'\gamma\gamma}}{t-m_{\eta'}^2}, \tag{120}$$

where the quantities $g_{\pi^0 NN}$, etc. are the meson-nucleon coupling constants and the quantities $F_{\pi^0\gamma\gamma}$, etc. the two-photon decay amplitudes. The last term in (117) represents the contribution of the scalar t-channel to the scattering amplitude. The integration in the upper half plane (for $t > 0$) runs through the unphysical region $4m_\pi^2 \le t < 4M^2$. In the latter region the t-channel partial wave expansion of $\mathrm{Im}_t A_i$ converges if $101° \le \theta_{\mathrm{lab}} \le 180°$ [1]. This statement shows that fixed-θ dispersion theory cannot be applied at all angles with equally good precision. At $\theta = 180°$ the application is rather straightforward so that backward-angle sum rules can be based on this approach. This will be discussed in Section 6.

3.7 Fixed-t dispersion relations

The natural extension of forward-angle dispersion theory to larger angles is given by fixed-t dispersion theory. Fixed-t dispersion theory has been proven to be successful in a wide range of Compton scattering angles and for energies up to about 1 GeV with high precision (see Section 5). A formal drawback, however, is that in fixed-t dispersion theory a strict separation of the s- and t-channel contributions is not possible but we may assume an approximate separation. In order to distinguish between the strict

separation in case of fixed-θ dispersion theory and the approximate separation in case of fixed-t dispersion theory we use the term "integral" amplitude instead of "s"-channel amplitude and "asymptotic" amplitude instead of "t-channel" amplitude.

The ansatz for a fixed-t dispersion relation may be given in the following form [58]:

$$\begin{aligned} \mathrm{Re}A_i(s,t,\tilde{u}) = A_i^B(s,t,\tilde{u}) &+ \frac{1}{\pi}\mathcal{P}\int_{s_0}^{s_{\max}(t)} \left(\frac{1}{s'-s}+\frac{1}{s'-\tilde{u}}\right) \times \mathrm{Im}_s A_i(s',t,\tilde{u})ds' \\ &+ \frac{1}{\pi}\mathcal{P}\int_{s_{\max}(t)}^{\infty} \left(\frac{1}{s'-s}+\frac{1}{s'-\tilde{u}}\right) \times \mathrm{Im}_s A_i(s',t,\tilde{u})ds' \\ &+ A_i^{t-\mathrm{pole}}(t) + A_i^{\mathrm{scalar}}(t) \end{aligned} \tag{121}$$

with the constraint

$$s' + \tilde{u} + t = 2M^2 \tag{122}$$

where use has been made of the crossing symmetry [58]

$$\mathrm{Im}_s A_i(s,t,u) = \mathrm{Im}_u A_i(u,t,s). \tag{123}$$

The terms in the first two lines in Eq. (121) represent the standard fixed-t dispersion relation [58]. The s-channel integral has been split up into one integral extending from s_0 to $s_{\max}(t)$ and an other extending from $s_{\max}(t)$ to ∞. This precaution has been taken in order to avoid the use of divergent s-channel integrals. The quantity $s_{\max}(t)$ in (121) has been proposed [68] to correspond to the excitation energy $E_{\max} = (s_{\max}(t) - M^2)/2M = 1.5$ GeV. The fourth term $A_i^{t-\mathrm{pole}}(t)$ is the analogue of the corresponding term in (117). The term $A_i^{\mathrm{scalar}}(t)$ replaces the t-channel integral in (117). It is interesting to mention that $A_i^{\mathrm{scalar}}(t)$ cannot be expressed through a t-channel integral in a strict sense, as in case of the fixed-θ dispersion theory. The reason for this is that in case of fixed-t dispersion theory parts of the t-channel strength is already contained in the integral amplitude. This is especially true for contributions which – in a diagrammatic representation – have a t-channel cut as well as a s-channel cut [91]. However, there are reasons to assume that the term A_i^{scalar} in (121) and the t-channel integral in (117) are approximately equivalent.

For the present case of a fixed-t dispersion relation it is useful to work with the variable $\nu = (s-u)/(4M)$, because the crossing operation $s \leftrightarrow u$ at fixed t is then simply a reflection $\nu \leftrightarrow -\nu$. In terms of the variable ν, the first term of the s-channel part of the fixed-t dispersion relation reads

$$\mathrm{Re}A_i^{\mathrm{NB}}(\nu,t) = \frac{1}{\pi}\mathcal{P}\int_{\nu_{\mathrm{thr}}(t)}^{\nu_{\max}(t)} d\nu' \mathrm{Im}A_i(\nu',t)\left[\frac{1}{\nu'-\nu}+\frac{1}{\nu'+\nu}\right] \tag{124}$$

$$= \frac{2}{\pi}\mathcal{P}\int_{\nu_{\mathrm{thr}}(t)}^{\nu_{\max}(t)} d\nu' \frac{\nu' \mathrm{Im}A_i(\nu',t)}{\nu'^2-\nu^2}. \tag{125}$$

where NB denotes non-Born. The integral given in Eq. (125) starts at the threshold

$$\nu_{\mathrm{thr}}(t) = \nu\left(s=(M+m_\pi)^2,t\right) = m_\pi + \frac{1}{2M}\left(m_\pi^2+\frac{t}{2}\right). \tag{126}$$

This function is shown in Figure 10 as a dotted line labeled $s = (M+m_\pi)^2$. It is easy to see that the threshold of the integral (125) is located in the physical region of the s-channel only for very small negative t. Outside the physical region $\nu_{\mathrm{thr}}(t)$ remains positive up to $t = -28.8\ m_\pi^2$ and then becomes negative. This unwanted property will be discussed in connection with the evaluation of the fixed-t dispersion integrals (see Section 4.5).

The second integral and the two terms in the last line of in (121) are dependent on t but not on s. Therefore, they can be added for each amplitude A_i to give one term which traditionally is termed the "asymptotic" contribution $A_i^{\rm as}(\nu,t)$ where we keep the ν dependence for sake of completeness. In a formal way this "asymptotic" contribution can be incorporated into the fixed-t dispersion theory formulated in a complex ν plane, by using a loop of finite size (a closed semicircle of radius $\nu_{\rm max}$) to close the Cauchy integral. This leads to the representation [68]:

$$ {\rm Re}A_i(\nu,t) = A_i^B(\nu,t) + A_i^{\rm int}(\nu,t) + A_i^{\rm as}(\nu,t), \tag{127} $$

with

$$ A_i^{\rm B}(\nu,t) = \frac{a_i(t)}{\nu^2 - t^2/16M^2} \ , \tag{128} $$

$$ A^{\rm int}(\nu,t) = \frac{2}{\pi}\mathcal{P}\int_{\nu_{\rm thr(t)}}^{\nu_{\rm max}(t)} {\rm Im}A_i(\nu',t)\frac{\nu' d\nu'}{\nu'^2 - \nu^2} \ , \tag{129} $$

$$ A_i^{\rm as}(\nu,t) = \frac{1}{\pi}{\rm Im}\int_{\nu'=\nu_{\rm max}(t)e^{i\phi},0<\phi<\pi} A_i(\nu',t)\frac{\nu' d\nu'}{\nu'^2 - \nu^2} \ . \tag{130} $$

Without loss of generality we may use $\nu_{\rm max}(t) \to \infty$, and this will be done in the following unless something else is stated.

In the foregoing, the non-Born (NB) amplitude has been partitioned into an integral part along the real axis of the complex ν plane and a contour integral in the upper half-plane. This partitioning is a formal procedure in the sense that only the integral part can be calculated, using the formula given in (129). The asymptotic (contour integral) part requires special considerations. The usual way to take it into account is to use the ansatz of a phenomenological effective σ-pole for the amplitude $A_1^{\rm as}(\nu,t)$ and poles due to pseudoscalar mesons for the amplitude $A_2^{\rm as}(\nu,t)$ as given in Eq. (120):

$$ A_1^{\rm as}(\nu,t) = A_1^{\sigma}(t) = \frac{g_{\sigma NN}F\sigma\gamma\gamma}{t - m_\sigma^2}, \quad A_2^{\rm as}(\nu,t) \equiv A_2^{\pi^0+\eta+\eta'}(t). \tag{131} $$

Experimental tests of this ansatz are described in Sections 5 and 6.

3.8 Propagator of the σ meson

For the practical application of the σ pole ansatz in the data analysis we assume that the σ meson has a composite structure with a $|q\bar{q}\rangle$ core and a $|\pi\pi\rangle$ cloud. Due to the coupling to the $\pi\pi$ hadronic exit channel the σ has a large width which modifies the structure of the corresponding pole term. This modification can be calculated by standard techniques [92] leading to the result that the mass m_σ has to be replaced by an effective mass $m_{\rm eff} = (m_\sigma^2 + \mathcal{P}(t))^{1/2}$. The width of the σ meson is taken into account via a $\pi\pi$ loop as depicted in Figure 12, leading to

$$ \frac{F_{\sigma\gamma\gamma}g_{\sigma NN}}{t - m_\sigma^2} \longrightarrow \frac{F_{\sigma\gamma\gamma}g_{\sigma NN}}{t - m_\sigma^2 - \mathcal{P}(t)} \tag{132} $$

with

$$ \mathcal{P}(t) = \frac{m_\sigma\Gamma_\sigma}{\pi\sqrt{1 - 4m_\pi^2/m_\sigma^2}}\left[-2 + \sqrt{\frac{1+y}{y}}\ln\left(\frac{\sqrt{\frac{1+y}{y}}+1}{\sqrt{\frac{1+y}{y}}-1}\right)\right], \tag{133} $$

$$ y = \frac{-t}{4m_\pi^2}. $$

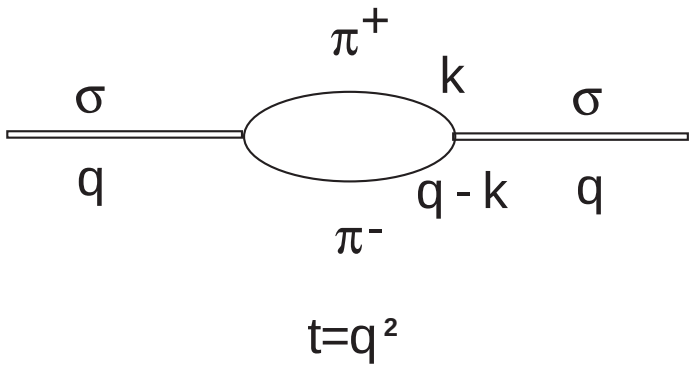

Figure 12: Propagator of a σ meson in the presence of a $\pi^+\pi^-$ loop. In addition, the $\pi^0\pi^0$ loop has to be taken into consideration.

This means that the width Γ_σ of the σ mesons leads to a shift of the pole parameter m_σ^2. For the data analysis we replace the t dependent effective mass $m_{\rm eff} = (m_\sigma^2 + \mathcal{P}(t))^{1/2}$ in the denomiator of the r.h.s of Eq. (132) by a constant and make a tentative prediction by assuming $m_\sigma = 500$ MeV, $\Gamma_\sigma = 500$ MeV (see Section 2.6.2) for the σ meson and $\theta_{\rm cm} = 125^\circ$ and $E_\gamma = 600$ MeV for the kinematics of the experiment. Then we arrive at the prediction $m_{\rm eff} = 630$ MeV.

For the data analysis we use the relations

$$2\pi(\alpha-\beta) + A_1^{\rm int}(0,0) = -A_1^{\rm as}(0) = \frac{g_{\sigma NN}F_{\sigma\gamma\gamma}}{m_{\rm eff}^2}, \quad A_1^{\rm as}(\nu,t) = \frac{g_{\sigma NN}F_{\sigma\gamma\gamma}}{t-m_{\rm eff}^2}. \tag{134}$$

In (134) $(\alpha-\beta)$ is the experimental value for the difference of electromagnetic polarizabilities measured at low energies where the $\mathcal{O}(\omega^2)$ approximation is valid, $A_1^{\rm int}(0,0)$ the integral part calculated from photomeson data (see Section 4) and $m_{\rm eff}$ an adjustable parameter to be determined from experimental Compton differential cross sections in the second resonance region and a range of large scattering angles. The fit parameter obtained for a given parameterization of photomeson amplitudes (see Section 5.5) is (589 ± 12) MeV. The error ± 12 only takes into account the uncertainties of the fit. The additional error due to the uncertainties in the parameterizations of photomeson amplitudes can only be estimated with a large margin of uncertainty. In view of this, the predicted and the experimental effective mass may be considered as being in good agreement with each other.

4 The imaginary parts of Compton amplitudes

In the following we discuss the method through which the imaginary parts ${\rm Im}A_i(\nu,t)$ of the amplitudes $A^{\rm int}(\nu,t)$ given in Eq. (125) and (129) are obtained. The main input are the single pion photoproduction data which are available with improving precision.

4.1 The unitarity relation

The integral contributions $A_i^{\rm int}$ are determined by the imaginary parts of the Compton scattering amplitudes which follow from the unitarity relation of the generic form [25]

$$T_{fi} - T_{if}^* = 2{\rm Im}T_{fi} = \sum_n (2\pi)^4 \delta^4(P_n - P_i) T_{nf}^* T_{ni}. \tag{135}$$

For the special case of forward Compton scattering where $f \equiv i$, we obtain

$$\mathrm{Im}T_{ii} = \frac{1}{2}(2\pi)^4 \sum_n |T_{in}|^2 \delta^4(P_i - P_n) = \frac{\omega}{4\pi}\sigma_{tot}(\omega). \tag{136}$$

The quantities P_i and P_n are the four-momenta before and after the absorption of the incident photon by the nucleon. The quantity $\delta^4(P_n - P_i)$ guarantees the energy and momentum conservation during the absorption process. In order to measure $\sigma_{tot}(\omega)$ all exit channels of the exited nucleon state have to be registered. This includes all particle channels as well as all photon decay channels. For the nucleon, in general only the elastic photon decay channel into the ground state is available in addition to meson photoproduction. This exit channel is termed elastic radiative decay and, of course, is not identical with the solid-angle integrated differential-cross section for Compton scattering. For the Δ resonance region it can be estimated that elastic radiative decay amounts to $\lesssim 1\%$ of the total decay. Below particle threshold we have $\sigma_{tot}(\omega) = 0$.

4.2 The CGLN amplitudes

The most precise data have been obtained for single-pion photoproduction for unpolarized photons and target nucleons. Based on the angular distribution of the emitted pions, multipole analyses have been carried out. The necessary tools for this have been worked out by Chew, Goldberger, Low and Nambu [93]:

Let the photoproduction amplitude be denoted by $\mathcal{F}$, such that the differential cross section for meson production in the c.m. system is

$$\frac{d\sigma}{d\Omega} = \frac{q}{k}|\langle \pi N|\mathcal{F}|\gamma N\rangle|^2, \tag{137}$$

where the matrix element is taken between initial and final Pauli (not Dirac) spinors. For a given isospin it is then possible to write $\mathcal{F}$ as follows

$$\mathcal{F} = i\boldsymbol{\sigma}\cdot\boldsymbol{\epsilon}\mathcal{F}_1 + \frac{\boldsymbol{\sigma}\cdot\mathbf{q}\,\boldsymbol{\sigma}\cdot(\mathbf{k}\times\boldsymbol{\epsilon})}{qk}\mathcal{F}_2 + \frac{i\boldsymbol{\sigma}\cdot\mathbf{k}\,\mathbf{q}\cdot\boldsymbol{\epsilon}}{qk}\mathcal{F}_3 + \frac{i\boldsymbol{\sigma}\cdot\mathbf{q}\,\mathbf{q}\cdot\boldsymbol{\epsilon}}{q^2}\mathcal{F}_4, \tag{138}$$

where $\mathcal{F}_1 \cdots \mathcal{F}_4$ are functions of energy and angle in the c.m. system and $\mathbf{q}$ and $\mathbf{k}$ are the meson and photon three-momenta. The angular dependence may be made explicit through a multipole expansion involving derivatives of Legendre polynomials:

$$\mathcal{F}_1 = \sum_{l=0}^{\infty}[lM_{l+} + E_{l+}]P'_{l+1}(x) + [(l+1)M_{l-} + E_{l-}]P'_{l-1}(x), \tag{139}$$

$$\mathcal{F}_2 = \sum_{l=1}^{\infty}[(l+1)M_{l+} + lM_{l-}]P'_l(x), \tag{140}$$

$$\mathcal{F}_3 = \sum_{l=1}^{\infty}[E_{l+} - M_{l+}]P''_{l+1}(x) + [E_{l-} + M_{l-}]P''_{l-1}(x), \tag{141}$$

$$\mathcal{F}_4 = \sum_{l=1}^{\infty}[M_{l+} - E_{l+} - M_{l-} - E_{l-}]P''_l(x). \tag{142}$$

Here x is the cosine of the angle of emission in the c.m. system.

The energy-dependent amplitudes $M_{l\pm}$ and $E_{l\pm}$ refer to transitions initiated by magnetic and electric radiation, respectively, leading to final states of orbital angular momentum l and total angular momentum $l \pm \frac{1}{2}$. Superscripts may be added to each amplitude in formulas (139) to (142) in order to designate the isospin of the transition.

The most prominent CGLN photomeson amplitudes at low and intermediate energies are the non-resonant E_{0+} amplitude where the pion is emitted as an s-wave, and the resonant $M_{1+}^{3/2}$ and $E_{1+}^{3/2}$ amplitudes leading to the $I = 3/2$ component of the Δ resonance via magnetic dipole or electric quadrupole transitions, respectively, whereafter the pion is emitted as a p-wave.

4.3 Helicity amplitudes

Walker [55,94] writes the integral cross section for pion photoproduction in terms of helicity "elements" (or amplitudes) $A_{l\pm}$ and $B_{l\pm}$, given in the form

$$\begin{aligned}
\sigma_T &= \frac{1}{2}\left(\sigma_{1/2} + \sigma_{3/2}\right), \\
\sigma_{1/2} &= \frac{8\pi q}{k}\sum_{l=0}^{\infty}(l+1)(|A_{l+}|^2 + |A_{(l+1)-}|^2), \\
\sigma_{3/2} &= \frac{8\pi q}{k}\sum_{l=0}^{\infty}\frac{1}{4}[l(l+1)(l+2)](|B_{l+}|^2 + |B_{(l+1)-}|^2),
\end{aligned} \tag{143}$$

where the subscript notation of the A's and B's is the same as that of CGLN [93]; e.g. $B_{l\pm}$ refers to a state with pion orbital angular momentum l and total angular momentum $j = l \pm \frac{1}{2}$. The A's and B's differ in the absolute values of the helicities $\Lambda = |\lambda|$ of the initial states given by $\lambda = \lambda_\gamma - \lambda_p$, where λ_γ is the helicity of the incident photon and λ_p the helicity of the nucleon in the initial state. For the A's the helicity is $\Lambda = 1/2$, for the B's $\Lambda = 3/2$. Walker [55] finds the following relations between the helicity elements and the CGLN multipole coefficients

$$E_{0+} = A_{0+}, \quad M_{1-} = A_{1-}, \tag{144}$$

and for $l \geq 1$,

$$\begin{aligned}
E_{l+} &= (l+1)^{-1}(A_{l+} + \frac{1}{2}lB_{l+}), \\
M_{l+} &= (l+1)^{-1}[A_{l+} - \frac{1}{2}(l+2)B_{l+}], \\
E_{(l+1)-} &= -(l+1)^{-1}[A_{(l+1)-} - \frac{1}{2}(l+2)B_{(l+1)-}], \\
M_{(l+1)-} &= (l+1)^{-1}(A_{(l+1)-} + \frac{1}{2}lB_{(l+1)-}).
\end{aligned} \tag{145}$$

Equivalently we may write

$$\begin{aligned}
A_{k+} &= \frac{1}{2}[(k+2)E_{k+} + kM_{k+}], \quad B_{k+} = E_{k+} - M_{k+}, \\
A_{(k+1)-} &= \frac{1}{2}[-kE_{(k+1)-} + (k+2)M_{(k+1)-}], \\
B_{(k+1)-} &= E_{(k+1)-} + M_{(k+1)-}.
\end{aligned} \tag{146}$$

For the three main multipoles this corresponds to

$$\begin{aligned} E1: &\qquad E_{0+} = A_{0+}, \\ M1: &\qquad M_{1+} = \frac{1}{2}(A_{1+} - \frac{3}{2}B_{1+}), \\ E2: &\qquad E_{1+} = \frac{1}{2}(A_{1+} + \frac{1}{2}B_{1+}). \end{aligned} \tag{147}$$

4.4 Imaginary parts of Compton amplitudes for πN intermediate states

Following L'vov [68] we express the invariant amplitudes $A_i(s,t)$ for Compton scattering through reduced helicity amplitudes τ_i for Compton scattering:

$$\begin{aligned} A_1 &= \frac{1}{(s-M^2)^2}\Big[-\frac{s}{M}\left(1-\sigma\frac{s+M^2}{2s}\right)\tau_4 - \frac{\sqrt{s}}{2}(\tau_5+\sigma\tau_6)\Big], \\ A_2 &= \frac{1}{(s-M^2)^3}\Big[-\frac{s}{M}(s+M^2)\left(1-\sigma\frac{s-M^2}{2s}\right)\tau_4 - \frac{\sqrt{s}}{2}(s-M^2)\tau_5 + 2s\sqrt{s}\left(1-\sigma\frac{s-M^2}{4s}\right)\tau_6\Big], \\ A_3 &= \frac{1}{(s-M^2)^2(s-M^2+t/2)}\Big[M^3[\tau_1+(1-\sigma)\tau_2] - 2M^2\sqrt{s}\left(1-\sigma\frac{s+M^2}{2s}\right)\tau_3\Big], \\ A_4 &= \frac{1}{(s-M^2)^2(s-M^2+t/2)}\Big[M^3\tau_1 - M^3\left(1+\sigma\frac{M^2}{s}\right)\tau_2 + \frac{2M^4}{\sqrt{s}}\sigma\tau_3\Big], \\ A_5 &= \frac{1}{(s-M^2)^2(s-M^2+t/2)}\Big[M(s+M^2)\sigma\tau_4 - M^2\sqrt{s}(\tau_5+\sigma\tau_6)\Big], \\ A_6 &= \frac{1}{(s-M^2)^2(s-M^2+t/2)}\Big[-\frac{M}{2}(s+M^2)[\tau_1+(1-\sigma)\tau_2] + 2M^2\sqrt{s}(1-\sigma)\tau_3\Big], \end{aligned} \tag{148}$$

where

$$\sigma = \sin^2\frac{\theta_s}{2} = -\frac{st}{(s-M^2)^2} \tag{149}$$

and θ_s the c.m. scattering angle.

The imaginary parts of the reduced helicity amplitudes τ_i may be written in the form [68]

$$\begin{aligned} \mathrm{Im}[\tau_1]^{(1\pi)} &= 8\pi q\sqrt{s}\sum_{k=0}^{\infty}(2k+2)(|A_{k+}|^2+|A_{(k+1)-}|^2)F(-k,k+2,1,\sigma), \\ \mathrm{Im}[\tau_2]^{(1\pi)} &= 8\pi q\sqrt{s}\sum_{k=1}^{\infty}\frac{k(k+1)(k+2)}{2}(|B_{k+}|^2+|B_{(k+1)-}|^2F(-k+1,k+3,1,\sigma), \\ \mathrm{Im}[\tau_3]^{(1\pi)} &= 8\pi q\sqrt{s}\sum_{k=1}^{\infty}k(k+1)(k+2)(-A_{k+}B^*_{k+}-A_{(k+1)-}B^*_{(k+1)-})F(-k+1,k+3,2,\sigma), \\ \mathrm{Im}[\tau_4]^{(1\pi)} &= 8\pi q\sqrt{s}\sum_{k=1}^{\infty}\frac{k(k+1)^2(k+2)}{2}(A_{k+}B^*_{k+}-A_{(k+1)-}B^*_{(k+1)-})F(-k+1,k+3,3,\sigma), \\ \mathrm{Im}[\tau_5]^{(1\pi)} &= 8\pi q\sqrt{s}\sum_{k=0}^{\infty}2(k+1)^2(|A_{k+}|^2-|A_{(k+1)-}|^2)F(-k,k+2,2,\sigma), \\ \mathrm{Im}[\tau_6]^{(1\pi)} &= 8\pi q\sqrt{s}\sum_{k=1}^{\infty}\frac{k^2(k+1)^2(k+2)^2}{12}(-|B_{k+}|^2+|B_{(k+1)-}|^2)F(-k+1,k+3,4,\sigma), \end{aligned} \tag{150}$$

where q is the pion momentum and the sum over different isotopic channels is implied. F is a hypergeometric polynomial of $\sigma = \sin^2(\theta_s/2)$:

$$F(a,b,c,x) = 1 + \frac{ab}{c}\frac{x}{1!} + \frac{a(a+1)b(b+1)}{c(c+1)}\frac{x^2}{2!} + \cdots . \tag{151}$$

For angular momenta $j \leq j_{\max} = 7/2$ predictions of imaginary parts related to single-pion photoproduction have been based on phenomenological analyses of photopion experimental data. Higher multipoles, $j > 7/2$, are assumed to be given by one-pion-exchange (OPE) diagrams. The corresponding formulae are given in [68]. Further information concerning the πN intermediate state and information on the $\pi\pi N$, the $\pi\Delta$ and the $\rho^0 N$ intermediate states may be found in the appendices of [68].

4.5 The integral parts of the amplitudes calculated in fixed-t dispersion theory for the unphysical region

As noted in connection with the Mandelstam plane (Figure 10), part of the integral amplitude of fixed-t dispersion theory has to be determined in the unphysical region between $\nu_{\rm thr}(t)$ and the borderline $\nu_\pi(t)$ of the physical region. As discussed in [68] the unphysical region corresponds to very small ν' and very high $-t$ which corresponds to an unphysical $z' = \cos\theta_s$ of the photon scattering angle arising in the integrand when taking into account Compton scattering at high energies and backward angles. For small angular momenta j the functions $\mathrm{Im}A_i(\nu', t)$ do not show any pathological behavior in the unphysical region. This, however, may not be the case when partial waves with high j are taken from experimental fits. For this case special procedures have been developed [68] involving model calculations which take care of the problem in a reliable way. In conclusion, the unphysical region did not provide problems in the range of the present investigation which is restricted to $E_\gamma < 1$ GeV and $\theta_{\rm lab} < 150°$.

4.6 Application of photomeson amplitudes in Compton scattering

In general the available pion photoproduction amplitudes have been applied without modification, but selections between different versions have been made in order to achieve optimum fits to the Compton differential cross sections. The sensitivity of this selection procedure has been demonstrated at an early stage of our investigations where it was shown that the resonance part of the M_{1+} amplitude which was available at that time [95, 96] had to be scaled down by 2.8% [97].

Updated versions of photomeson amplitudes are published regularly in the SAID and MAID data bases [98]. Though large improvements have been made in recent years, the application of the photomeson amplitudes to the calculation of Compton scattering amplitudes requires a very sophisticated procedure. One example is given in Section 5.3.3 where the selection procedure is described to find an optimal representation of differential cross sections for Compton scattering by the neutron. In the course of our work it also was noticed that updates of photomeson amplitudes may lead to less good agreement with Compton scattering data than the versions published before. This shows that Compton scattering is well suited to make independent constraints on these amplitudes.

5 Recent experiments on Compton scattering and polarizabilities of the proton and the neutron

5.1 Electromagnetic polarizabilities of the proton

A common feature of experiments carried out in the 1950's to 1970's has been the use of continuous-energy bremsstrahlung photon beams and photon detectors having poor energy resolution. These factors made it difficult to determine the incident photon flux accurately. With the advent of high duty factor electron accelerators and large-volume NaI(Tl) detectors these problems were largely overcome. The first experiment making use of these new achievements was carried out at the University of Illinois at Urbana-Champaign [99]. Photons were produced via the bremsstrahlung process in a thin Al foil. The post-bremsstrahlung electrons were momentum analyzed in a magnetic spectrometer and detected in an array of plastic scintillators, thereby tagging the associated photons through their time-coincidence with the scattered photons. In this way quasi-monochromatic photons were obtained with an energy resolution of few MeV. The advantage of the quasi-monochromatic photons is paid for by low intensity which is limited to $10^5 - 10^6 s^{-1}$ per channel as defined through a plastic scintillator. The result obtained was $\alpha_p = 10.9 \pm 2.2 \pm 1.3$, $\beta_p = 3.3 \mp 2.2 \mp 1.3$ using the constraint $\alpha_p + \beta_p = 14.2$ calculated in an early evaluation [100] from photo-absorption data assuming the validity of Baldin's sum rule.

A different method was used [101] at the low duty-cycle linear accelerator at Mainz where bremsstrahlung was used for Compton scattering by the proton through $\theta^{\rm lab} = 180^\circ$. The forward scattered protons were deflected by a magnetic spectrometer with 12 detector channels to measure the energies of the recoil protons. Rather thin targets (5 –10 mm lq. H_2) had to be used so that the recoil protons had to be separated from protons produced in the thin windows of the target. The result obtained was $\alpha_p = 10.62 \pm 1.22 \pm 1.05$, $\beta_p = 3.58 \mp 1.22 \mp 1.05$, using the constraint $\alpha_p + \beta_p = 14.2$.

Two experiments were carried out in the SAL laboratory in Saskatoon. In the 1993 experiment [102] a high duty-factor bremsstrahlung beam and a high-resolution NaI(Tl) detector was used to measure Compton scattering using the end-point technique. This method has the disadvantage that the shape of the bremsstrahlung spectrum at the endpoint has to be known. Furthermore, the energies (150 - 300 MeV) were far outside the range of validity of the low-energy approximation, leading to possible large uncertainties in the polarizabilities due to model-dependent effects. The result obtained was $\alpha_p = 9.8 \pm 0.4 \pm 1.1$, $\beta_p = 4.4 \mp 0.4 \mp 1.1$, using the constraint $\alpha_p + \beta_p = 14.2$. In the 1995 experiment [103] tagged photons with energies from 70 to 100 MeV and un-tagged photons with energies from 100 to 148 MeV were used. The entire energy region from 70 to 148 MeV was measured simultaneously. The result obtained is $\alpha_p = 12.5 \pm 0.6 \pm 0.7 \pm 0.5$, $\beta_p = 1.7 \mp 0.6 \mp 0.7 \mp 0.5$, using the constraint $\alpha_p + \beta_p = 14.2$. Here a model dependent error is given in addition to the statistical and systematic error.

Recently a re-evaluation of the experiments on the electromagnetic polarizabilities of the proton has been carried out using the data cited above and using also all the other data from the data base of the 1950's – 1990's. The overall (global) average obtained from these data is [17]

$$\begin{aligned} \alpha_p &= 11.7 \pm 0.8(\text{stat} + \text{syst}) \pm 0.7(\text{model}), \\ \beta_p &= 2.3 \pm 0.9(\text{stat} + \text{syst}) \pm 0.7(\text{model}) \end{aligned} \tag{152}$$

where no use has been made of the Baldin sum rule result for $\alpha_p + \beta_p$ as obtained from photo-absorption data. The sum of polarizabilities following from (152) is

$$\alpha_p + \beta_p = 14.0 \pm 1.3(\text{stat} + \text{syst}) \pm 0.6(\text{model}). \tag{153}$$

5.1.1 Electromagnetic polarizabilities of the proton measured at MAMI (Mainz)

A new precise determination of the electromagnetic polarizabilities of the proton α_p and β_p has been performed using the TAPS apparatus set up at the tagged-bremsstrahlung facility at MAMI (Mainz) [2, 104]. This facility provided quasi-monochromatic photons with an energy resolution of $\Delta E_\gamma \approx 2$ MeV at energies in the range between $E_\gamma \approx 60$ MeV and 160 MeV. At these low energies the low-energy approximation is valid to a large extent so that model dependencies arising from higher-oder terms in the photon energy are small in a major part of this interval. This experiment was the first which covered a large angular interval with one experimental setting ranging from $\theta_{\rm lab} = 59^\circ$ to 155°. The set-up is depicted in the left panel of Figure 13. The coverage of this large angular range was achieved by using

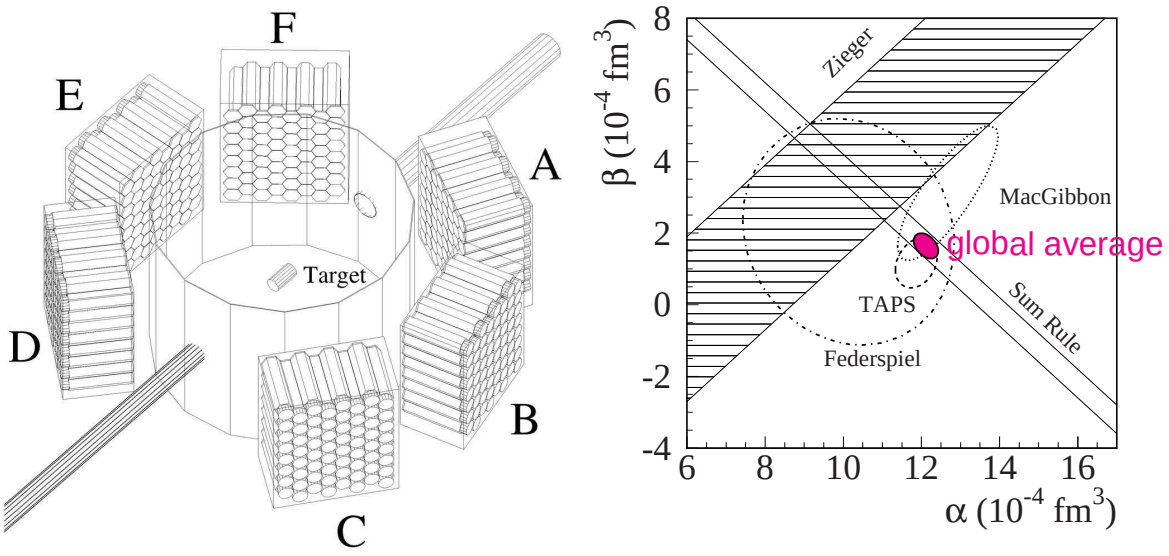

Figure 13: Left panel: The TAPS arrangement at MAMI. The photon beam enters the setup between the blocks A and F. Also shown are the target cell and the scattering chamber. Right panel: Error contour plot $\chi^2(\alpha, \beta) = \chi^2_{\rm min} + 1$ for which the errors are taken as the statistical ones only. Also shown are the constraint form the Baldin sum rule and the value $\alpha - \beta$ as follows from the experiment by Zieger et al. [101]. The grey ellipse corresponds to the global fit of [2, 104].

6 blocks A to F of the TAPS detector, each consisting of 64 BaF_2 detectors. The procedure used for the data analysis was to take α_p and β_p as free parameters and to make no use of the constraints provided by Baldin's sum rule. The result obtained in this way was

$$\begin{aligned} \alpha_p &= 11.9 \pm 0.5({\rm stat}) \mp 1.3({\rm syst}), \\ \beta_p &= 1.2 \pm 0.7({\rm stat}) \mp 0.3({\rm syst}). \end{aligned} \tag{154}$$

The sum of electromagnetic polarizabilities obtained from these data is

$$\alpha_p + \beta_p = 13.1 \pm 0.9({\rm stat}) \mp 1.0({\rm syst}). \tag{155}$$

Comparing the results of the TAPS experiment as given in Eqs. (154) and (155) with the average of all results obtained in previous experiments as given in Eqs. (152) and (153) we recognize that the precision achieved in the TAPS experiment is comparable with the precision of all the previous experiments taken together. This finding is illustrated in the right panel of Figure 13.

The right panel of Figure 13 shows a comparison of the result of the recent TAPS experiment [104] with other experiments carried out in the 1990's. Also shown is the constraint given by Baldin's sum rule. The results are shown in a two-dimensional diagram α_p versus β_p. The contours correspond to $\chi^2(\alpha_p, \beta_p) = \chi^2_{\rm min} + 1$. The result obtained for $\alpha_p - \beta_p$ when taking into account the constraints of Baldin's sum rule (taken to be $\alpha_p + \beta_p = 13.8 \pm 0.4$ [104]) is represented by the small grey ellipse corresponding to

$$\alpha_p - \beta_p = 10.5 \pm 0.9({\rm stat + syst}) \pm 0.7({\rm model}). \tag{156}$$

From the numbers given in Eqs. (153) and (155) we obtain as the global – i.e. all existing data for low-energy Compton scattering containing – result

$$\alpha_p + \beta_p = 13.6 \pm 0.8({\rm stat + syst}) \pm 0.5({\rm model}). \tag{157}$$

As a *recommended* final result of the experimental electromagnetic polarizabilities of the proton we propose to used the weighted average of the data obtained from low-energy Compton scattering by the proton given in Eqs. (152) and (154) and from the adopted result for $\alpha_p + \beta_p$ obtained from photo-absorption data via the Baldin sum rule. The corresponding numbers are given Table 8.

Table 8: *Recommended* values for the experimental electromagnetic polarizabilities of the proton. The values are constrained by Baldin's sum rule using $\alpha_p + \beta_p = 13.9 \pm 0.3$ (see Table 13). The unit is $10^{-4}{\rm fm}^3$.

α_p	β_p
12.0 ± 0.6	1.9 ∓ 0.6

5.2 Spin polarizability of the proton

The spin polarizability of the proton for the backward direction has first been extracted from experimental data by Tonnison et al. (LEGS) [105] leading to $\gamma_\pi^{(p)} = -[27.1 \pm 2.2({\rm stat + syst})^{+2.8}_{-2.4}({\rm model})] \times 10^{-4}{\rm fm}^4$. This result received great attention because it differed considerably from the prediction based on dispersion theory with the asymptotic contribution calculated from the π^0, η and η' poles. One possible interpretation of this finding was that a new contribution to the spin structure of the proton was discovered.

However, a Compton scattering experiment carried out at MAMI using the 48 cm $\oslash\times$ 64 cm NaI(Tl) detector [106] confirmed the predicted value of $\gamma_\pi^{(p)} = -37.6$ [106]. This latter result has recently been confirmed in two further experiments carried out at MAMI using the large acceptance arrangement LARA [107, 108] and the TAPS detector [104]. The result obtained with LARA through fits to the experimental differential cross sections [107, 108] is

$$\gamma_\pi^{(p)} = -37.1 \pm 0.6({\rm stat + syst}) \pm 3.0({\rm model}) \tag{158}$$

when using the SAID-SM99K parameterization [95,96] as a basis in the un-subtracted fixed-t dispersion theory [68] and

$$\gamma_\pi^{(p)} = -40.9 \pm 0.6({\rm stat + syst}) \pm 2.2({\rm model}) \tag{159}$$

when using the MAID2000 parameterization [109]. The difference between the results given in (158) and (159) may be considered as a typical example of a model dependence introduced by inconsistencies

in the parameterizations of photomeson amplitudes. In the present case these parameterizations are used unmodified, i.e. without adjustments to the Compton scattering data whereas the asymptotic part of the spin-polarizability is treated as an adjustable parameter. The result obtained from low energy Compton scattering using the TAPS detector [104] is

$$\gamma_\pi^{(p)} = -35.9 \pm 2.3(\text{stat} + \text{syst}) \tag{160}$$

where the model error has been included into the systematic error.

It has been shown [106–108] that these discrepancies between MAMI and LEGS can be traced back to a discrepancy in the experimental differential cross sections for Compton scattering by the proton obtained in the Δ resonance region. This finding has recently been confirmed [110] at MAMI using the apparatus shown in the left panel of Figure 14. This apparatus consists of the Mainz 48

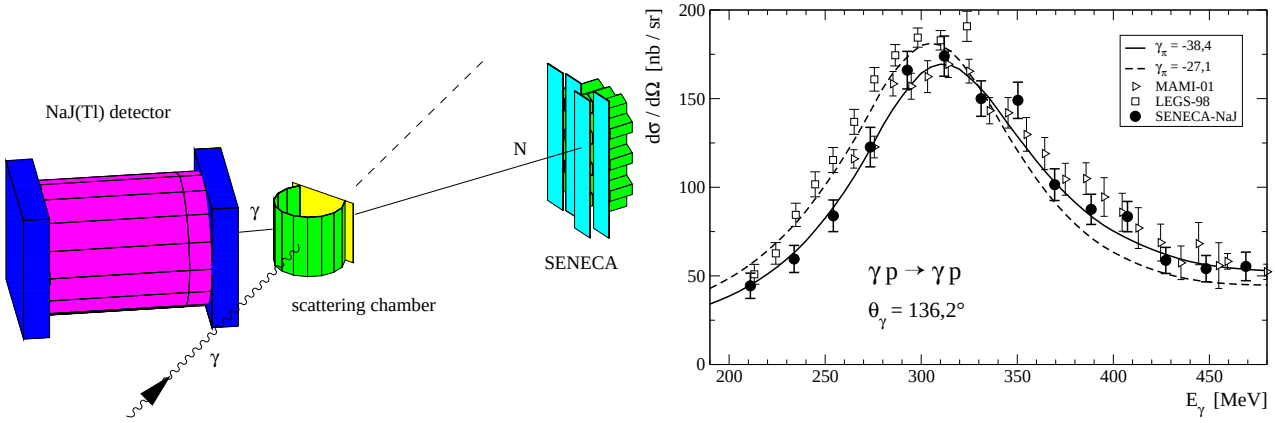

Figure 14: Left panel: Experimental arrangement used for Compton scattering by the proton [110]. Compton scattering events are identified through coincidences between the Mainz 48 cm ⌀× 64 cm NaI(Tl) photon detector positioned under 136° and the Göttingen segmented recoil counter SENECA positioned under 18°. Right panel: Experimental differential cross sections for Compton scattering by the proton at $\theta_\gamma^{\text{lab}} = 136.2°$. Closed circles: SENECA-NaI (left figure) data [110]. Open triangles Mainz-LARA data [107, 108]. Open squares: LEGS data [105, 111]

cm ⌀ × 64 cm NaI(Tl) photon detector positioned under 136° to the incoming photon beam and the Göttingen segmented recoil spectrometer SENECA positioned under 18°. This apparatus was set up for an experiment to measure the electromagnetic polarizabilities of the neutron via quasi-free Compton scattering by neutrons bound in the deuteron above π photoproduction threshold. As a test of the apparatus the target cell was filled with liquid hydrogen so that Compton differential cross sections for the proton were measured. The experimental result is shown in the right panel of Figure 14 together with the LEGS data [105, 111]. The backward spin polarizability extracted from the MAMI data of Figure 14 is

$$\gamma_\pi^{(p)} = -36.5 \pm 1.6(\text{stat}) \pm 0.6(\text{syst}) \pm 1.8(\text{model}) \quad \text{(SAID-SM99K)}, \tag{161}$$
$$\gamma_\pi^{(p)} = -39.1 \pm 1.2(\text{stat}) \pm 0.8(\text{syst}) \pm 1.5(\text{model}) \quad \text{(MAID2000)}. \tag{162}$$

From the Mainz values of Eqs. (158) - (162) given above we obtain [110] a the weighted average given in Table 9. We recommend to consider the weighted average given in Table 9 as the accepted result for the experimental backward spin-polarizability of the proton.

Table 9: *Recommended* value for the experimental backward spin polarizability of the proton (MAMI weighted average). The unit is 10^{-4}fm^4.

$$\boxed{\gamma_\pi^{(p)} = -38.7 \pm 1.8}$$

5.3 Electromagnetic polarizabilities of the neutron

For a long time the determination of the electromagnetic polarizabilities of the neutron via Compton scattering was considered as impossible. Therefore, the application of electromagnetic scattering of neutrons in the Coulomb field of heavy nuclei was given preference, as discussed in the introduction. However, these early results remained unsatisfactory.

5.3.1 Electromagnetic scattering of neutrons in a Coulomb field in the 1990's

The only experiment on electromagnetic scattering of neutrons in the Coulomb field of heavy nuclei leading to a value for α_n with a meaningful precision was carried out in Oak Ridge [112] using a Pb target enriched in ^{208}Pb in order to reduce the uncertainties arising from nuclear neutron scattering. The result of this experiment was

$$\alpha_n = 12.6 \pm 1.5 \pm 2.0. \tag{163}$$

The number given here has been corrected by adding the Schwinger term [3] $e^2\kappa_n^2/4M^3 = 0.6$, containing the neutron anomalous magnetic moment κ_n and the neutron mass M. This term compensates for a missing term (see [3]) in the original evaluation of this experiment. After including the Schwinger term the number is directly comparable with the one defined through Compton scattering. A later experiment carried out in Munich [113] lead to $\alpha_n = 0.6 \pm 5$. This value for α_n appears to us unreasonable and, furthermore, has a large error. Therefore, we consider it advisable to disregard this result in the following considerations. The Oak Ridge experiment [112] is of very high precision. However this precision has been questioned by a number of researchers active in the field of neutron scattering [114]. Their conclusion is that the Oak Ridge result [112] possibly might be quoted as $7 \leq \alpha_n \leq 19$. (For a more detailed discussion see [115].) Certainly, this criticism has to be kept in mind. On the other hand we feel obliged to the rule that authors have to be trusted in a first place and, therefore, cite and adopt the result of [112] as it is given in Eq. (163).

5.3.2 Compton scattering by neutrons below meson photoproduction threshold

The electromagnetic polarizabilities α_p and β_p of the proton have been measured through Compton scattering at energies below π-photoproduction threshold. The differential cross section for Compton scattering is comparatively large in this case because of the sizable interference term between the Born and the non-Born amplitude. In fact, it is this interference term which is of essential help in experiments on the proton.

A corresponding experiment for the neutron is extremely difficult, because there is no Thomson amplitude to interfere with the non-Born part of the scattering amplitude. Therefore, differential cross sections for Compton scattering by the neutron at energies below π-photoproduction threshold are extremely small. Furthermore, there are no free-neutron targets with sufficient density, and for neutrons bound in the deuteron sizable corrections are expected to the quasi-free differential cross section due to

final-state interaction between the outgoing nucleons. Therefore, any experiment of this kind has to be accompanied by a carefully carried out theory [116].

The first experiment on low-energy γn scattering with subsequent extraction of the polarizabilities of the neutron has been carried out by the Göttingen-Mainz group [117] which followed an earlier theoretical suggestion [116] to exploit the reaction $\gamma d \to \gamma np$ in the quasi-free kinematics. The experiment was carried out using non-tagged bremsstrahlung produced by a 130 MeV 20 μA c.w. electron beam of MAMI A which was available for a small period of time during the MAMI construction. Quasi-free Compton scattering by the neutron was investigated via the $^2\mathrm{H}(\gamma,\gamma' n)^1\mathrm{H}$ reaction by detecting Compton scattered photons in two 25 cm $\varnothing \times$ 36 cm NaI(Tl) detectors positioned at lab scattering angles of $\theta_{\gamma'} = 90^\circ$ and 135°. The energy spectrum and angular distribution of recoiling neutrons were measured in coincidence with the Compton scattered photons via time of flight using a plastic-scintillator hodoscope.

This experiment was successful in the sense that the relevant effect, i.e. coincidence events between Compton scattered photons and recoil neutrons, was definitely identified. It was possible to extract the value $\alpha_n = 10.7$ for the electric polarizability from the experimental data with an upper error of +3.3. The determination of a lower error failed because of the rather large lower error of 18% of the differential cross section, so that its lower bound did not correspond to a possible electromagnetic polarizability. In order to avoid this difficulty, the lower error of the differential cross section should have been 10% or smaller. The result of this first and only experiment carried out below the meson photoproduction threshold may be quoted as

$$\alpha_n = 10.7^{+3.3}_{-10.7}. \tag{164}$$

5.3.3 Quasi-free Compton scattering by neutrons bound in the deuteron above meson photoproduction threshold

Because of the difficulties involved in a Compton scattering experiment at energies below meson photoproduction threshold it has been proposed [116] to measure quasi-free Compton scattering by the neutron at energies between pion threshold and the Δ peak to determine $\alpha_n - \beta_n$. The underlying properties of the method are depicted in Figure 15. Compton scattering by the nucleon has to be calculated under kinematical conditions fulfilled for Compton scattering by a free nucleon. Under these kinematical conditions the quasi-free peak is expected. The calculation is performed in a diagrammatic approach. As a first approximation, the nucleon wave functions in the final state are treated as plane waves. Thereafter, the modification of the wave-functions due to the nucleon-nucleon potential is taken into account. Since the nucleon-nucleon potential is isospin dependent, additional diagrams taking into account meson exchange currents (MEC) (see Figure 15 e) and f)) have to be taken into account. The result of the calculation is the quasi-free peak either for the recoiling proton or recoiling neutron having a width which is larger than the one expected from Fermi motion alone. This increase of width is large at energies below meson photoproduction threshold and becomes small at higher energies. The further steps of the calculation are (i) to relate the area underneath the quasi-free peak to the triple differential cross section in the center of the quasi-free peak and (ii) to relate the triple differential cross section in the center of the quasi-free peak to the differential cross section for the free nucleon. With this theoretical input, the number of events found experimentally in the range of recoil energies where the quasi-free peak is expected can be used (i) to calculate the experimental triple differential cross section in the center of the quasi-free peak and (ii) to calculate the corresponding experimental differential cross section for a "free" nucleon obtained by the quasi-free method.

Compton scattering experiments on the free proton and quasi-free Compton scattering on the proton bound in the deuteron can be used to test the validity of the procedure. The first experiment of this

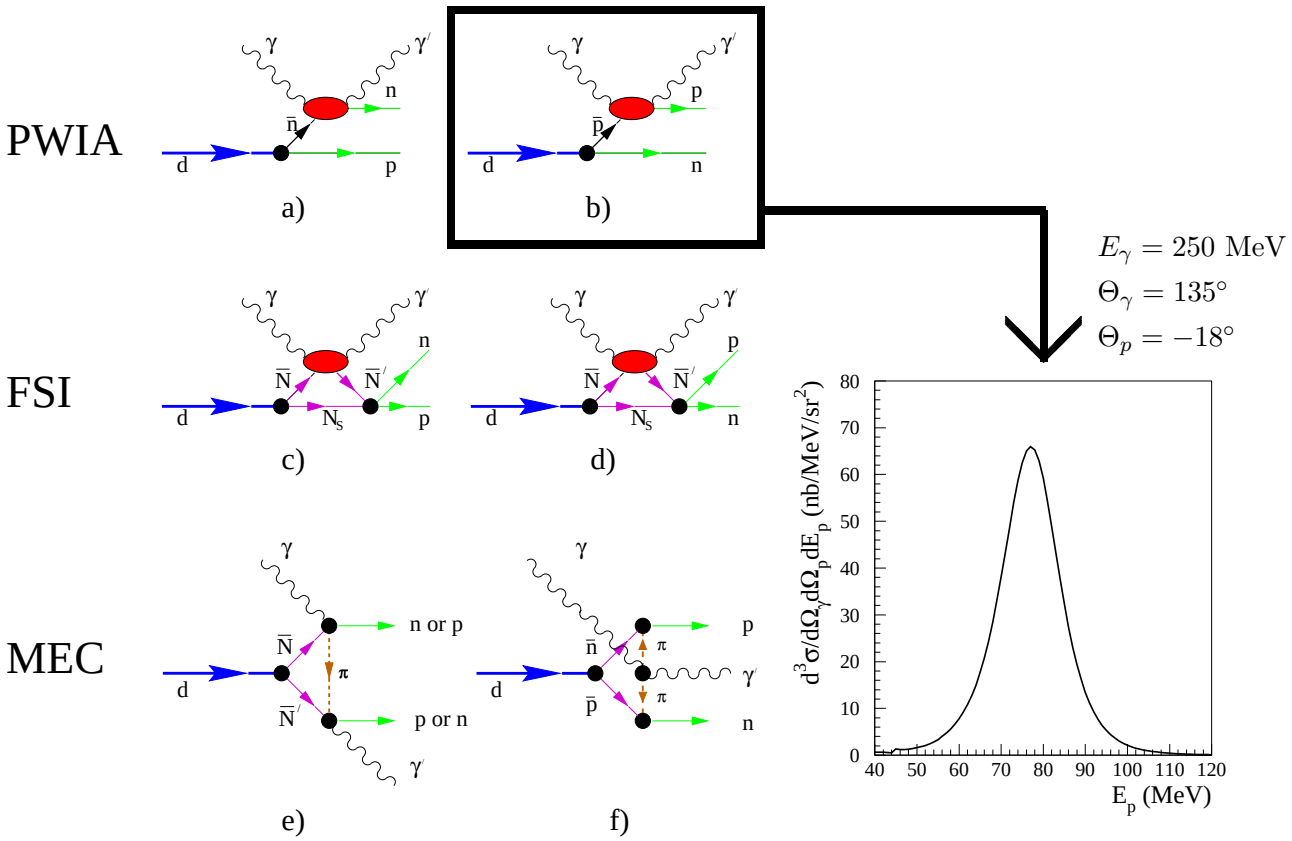

Figure 15: Left panel: Feynman diagrams for quasi-free Compton scattering by the proton and neutron bound in the deuteron. a) Compton scattering by the neutron in quasi-free kinematics calculated in plane-wave approximation. b) Same as a) but calculated for the proton. c) and d) final-state interactions due to the nucleon-nucleon interaction in the final state. e) and f) meson-exchange corrections. Right panel: Triple differential $d^3\sigma/d\Omega_\gamma d\Omega_p dE_p$ cross section for Compton scattering by the proton in the quasi-free peak including final-state interactions and corrections due to meson-exchange.

kind has been carried out by Wissmann et al. [106] at MAMI (Mainz) using the Mainz 48 cm$\varnothing$ × 64 cm NaI(Tl) spectrometer for the free-proton experiment and the TAPS spectrometer for the quasi-free proton experiment. Differential cross sections sections for Compton scattering by the free proton were measured in the energy range from $E_\gamma = 200$ MeV to 400 MeV at a scattering angle of $\theta^{\rm lab}_{\gamma'} = 131°$. Triple differential cross sections in the center of the proton quasi-free peak (PQFP) at $\theta^{\rm lab}_{\gamma'} = 149°$ were measured in the energy range from $E_\gamma = 200$ MeV to 290 MeV. The results were encouraging enough to carry out a dedicated experiment on quasi-free Compton scattering by the neutron (see also Section 5.2).

This dedicated experiment [118] was carried out using the experimental arrangement shown in Figure 14. Though the foregoing experiments had shown that the basis of the data-evaluation procedure is sound, this experiment was carried out in a self-testing way containing the following steps:
(i) The target-container was filled with liquid hydrogen so that Compton scattering by the free proton was measured in an energy range from $E_\gamma = 200$ to 400 MeV. The results of this experiment led to the following information. The asymptotic part of the spin-polarizability $\gamma_\pi^{(p)}$ is in agreement with the prediction obtained from the π^0, η and η' poles. Therefore, there is a good reason to use the corresponding prediction to calculate the spin-polarizability for the neutron, leading to $\gamma_\pi^{(n)} = 58.6$. This value was used as a fixed input for the evaluation of $\alpha_n - \beta_n$ from the quasi-free data. The other fixed input is $\alpha_n + \beta_n = 15.2 \pm 0.5$ [119] obtained via Baldin's sum rule from photo-absorption data. From the large

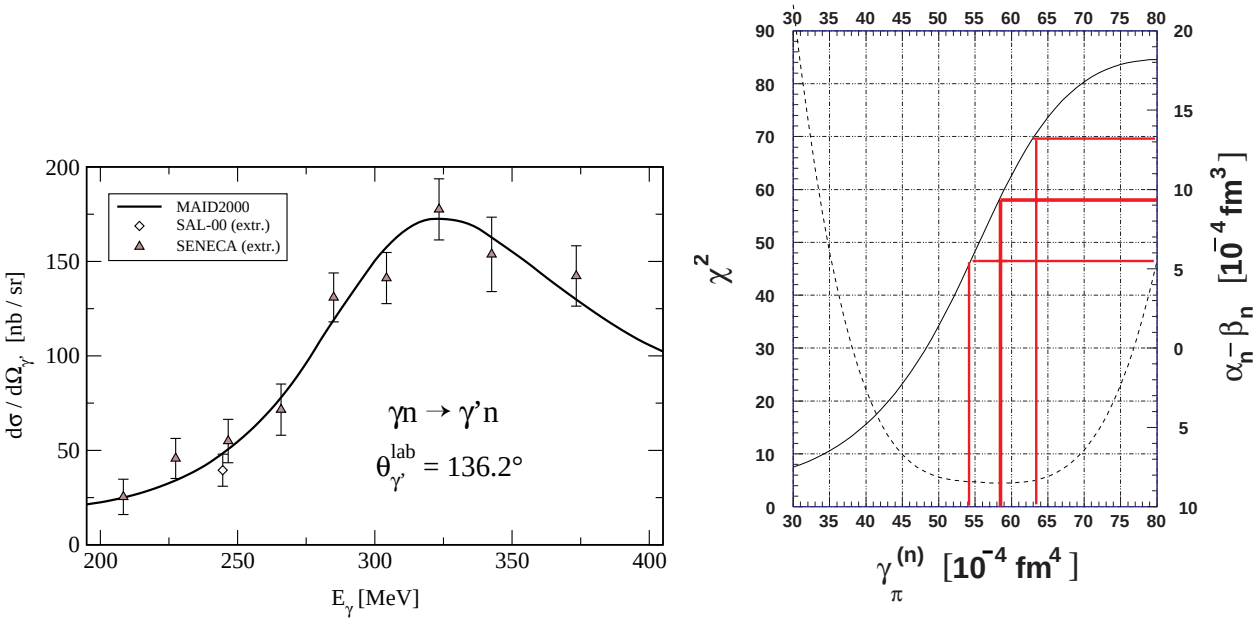

Figure 16: Results of the NaI-SENECA experiment on quasi-free Compton scattering on neutrons bound in the deuteron. Left panel: Differential cross-section for the "free" neutron extracted from the quasi-free cross-sections for the bound neutron at $\theta_\gamma^{\rm lab} = 136.2°$ (triangles). The SAL result [120] is shown by a diamond. Only statistical errors are given. Right panel: The solid curve shows pairs of values $\alpha_n - \beta_n$ and $\gamma_\pi^{(n)}$ used as independent parameters in fits to the experimental differential cross sections shown in the left panel of this figure. The corresponding χ^2 is depicted by the dashed line. The center horizontal and vertical bars correspond to the best fit obtained for $\gamma_\pi^{(n)} = 58.6$. The outer horizontal and vertical bars correspond to the statistical errors to be attributed to the best fits.

number of parameterizations of the photomeson amplitudes the MAID2000 parameterization led to the best overall agreement with the experimental differential cross-sections measured in this experiment for the free proton. This parameterization, therefore, served as the leading one in the data analysis. Other parameterizations which led to an almost equivalent quality of agreement were used to obtain information on the model error.

(ii) The target-container was filled with liquid deuterium so that "free" differential cross sections for Compton scattering by the proton and the neutron were obtained from quasi-free data. The "free" differential cross sections obtained for the proton were not in a complete agreement with the corresponding differential cross section for the free proton. But the agreement was good enough to justify the application of the theory of quasi-free Compton scattering in its present form for the data analysis and to use the remaining inconsistencies for an estimate of the model error. The measured "free" differential cross-sections extracted from quasi-free data on Compton scattering by the neutron is displayed in the left panel of Figure 16. There is consistency with the one existing SAL [120] data point. The fit to the data was obtained by keeping $\alpha_n + \beta_n = 15.2$ [119] and $\gamma_\pi^{(n)} = 58.6$ and the MAID2000 parameterization fixed and treating $\alpha_n - \beta_n$ as an adjustable parameter. The result obtained for the polarizability difference of the neutron obtained in this way is [118]

$$\alpha_n - \beta_n = 9.8 \pm 3.6({\rm stat})^{+2.1}_{-1.1}({\rm syst}) \pm 2.2({\rm model}). \tag{165}$$

Using $\alpha_n + \beta_n = 15.2 \pm 0.5$ obtained from the photo-absorption cross section [119] as a constraint we obtain

$$\begin{aligned} \alpha_n &= 12.5 \pm 1.8({\rm stat})^{+1.1}_{-0.6}({\rm syst}) \pm 1.1({\rm model}), \\ \beta_n &= 2.7 \mp 1.8({\rm stat})^{+0.6}_{-1.1}({\rm syst}) \mp 1.1({\rm model}). \end{aligned} \tag{166}$$

5.3.4 Coherent-elastic scattering of photons by deuterons

In-medium nucleon polarizabilities are an interesting field of research. Whereas in complex nuclei the interest is directed to the question whether or not the in-medium electromagnetic polarizabilities are the same as the free polarizabilities [36], for the deuteron no medium-modifications are expected because of the weak binding of the nucleons. Since the polarizabilities of the proton are known with comparatively good precision it may be expected that the neutron polarizabilities can be extracted from the isospin-averaged nucleon polarizabilities. The latter can be investigated in elastic Compton scattering experiments by deuterons. An advantage of this method is that the effect of the isospin-averaged polarizabilities is strongly enhanced in comparison with Compton scattering by free neutrons due to interference of the polarizability-dependent term with the Born term. This situation resembles that of Compton scattering by the free proton. The price we have to pay for the advantage is the necessity of taking into account the *np*-interaction in the intermediate state, meson exchange currents and two-body seagull amplitudes. All these effects introduce noticeable model dependencies in the extracted values of the polarizabilities. For details we refer the reader to [119, 121].

Differential cross sections for Compton scattering from the deuteron were measured at MAX-Lab (Lund) [121] for incident photon energies of 55 and 66 MeV at nominal laboratory angles of 45°, 125°, and 135°. Tagged photons were scattered from liquid deuterium into three NaI(Tl) spectrometers. By comparing the data with theoretical calculations in the framework of a one-boson-exchange model [119], the sum and the difference of the isospin-averaged nucleon polarizabilities, $\alpha_N + \beta_N = 17.4 \pm 3.7$ and $\alpha_N - \beta_N = 6.4 \pm 2.4$ have been determined. By combining the latter with the global-average value for $\alpha_p - \beta_p$ and using the predictions of the Baldin sum rule for the sum of the nucleon polarizabilities, the following values for the neutron electric and magnetic polarizabilities

$$\begin{aligned} \alpha_n &= 8.8 \pm 2.4(\text{total}) \pm 3.0(\text{model}), \\ \beta_n &= 6.5 \mp 2.4(\text{total}) \mp 3.0(\text{model}) \end{aligned} \tag{167}$$

have been obtained [121].

5.3.5 Summary on the experimental results for the electromagnetic polarizabilities of the neutron

Table 10: Electromagnetic polarizabilities of the neutron determined by three different methods and their weighted average. The unit is 10^{-4}fm^3

experimental method	polarizability
electromagnetic scattering [112]	$\alpha_n = 12.6 \pm 2.5$
quasi-free Compton scattering [118]	$\alpha_n = 12.5 \pm 2.3$
coherent Compton scattering [121]	$\alpha_n = 8.8 \pm 3.8$
weighted average	$\alpha_n = 11.9 \pm 1.5$
constrained by $\alpha_n + \beta_n = 15.2 \pm 0.5$	$\beta_n = 3.3 \mp 1.5$

Table 10 shows a summary of the experimental results obtained for the electromagnetic polarizabilities of the neutron. It is satisfactory that the three different methods led to results for α_n which are in agreement with each other within the given errors. It cannot be excluded that a recalculation of

Table 11: *Recommended* results for the electromagnetic polarizabilities of the neutron obtained from the Baldin sum rule constraint, from quasi-free Compton scattering and from electromagnetic neutron scattering. The unit is 10^{-4}fm^3.

α_n	β_n
12.5 ± 1.7	2.7 ∓ 1.8

the nuclear scattering amplitude of the deuteron which still is under discussion[6] may shift the coherent Compton scattering result [121] to some extent. Therefore, without further clarification we recommend to use the Baldin sum-rule constraint $\alpha_n + \beta_n = 15.2 \pm 0.5$ and the values for the electric polarizability from electromagnetic scattering and quasi-free Compton scattering of Table 10 to arrive at *recommended* values for the electromagnetic polarizabilities of the neutron as given in Table 11.

5.4 Spin polarizability of the neutron

In the frame of the invariant amplitudes and in frame of fixed-t dispersion theory, the backward spin polarizability is given by

$$\gamma_\pi = -\frac{1}{2\pi M}[A_2^{\text{int}}(0,0) + A_2^{\text{as}}(0,0) + A_5^{\text{int}}(0)] \tag{168}$$

with the integral parts being the smaller contribution. In case of fixed-t dispersion theory it is not granted that $A_2^{\text{as}}(t)$ is exhausted by the t-channel poles due to π^0, η and η' exchanges, though it has been shown for the proton that this is the case. Nevertheless, it may be of interest to find out whether or not the adopted quantity $\gamma_\pi^{(n)} = 58.6$ is the optimum for the data shown in the left panel of Figure 16. This investigation is carried out in the right panel of Figure 16. The main difference as compared to the analysis procedure described so far is that $\alpha_n - \beta_n$ and $\gamma_\pi^{(n)}$ are treated as free parameters when fitting the predicted Compton differential cross-section to the experimental "free" differential cross sections. In this way for each pair of values $\alpha_n - \beta_n$ and $\gamma_\pi^{(n)}$ a χ^2 was obtained which is shown by a dashed line in Figure 16. It is apparent that the adopted values $\alpha_n - \beta_n = 9.8$ and $\gamma_\pi^{(n)} = 58.6$ both are in line with the center of the rather broad χ^2 distribution. This means that this pair of data is supported by the experiment on quasi-free Compton scattering as evaluated here. According to Figure 16 it is also possible to attribute an experimental error to $\gamma_\pi^{(n)}$, leading to the number given in Table 12.

Table 12: *Recommended* experimental value for the spin polarizability of the neutron. The unit is 10^{-4}fm^4.

$\gamma_\pi^{(n)} = 58.6 \pm 4.0$

5.5 Compton scattering by the proton using the large acceptance arrangement LARA

For a long time dispersion theories for Compton scattering by the proton existed only for the Δ range. This restriction was overcome in the 1990's [68] when a non-subtracted dispersion theory at fixed-t

[6] Very recently the data have been re-evaluated in the framework of chiral effective field theory to next-to-leading order. The results obtained are $\alpha_n = 14.2 \pm 2.0(\text{stat}) \pm 1.9(\text{syst})$, $\beta_n = 1.8 \pm 2.2(\text{stat}) \pm 0.3(\text{syst})$ [122]. In [123] $1/2(\alpha_p + \alpha_n) = (13.0 \pm 1.9(\text{stat}))^{+3.9}_{-1.5}(\text{theory})$ was obtained.

was developed with an applicability extending through the second resonance region. This apparent success led to an experimental program at MAMI (Mainz) aimed to carry out a rigorous test of the predictions. In order to save beam time is was necessary to develop an apparatus with which large energy and angular ranges could be covered with one experimental set up. One essential difficulty of Compton scattering above π-threshold is that a very small rate of Compton scattered photons has to be identified in the presence of a large rate of photons from π^0 decay. Though the largest part of these

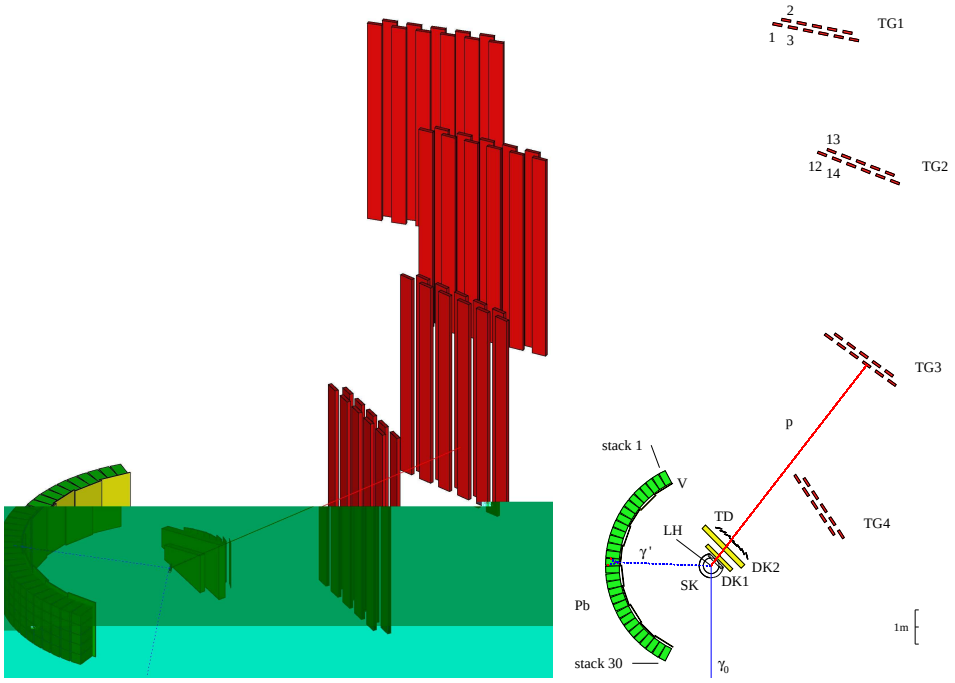

Figure 17: Perspective view (left panel) and vertical projection (right panel) of the LARA arrangement. The photon arm consists of 10 blocks of 3 (horizontal) $\times$ 5 (vertical) lead glass detectors (Pb), each block equipped with a 1 cm plastic scintillator (V). The proton arm consists of two wire chambers (DK1,DK2) at distances of 25 and 50 cm from the target center, 8 plastic scintillators serving as trigger detectors (TD) and 43 bars of 20 cm $\times$ 300 cm $\times$ 5 cm plastic scintillators serving as time-of flight (TOF) stop detectors. The scattering target consists of liquid H_2 contained in a 3 cm $\varnothing$ $\times$ 20 cm Kapton cylinder.

latter photons have a kinematics which is considerably different from the Compton kinematics, there is a sizable rate of photons from π^0 photoproduction which has an almost identical kinematics. These are those decays where one of the decay photons is emitted almost parallel to the direction of the π^0 velocity. In this case a high-energy photon is emitted with an energy almost equal to the energy of the Compton scattered photon. The only way to overcome this difficulty is to determined the kinematical variables of all particles with the highest possible precision. Before constructing a large acceptance arrangement several experiments were carried out where some of the experimental principles to be applied later were tested on a smaller scale [97, 124].

For the construction of the large acceptance arrangement LARA shown in Figure 17 [107,108] it had to be taken into account that one principal limitation is given by the angular straggling of the recoil protons which limits the angular resolution to about $\pm 0.5^\circ$ to $\pm 1^\circ$. Due to kinematics the angular spread of the Compton scattered photons is about twice that of the corresponding recoil protons. Therefore, a wall of lead glass photon-detectors was built with an angular resolution of about $\pm 2^\circ$ both in the horizontal and in the vertical direction. The trajectories of the recoil protons were determined

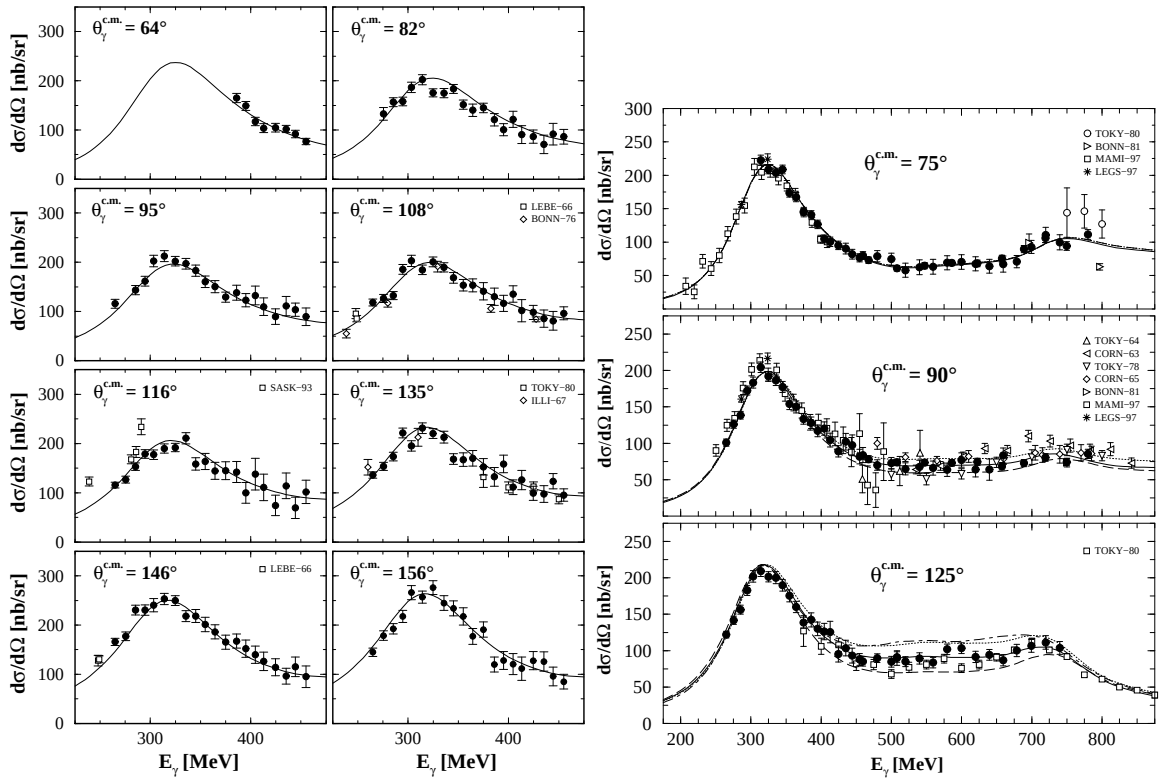

Figure 18: Left panel: Eight out of 24 measured energy distributions from $\theta_\gamma^{\rm c.m.} = 59°$ to 156° obtained with the LARA arrangement (•) in the first resonance range compared with predictions from dispersion theory. The previous data are taken from [125](LEBE-66); [126] (ILLI-67); [127] (BONN-76); [102] (SASK-93); [128] (TOKYO-80). Right panel: Differential cross sections for Compton scattering by the proton versus photon energy [107,108]. The three panels contain data corresponding to the c.m.-angles of 75°, 90° and 125°. The three curves are calculated for different mass parameters $m_{\rm eff} = 800$ MeV (upper), 600 MeV (center) and 400 MeV (lower). A good sensitivity to a variation of $m_{\rm eff}$ is observed at $\theta_\gamma^{\rm c.m.} = 125°$ with an optimum fit for $m_{\rm eff} = 589 \pm 12$ MeV.

by a pair of wire chambers with an angular resolution of better than 1°. The reaction point in the scattering target was determined in this way with a precision of about ±0.7 cm. The proton energies were determined via time-of-flight with flight paths ranging from 2.6 to 12.0 m, depending on the energies of the recoil protons. The energies of the incoming photons were fixed by tagging to about 2 MeV whereas the energy resolution of the lead glass detectors was poor. With this arrangement it was possible to measure differential cross sections for Compton scattering by the proton in the energy range $250 \lesssim E_\gamma \lesssim 800$ MeV and angular range $30° \lesssim \theta_\gamma^{\rm lab} \lesssim 150°$, with the exception of small scattering angles and small photon energies where the energies of the recoil protons were too small for an escape from the liquid hydrogen target.

Figure 18 shows a selection of Compton differential cross sections obtained by the LARA experiment. The experimental data are compared with the predictions of fixed-t dispersion theory [68] where the SAID-SM99K parameterization of photomeson amplitudes is used as a basis and the difference $\alpha_p - \beta_p$ measured at energies below meson photoproduction threshold is used as an external input. It is remarkable to note that in the Δ resonance range and for $\theta_\gamma^{\rm c.m.} = 75°$ also at higher energies, an excellent fit to the experimental data is obtained without any major effect of the scalar t-channel – or, in an other language – the effective σ pole. This proves that the basic concept of the fixed-t dispersion theory in the present form is correct. At $\theta_\gamma^{\rm c.m.} = 90°$ and 125° the differential cross sections show a sensitivity to the effective mass of the σ pole as discussed in Section 3.8. This sensitivity increases with

increasing scattering angle as expected. From the fit to the experimental differential cross sections it is possible to determine the effective mass leading to $m_{\rm eff} = 589 \pm 12$ MeV. This value obtained for the effective mass is in agreement with the prediction we obtained from our general knowledge about the σ meson (see Section 3.8). In spite of this apparent success of fixed-t dispersion theory an independent interpretation in terms of fixed-θ dispersion theory appears to us highly desirable.

6 Sum rules

6.1 The Baldin (BL) sum rule

Using (106) Baldin's sum rule (50) may be formulated in the form

$$\alpha + \beta = -\frac{1}{2\pi}[A^{\rm int}_{3+6}(0,0) + A^{\rm as}_{3+6}(0,0)], \tag{169}$$

with

$$A^{\rm int}_{3+6}(0,0) = \frac{2}{\pi}\int_{\nu_{\rm thr}}^{\nu_{\rm max}} {\rm Im}A_{3+6}(\nu',0)\frac{d\nu'}{\nu'} \tag{170}$$

$$A^{\rm as}_{3+6}(0,0) = \frac{2}{\pi}\int_{\nu_{\rm max}}^{\infty} {\rm Im}A_{3+6}(\nu',0)\frac{d\nu'}{\nu'}, \tag{171}$$

where $\nu_{\rm max}$ separates the sum of electromagnetic polarizabilities into an integral part and into an asymptotic part

$$\alpha + \beta = (\alpha + \beta)^{\rm int} + (\alpha + \beta)^{\rm as}. \tag{172}$$

Numbers may be found in the recent work of Wissmann [2] where the following results have been obtained

$$(\alpha_p + \beta_p)^{\rm int} = 12.6, \quad (\alpha_p + \beta_p)^{\rm as} = 1.2, \quad \text{for } \nu_{\rm max} = 1.5 \text{ GeV}, \tag{173}$$

$$(\alpha_p + \beta_p)^{\rm int} = 13.1, \quad (\alpha_p + \beta_p)^{\rm as} = 0.7, \quad \text{for } \nu_{\rm max} = 2.0 \text{ GeV}, \tag{174}$$

using a choice of $\nu_{\rm max}$ as proposed in [68]. Apparently, the asymptotic part of $(\alpha + \beta)_p$ is only of the order of $5 - 10\%$ of the integral part. This finding is partly responsible for the validity of Baldin's sum rule since deviations are expected only from the asymptotic part. An other essential point in connection with the validity of Baldin's sum rule is that $A^{\rm as}_{3+6}(0,0)$ is given by an integral along the real ν-axis and that there is no additional real part stemming from a non-vanishing contour integral or – in the language of fixed-θ dispersion theory – from a t-channel contribution. This follows from the discussion given in Section 2.7.1. According to this discussion it may be expected that the expression given in Eq. (171) is complete, since – in the forward direction – the candidate for a t-channel contribution, *viz.* the $f_2(1270)$ meson, is absorbed into the total photo-absorption cross section via vector meson dominance (VMD) together with the $a_2(1320)$ meson and the Pomeron. Predictions for $\alpha + \beta$ made on the basis of Eq. (169) are shown in Table 13. Of these, the predictions made by Olmos et al. [104] and Levchuk et al. [119] are based on recent sets of photo-absorption data. Furthermore they take into account the $\lesssim 1\%$ radiative decay channel of the total photoabsorption cross section. Therefore, we consider the averages of these two results as the adopted values, listed in the last line of Table 13.

Table 13: The Baldin sum rule evaluated from total photo-absorption cross sections. The adopted value is the weighted average of the data of Olmos(01) and Lvov(00). The unit is 10^{-4}fm^3.

Absorption-Exp.	$\alpha_p + \beta_p$	$\alpha_n + \beta_n$
Damashek(70) [129]	14.2 ± 0.3	
Lvov(79) [100]	14.2 ± 0.5	15.8 ± 0.5
Babusci(98) [54]	13.69 ± 0.14	14.40 ± 0.66
Olmos(01) [104]	13.8 ± 0.4	
Lvov(00) [119]	14.0 ± 0.3	15.2 ± 0.5
adopted value	13.9 ± 0.3	15.2 ± 0.5

Table 14: Experimental results for $\alpha_p + \beta_p$ obtained by measuring Compton scattering below meson photoproduction threshold without using the constraint from Baldin's sum rule in the data evaluation. The adopted value is equal to the weighted average. The unit is 10^{-4}fm^3.

Scattering-Exp.	$\alpha_p + \beta_p$
1950's–1990's [17]	14.0 ± 1.4
Olmos(01) [104]	13.1 ± 1.3
adopted value	13.6 ± 1.0

6.1.1 Experimental tests of the Baldin (BL) sum rule

Experimentally, the validity of the Baldin sum rule can be tested by measuring the electromagnetic polarizabilities α and β below the meson photoproduction threshold. The relevant experiments and the results obtained have been discussed in Section 5.1 and are summarized in Table 14. The numbers given as the adopted results in Tables 13 and 14, *viz.* $(\alpha_p + \beta_p)^{\text{absorption}} = 13.9 \pm 0.3$ and $(\alpha_p + \beta_p)^{\text{scattering}} = 13.6 \pm 1.0$ deviate from each other by not more than 30% of the standard deviation. We may consider this as a firm verification of the Baldin sum rule.

An interesting aspect of the Baldin sum rule has been discussed by Drechsel et al. [1] in the frame of fixed-θ dispersion theory. The structure of the two dispersion integrals shows that the integral part of the fixed-t dispersion theory at $t = 0$ and the s-channel part of fixed-θ dispersion theory at $\theta_s = \theta_{\text{lab}} = 0$ coincide. The number obtained for the s-channel part of $\alpha_p + \beta_p$ is

$$(\alpha_p + \beta_p)^s = 11.94, \quad \theta_{\text{lab}} = 0^\circ \quad \text{for } \nu_{\text{max}} = 1.5 \text{ GeV} \tag{175}$$

which indeed is not too much different form the fixed-t counterpart given in Eq. (173), but again the Baldin sum rule is not completely saturated at an energy of $\nu_{max} = 1.5$ GeV. In fixed-θ dispersion theory and at non-forward angles the $f_2(1270)$ meson is expected to contribute to $\alpha + \beta$ via the t-channel integral due to its direct coupling to two photons. Calculations of the t-channel integral have been found feasible [1] in the angular range between $\theta_{\text{lab}} = 100^\circ$ and 180°. The results obtained are summarized in Table 15. Unfortunately, the reason for the large deviation of the prediction from the experimental value of the Baldin sum rule shown in the 5th row of Table 15 has only been discussed qualitatively. As a test case for the validity of fixed-θ dispersion theory at large angles it would be highly desirable to investigate in what way Baldin's sum rule can be saturated.

Table 15: Fixed-θ dispersion theory prediction for $\alpha_p + \beta_p$. $(\alpha+\beta)_p^s$: s-channel contribution, $(\alpha+\beta)_p^t$: t-channel contribution, $(\alpha+\beta)_p^{(s+t)}$: total prediction, $(\alpha+\beta)_p^{\exp-(s+t)}$: deviation of prediction from the experimental value. The unit is 10^{-4}fm^3.

θ_{lab}	$(\alpha+\beta)_p^s$	$(\alpha+\beta)_p^t$	$(\alpha+\beta)_p^{(s+t)}$	$(\alpha+\beta)_p^{\exp-(s+t)}$
180°	7.52	3.28	10.80	3.1
140°	7.65	3.28	10.93	3.0
100°	8.13	3.28	11.41	2.5

6.2 The GDH sum rule

The GDH sum rule [60,61] relates the anomalous magnetic moment, κ, and mass, M, of the nucleon, i.e. static properties, to its dynamic observables, like the total absorption cross sections, $\sigma_{3/2,1/2}$, of circularly polarized real photons on longitudinally polarized nucleons in the two relative spin configurations, parallel (3/2) and antiparallel (1/2):

$$\int_{\nu_{\text{thr}}}^{\infty} (\sigma_{1/2}(\nu) - \sigma_{3/2}(\nu)) \frac{d\nu}{\nu} = -\frac{2\pi^2\alpha_e}{M^2}\kappa^2 = \begin{cases} -205\mu b, & \text{proton,} \\ -233\mu b, & \text{neutron.} \end{cases} \tag{176}$$

Here $\alpha_e = 1/137.04$ denotes the fine-structure constant and ν the photon energy. Since the dispersion theory has been tested through Compton scattering experiments to a high level of precision, the only crucial assumption in the dispersion theoretic approach applied to the Compton forward amplitude, is the *no-subtraction-hypothesis*. Furthermore, the energy dependence of the cross section in the two spin configurations gives important information for multipole analyses in the resonance region and for parameters of Regge models in the higher energy regime.

In connection with a possible violation of the GDH sum rule a fixed pole existing in the framework of Regge theory has been discussed in the literature. For sake of completeness we wish to summarize the essential features of these considerations here. Starting from invariant amplitudes we write the relevant dispersion integral in the following form

$$\text{Re}A_4(\nu, 0) = -\frac{\alpha_e\kappa^2}{4M\nu^2} + \frac{2}{\pi}\mathcal{P}\int_{\nu_{\text{thr}}}^{\infty} \frac{\nu' \text{Im}A_4(\nu', 0)}{\nu'^2 - \nu^2} d\nu'. \tag{177}$$

The existence of a fixed pole then implies that the l.h.s. of Eq. (177) converges to an asymptotic contribution in the form

$$A_4^{\text{as}}(\nu, t) = a_4(t)\nu^{-2} \tag{178}$$

where $a_4(t)$ is a real function of t. Using (178) and multiplying both sides of (177) with ν^2 we arrive at

$$a_4(0) = -\frac{\alpha_e\kappa^2}{4M} - \frac{2}{\pi}\int_{\nu_{\text{thr}}}^{\infty} \nu \text{Im}A_4(\nu, 0) d\nu. \tag{179}$$

in the limit $\nu \to \infty$. Using the unitarity condition

$$\text{Im}A_4(\nu, 0) = \frac{M}{16\pi\nu^2}\left(\sigma_{1/2}(\nu) - \sigma_{3/2}(\nu)\right) \tag{180}$$

we arrive at a generalized GDH sum rule in the form

$$\int_{\nu_{\text{thr}}}^{\infty} \frac{\sigma_{1/2}(\nu) - \sigma_{3/2}(\nu)}{\nu} d\nu = -\frac{2\pi\alpha_e\kappa^2}{M^2} - \frac{8\pi^2}{M}a_4(0). \tag{181}$$

The generalized GDH sum rule (181) allows an under-fulfillment or over-fulfillment of the GDH sum rule depending on the the sign of $a_4(0)$. Indeed, a first evaluation of the GDH sum rule [94] led to deviations from the GDH prediction which appeared to be isovector, i.e. different in sign for the proton and the neutron. This evaluation was based on photomeson amplitudes measured without polarization and estimated corrections for double-pion photoproduction. Later on this first evaluation was confirmed by several authors [130] and lead to results ranging between -289 and -257 μb, and between -189 and -169 μb, for the proton and neutron, respectively, where – in absolute numbers – the proton results were much larger and the neutron results much smaller than the GDH integral predictions given in Eq. (176). These findings on the basis of experimental data led to several investigations of the possible origin of these deviations from the theoretical value of the GDH integral [131]. In these investigation a fixed $J = 1$ pole entering into Regge phenomenology as well as current algebra arguments were taken into consideration. These speculations provided part of the motivation to measure the GDH sum rule with circularly polarized photons and spin-polarized nucleons. An other part was provided by the desire to get a better understanding of the spin-structure of the nucleon.

6.2.1 Verification of the GDH sum rule

The GDH integrand on the l.h.s. of Eq. (176) was determined at two electron accelerators. While the measurement from 0.2 to 0.8 GeV was carried out at MAMI [132–134], the energy range from 0.68 to 2.9 GeV was covered at the electron stretcher ring ELSA [135, 136]. In total the range from the resonance region up to the Regge regime was covered. This range is wide enough to reliably make conclusions on the validity of the GDH sum rule for the first time. Only the ranges from 0.14 – 0.20 GeV and $>$ 2.9 GeV had to be covered using model predictions. For the photon energies below 0.20 GeV the unitary isobar model MAID2002 gives a contribution of (-27.5 $\pm$ 3) μb [137]. Above 2.9 GeV the Regge approach of Ref. [87] gives -14 μb while the prediction of Ref. [138] is -13 μb. The results

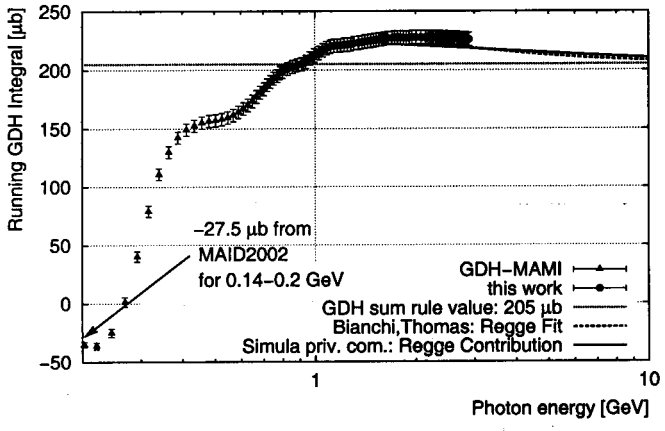

Figure 19: Running GDH integral, I_{GDH}, for the proton up to 2.9 GeV. Error bars indicate statistical errors only. $I_{\mathrm{GDH}}(\omega) = \int_{\nu_{\mathrm{thr}}}^{\omega} (\sigma_{3/2}(\nu) - \sigma_{1/2}(\nu)) d\nu/\nu$ with ω being the photon energy is shown on the abscissa.

of the MAMI – ELSA series of experiments are shown in Figure 19 and Table 16. The experimental running GDH-integral clearly overshoots the value predicted by the GDH sum rule even when the reduction due to the negative contribution of the range 0.14–0.20 GeV is taken into account. However, there is a tendency visible of a decrease of the GDH integral beyond 2 GeV, which is supported by the predictions from Regge theory [87, 138]. Taking the predicted high-energy extrapolation into account

Table 16: Measured values of the GDH integral for the proton $I_{\rm GDH}$ and model predictions for the unmeasured ranges.

	E_γ [GeV]	$I_{\rm GDH}$ [μ b]
MAID2002 [137]	0.14-0.20	-27.5 $\pm$ 3
measured (GDH-Collaboration)	0.20-2.90	254 $\pm$ 5 $\pm$ 12
Bianchi and Thomas [87]	> 2.9	-14
Simula et al. [138]	> 2.9	-13
GDH integral	$0.14 - \infty$	≈ 213
GDH sum rule	$\nu_{\rm thr} - \infty$	205

the remaining difference $213\mu b - 205\mu b = 8\mu b$ is well below the estimated error $\approx \pm 13\mu b$ so that the tentative conclusion is allowed that the GDH sum rule has been confirmed for the proton.

6.3 The Lvov-Nathan sum rule

The Lvov-Nathan sum rule [67] uses the fixed-angle $\theta = \pi$ sum rule to make predictions for the backward spin polarizability γ_π. For the non-Born part of the relevant amplitude

$$\tilde{A}_2(s,u,t,) \equiv A_2(s,u,t) + \left(1 - \frac{t}{4M^2}\right) A_5(s,u,t) \tag{182}$$

we obtain

$$\begin{aligned} \tilde{A}_2^{\rm NB}(s,u,t,) &= \frac{1}{\pi}\mathcal{P}\int_{s_0}^{\infty}\left(\frac{1}{s'-s}+\frac{1}{s'-u}-\frac{1}{s'}\right){\rm Im}_s\tilde{A}_2(s',u',t')ds' \\ &+ \frac{1}{\pi}\mathcal{P}\int_{t_0}^{\infty}{\rm Im}_t\tilde{A}_2(s',u',t')\frac{dt'}{t'-t}, \end{aligned} \tag{183}$$

where

$$s'+u'+t' = 2M^2 \quad \text{and} \quad s'u' = M^4. \tag{184}$$

When $s = u = M^2$ and $t = 0$, these integrals determine the backward spin polarizability of the nucleon

$$\gamma_\pi \equiv \frac{\tilde{A}_2^{\rm NB}(M^2,M^2,0)}{2\pi M} = \gamma_\pi^s + \gamma_\pi^t, \tag{185}$$

where

$$\gamma_\pi^s = -\frac{1}{2\pi^2 M}\int_{s_0}^{\infty}\frac{s'+M^2}{s'-M^2}{\rm Im}_s\tilde{A}_2(s',u',t')\frac{ds'}{s'}, \tag{186}$$

$$\gamma_\pi^t = -\frac{1}{2\pi^2 M}\int_{t_0}^{\infty}{\rm Im}_t\tilde{A}_2(s',u',t')\frac{dt'}{t'}. \tag{187}$$

6.3.1 The s-channel part of the LN sum rule

We now replace the Mandelstam variables by the photon energy ω in the lab frame and the imaginary part of scattering amplitudes by the appropriate photoabsorption cross sections. This is achieved by

using the relation derived for $\mathrm{Im}g_\pi(\omega)$ in Eq. (62) and by using the relation between $g_\pi(\omega)$ and $\tilde{A}_2$ derived in Eq. (104). For the Mandelstam variable we obtain the replacement

$$s' = m^2 + 2m\omega. \tag{188}$$

Then, after some calculation we arrive at [67]

$$\gamma_\pi^s = \int_{\omega_0}^{\infty} \frac{d\omega}{4\pi^2\omega^3}\sqrt{1+\frac{2\omega}{M}}\left(1+\frac{\omega}{M}\right)\sum_n P_n[\sigma_{3/2}^n(\omega)-\sigma_{1/2}^n(\omega)] \tag{189}$$

with

$$\sum_n P_n[\sigma_{3/2}^n(\omega)-\sigma_{1/2}^n(\omega)] = \left\{\left(\sigma_{1/2}(\omega,\Delta P=\text{yes})-\sigma_{1/2}(\omega,\Delta P=\text{no})\right)-(1/2\to 3/2)\right\}. \tag{190}$$

The dominant contribution to γ_π^s comes from single-pion photoproduction, $\gamma N\to\pi N$, which yields the cross section (see Eq. (62) and [67])

$$\sum_n P_n[\sigma_{3/2}^n(\omega)-\sigma_{1/2}^n(\omega)]^{\pi N} = 8\pi\frac{q}{k}\sum_{l=0}^{\infty}(-1)^l(l+1)\left\{|A_{l+}|^2-|A_{(l+1)-}|^2-\frac{l(l+2)}{4}(|B_{l+}|^2-|B_{(l+1)-}|^2)\right\}. \tag{191}$$

where $q=|\mathbf{q}|$ and $k=|\mathbf{k}|$ are the momenta of the pion and photon in the c.m. system, respectively. Here a sum over channels with charged and neutral pions is implied, where $A_{l\pm}$ and $B_{l\pm}$ are the standard Walker photoproduction multipoles [55].

6.3.2 The t-channel part of the LN sum rule

Each pseudoscalar meson M makes a contribution [67]

$$\tilde{A}_2^M(t) = \frac{g_{MNN}F_{M\gamma\gamma}}{t-m_M^2-i0}\tau_M \tag{192}$$

to the amplitude entering into Eq. (187). Here g_{MNN} is the meson-nucleon coupling constant and $F_{M\gamma\gamma}$ the constant of the two-photon decay of the meson. The isospin factor τ_M is either 1 or τ_3 for isoscalar and isovector mesons, respectively. Making use of the symbolic equality

$$\frac{1}{x-i0} = \mathcal{P}\frac{1}{x}+i\pi\delta(x) \tag{193}$$

we arrive at

$$\gamma_\pi^{(M)} = -\frac{\tilde{A}_2^M(0)}{2\pi M} = \frac{g_{MNN}F_{M\gamma\gamma}}{2\pi m_M^2 M}\tau_M. \tag{194}$$

For the further discussion of γ_π^t we refer to the paper of L'vov and Nathan [67].

6.3.3 Comparison between theory and experiment

Table 17 summarizes the results obtained for the backward spin polarizabilities of proton and neutron in comparison with the LN sum rule predictions. The experimental results have been obtained from the invariant amplitudes adjusted to the experimental Compton differential cross sections using the formula

$$\gamma_\pi(\text{fixed}-t) = -\frac{1}{2\pi M}\tilde{A}_2^{\mathrm{NB}}(0,0) = -\frac{1}{2\pi M}\left[A_2^{\mathrm{NB}}(0,0)+A_5^{\mathrm{NB}}(0,0)\right] \tag{195}$$

where NB denotes the non-Born part of the scattering amplitude. During the adjustment procedure the photo-absorption cross sections as calculated from the pion photoproduction data and the difference $\alpha - \beta$ of electromagnetic polarizabilities obtained from low-energy Compton scattering experiments have been kept constant, whereas the spin-polarizability $\gamma_\pi(\text{fixed} - t)$ has been used as an adjustable parameter. In fixed-t dispersion theory the non-Born part of the amplitude is a superposition of an integral part and an asymptotic part

$$\tilde{A}_2^{\rm NB}(\nu, t) = \tilde{A}_2^{\rm int}(\nu, t) + \tilde{A}_2^{\rm as}(\nu, t) \tag{196}$$

where the integral part can be calculated from pion photoproduction data alone, whereas the asymptotic

Table 17: Experimental results obtained for the backward spin-polarizabilities of proton and neutron compared with predictions from the LN sum rule. The unit is 10^{-4}fm^4

spin polarizabilities	proton	neutron	
$\gamma_\pi(\text{fixed} - t)$	-38.7 ± 1.8	$+58.6\pm4.0$	experiment [110, 118]
$\gamma_\pi\text{fixed} - \theta$	-39.5 ± 2.4	$+52.5\pm2.4$	sum rule [67]
$\gamma_\pi^t \equiv \gamma_\pi^{\rm as}$	-46.6	$+43.4$	$\pi^0 + \eta + \eta'$ -poles [67]
$\gamma_\pi^{\rm int}$	$+7.9 \pm 1.8$	$+15.2\pm 4.0$	experiment [110, 118]
γ_π^s	$+7.1 \pm 1.8$	$+9.1\pm 1.8$	sum rule [67]

part is not exactly known. However, it may be assumed that this part is essentially given by the pseudoscalar poles which are expected to exhaust the t-channel of fixed-θ dispersion theory. This contribution to γ_π is given by

$$\gamma_\pi^t = \frac{1}{2\pi M}\left[\frac{g_{\pi NN}F_{\pi^0\gamma\gamma}}{m_{\pi^0}^2}\tau_3 + \frac{g_{\eta NN}F_{\eta\gamma\gamma}}{m_\eta^2} + \frac{g_{\eta' NN}F_{\eta'\gamma\gamma}}{m_{\eta'}^2}\right]. \tag{197}$$

In Table 17 the numbers in line 2 and 3 represent the spin-polarizabilities obtained from the experimental Compton differential cross sections on the basis of fixed-t dispersion theory and the LN sum-rule prediction, respectively. For the proton the agreement of the two different results is well within the errors, whereas for the neutron the difference of the two results is of the order of the errors. It has to be kept in mind, that for the neutron the experimental result for $\gamma_\pi(\text{fixed} - t)$ has a comparatively large error so that the major part of the conclusions has to rest on the proton data. The numbers in line 4 represent the t-channel results as obtained from the pseudoscalar poles, where it has been assumed that these numbers coincide with the asymptotic contributions entering into fixed-t dispersion theory. Subtracting the numbers in line 4 from the corresponding numbers in lines 2 and 3, we arrive at the numbers in line 5 and 6, respectively.

The conclusions to be drawn from Table 17 are the following. The LN sum rule has been shown to be fulfilled with good precision and there is no major difference between γ_π^t as entering into fixed-θ dispersion theory and $\gamma_\pi^{\rm as}$ as entering into fixed-t dispersion theory. This result is nontrivial because γ_π^t has been calculated from the LN sum rule and $\gamma_\pi^{\rm as}$ has been obtained by adjustments to experimental data by using this quantity as the adjustable parameter. This finding contrasts with the findings made in the following subsection in connection with the t-channel and asymtotic contributions in case of the BEFT sum rule.

6.4 The Bernabeu-Ericson-FerroFontan-Tarrach sum rule

The BEFT sum rule [65,66,139–142] may be derived from the non-Born part of the invariant amplitude

$$\tilde{A}_1(s,u,t) \equiv A_1(s,u,t) - \frac{t}{4M^2} A_5(s,u,t) \tag{198}$$

by applying the fixed-θ dispersion relation for $\theta = 180^\circ$ ($a = 0$). Then we arrive at

$$\begin{aligned} \tilde{A}_1(s,u,t) &= \frac{1}{\pi}\mathcal{P}\int_{s_0}^{\infty}\left(\frac{1}{s'-s}+\frac{1}{s'-u}-\frac{1}{s'}\right)\mathrm{Im}_s\tilde{A}_1(s',u',t')ds' \\ &+ \frac{1}{\pi}\mathcal{P}\int_{t_0}^{\infty}\mathrm{Im}_t\tilde{A}_1(s',u',t')\frac{dt'}{t'-t}\ , \end{aligned} \tag{199}$$

where $s_0 = (M+m_\pi)^2$, $t_0 = 4m_\pi^2$, $s'+u'+t' = 2M^2$ and $s'u' = M^4$. Using

$$\alpha - \beta = -\frac{1}{2\pi}\tilde{A}_1(M^2,M^2,0) = (\alpha-\beta)^s + (\alpha-\beta)^t \tag{200}$$

we arrive at

$$(\alpha-\beta)^s = -\frac{1}{2\pi^2}\int_{s_0}^{\infty}\frac{s'+M^2}{s'-M^2}\mathrm{Im}_s\tilde{A}_1(s',u',t')\frac{ds'}{s'}\ , \tag{201}$$

$$(\alpha-\beta)^t = -\frac{1}{2\pi^2}\int_{t_0}^{\infty}\mathrm{Im}_t\tilde{A}_1(s',u',t')\frac{dt'}{t'}. \tag{202}$$

6.4.1 The s-channel part of the BEFT sum rule

Using the relation for f_π derived in Eq. (103) and the relation for $\mathrm{Im}f_\pi$ derived in Eq. (61) we arrive at

$$(\alpha-\beta)^s = \frac{1}{2\pi^2}\int_{m_\pi+\frac{m_\pi^2}{2M}}^{\infty}\sqrt{1+\frac{2\omega}{M}}\left[\sigma(\Delta P = \text{yes}) - \sigma(\Delta P = \text{no})\right]\frac{d\omega}{\omega^2}. \tag{203}$$

This integral contains the s-channel part of the BEFT sum rule in terms of quantities which are convenient for calculations. The main contribution to $(\alpha-\beta)^s$ comes from the photoproduction of πN states. For these states, the cross-section difference can be expressed in terms of the standard CGLN amplitudes via [52]

$$\begin{aligned} \left[\sigma(\Delta P = \text{yes}) - \sigma(\Delta P = \text{no})\right]^{\pi N} &= 4\pi\frac{q}{k}\sum_{k=0}^{\infty}(-1)^k(k+1)^2\Big\{(k+2)\left(|E_{k+}|^2 - |M_{(k+1)-}|^2\right) \\ &\quad +k\left(|M_{k+}|^2 - |E_{(k+1)-}|^2\right)\Big\}^{\pi N}, \end{aligned} \tag{204}$$

where $q = |\mathbf{q}|$ and $k = |\mathbf{k}|$ are the pion and photon momenta in the c.m. system, respectively.

6.4.2 The t-channel part of the BEFT sum rule

The imaginary part of the amplitude $\tilde{A}_1$ in the t-channel can be found using the general unitarity relation

$$\mathrm{Im}_t T(\gamma\gamma \to N\bar{N}) = \frac{1}{2}\sum_n (2\pi)^4\delta^4(P_n - P_i)T(\gamma\gamma\to n)T^*(N\bar{N}\to n), \tag{205}$$

where the sum on the right-hand side is taken over all allowed intermediate states n having the same total 4-momentum as the initial state. In the following we restrict ourselves to two-pion intermediate states, i.e. $n = \pi\pi$.

The amplitudes $T(\gamma\gamma \to \pi\pi)$ and $T(\pi\pi \to \bar{N}N)$ are constructed making use of available experimental information on two different reactions. For the amplitude $T(\gamma\gamma \to \pi\pi)$ this is the two-photon fusion reaction $\gamma\gamma \to \pi\pi$. Since there are no data on the reaction $\pi\pi \to \bar{N}N$, the amplitude $T(\pi\pi \to \bar{N}N)$ is constructed in a dispersive approach using the well known amplitudes of the pion-nucleon scattering reaction $\pi N \to N\pi$. At $t > m_\pi^2$ unitarity shows that the phases of the amplitudes $T(\gamma\gamma \to \pi\pi)$ and $T(\pi\pi \to \bar{N}N)$ are the same and equal to the phases of pion-pion scattering, δ_I^J, which are known from the data on the reaction $\pi p \to p\pi\pi$.

The phase-dependent factor entering into the amplitude of a narrow resonance is described by a Breit-Wigner curve, whereas for the present case of a very broad resonance as given by the functions $\delta_I^J(t)$, a generalized version of the Breit-Wigner curve has to be used. This generalized phase-dependent factor is given by the Omnès [143] function $\Omega_I^J(t)$ defined through

$$\Omega_I^J(t) = \exp\left[\frac{t}{\pi}\int_{4m_\pi^2}^{\infty} dt' \frac{\delta_I^J(t')}{t'(t'-t-i0)}\right] \equiv e^{i\delta_I^J(t)} \exp\left[\frac{t}{\pi}\mathcal{P}\int_{4m_\pi^2}^{\infty} \frac{\delta_I^J(t')dt'}{t'(t'-t)}\right], \tag{206}$$

where use is made of Eq. (193). For the discussion, it is helpful to know that for a narrow resonance with infinitesimal width Γ the Omnès function can be written in the form

$$\Omega(t) = \frac{m^2}{m^2 - t - im\Gamma}, \tag{207}$$

where $m^2 = t(\delta = \pi/2)$ is the "bare mass" of the resonance. This means that for small Γ the Omnès function has the structure of a pole located on the t-axes at a position where the phase is equal to $\delta = \pi/2$. For energies far below the resonance energy, i.e. $t \ll m^2$, the Omnès function is only slightly dependent on t. Note that according to Eq. (207) $\Omega(0) = 1$. In the general case the Omnès function retains the essential parts of these properties. Instead of the Omnès function in most treatments the function $D_I^J(t) = 1/\Omega_I^J(t)$ is in use. The procedure of taking into account the $\pi\pi$ phase relation is based on dispersion relations termed the N/D method (see e.g. [58]).

For the discussion of the properties of the $T(\pi\pi \to \bar{N}N)$ amplitude in the unphysical region $4m_\pi^2 \leq t \leq 4M^4$ we use the backward amplitude $F^{(+)}(t)$ discussed by Bohannon [144]. For the pion scattering process the quantity t is negative, whereas for positive t the analytic continuation of $F^{(+)}(t)$ describes the $N\bar{N} \to \pi\pi$ annihilation process for the case that the helicities of the nucleon and the antinucleon are the same, $\lambda = \bar{\lambda}$. This provides us with a tool to construct the $N\bar{N} \to \pi\pi$ amplitude from the measured $\pi N \to \pi N$ amplitude. Since the backward $\pi N \to N\pi$ scattering amplitude implies also backward $N\bar{N} \to \pi\pi$ annihilation, it can be shown that the first two terms of the expansion for $F^{(+)}(t)$ at positive t are

$$F^{(+)}(t) = \frac{16\pi}{M(4M^2 - t)} f_+^0(t) - \frac{5\pi(t - 4m_\pi^2)}{M} f_+^2(t). \tag{208}$$

The amplitudes $f_+^J(t)$ are the partial wave amplitudes introduced by Frazer and Fulco [145], where J denotes the angular momentum of the $\pi\pi$ intermediate state. The + sign denotes that the two helicities λ and $\bar{\lambda}$ of N and $\bar{N}$, respectively, are the same, $\lambda = \bar{\lambda}$. The construction of these amplitudes follows the standard N/D procedure which is described at many places (see e.g. [58]).

The construction of both amplitudes, $T(\gamma\gamma \to \pi\pi)$ and $T(\pi\pi \to \bar{N}N)$, in connection with the scalar-isoscalar t-channel of Compton scattering has first been described and worked out in some detail

by Köberle [50] and later discussed by several authors, of whom we wish to cite [1, 52, 80, 146, 147]. For a very broad resonance the appropriate ansatz reads

$$F^J_{I\lambda}(t) = \Omega^J_I(t) P^J_{I\lambda}(t). \tag{209}$$

where $P^J_{I\lambda}(t)$ is a real amplitude in the $\gamma\gamma \to \pi\pi$ physical region and $\Omega^J_I(t)$ the phase-dependent Omnès function discussed above. In (209) I is the isospin of the transition, J the angular momentum and $\lambda \equiv \Lambda^t_{\gamma\gamma}$ the helicity difference of the two photons. In the present case we have $\lambda \equiv \Lambda^t_{\gamma\gamma} \equiv 0$, so that we can omit the index λ without loss of generality.

The amplitudes $F^J_I(t)$ have to be constructed such that they have the correct low-energy properties, reproduce the cross section of the photon fusion reaction $\gamma\gamma \to \pi\pi$ and incorporate the phases $\delta^J_I(t)$ [78, 148–151]. For $J = 0$ the following form of Eq. (209) has been obtained [52, 147]:

$$\begin{aligned} F^0_I(t) &= \Omega^0_I(t)\Big\{ \Big[F^{B,0}_I(t) + \Delta F^0_I(t)\Big] \mathrm{Re}\frac{1}{\Omega^0_I(t)} - \frac{t^2}{\pi}\Big[\mathcal{P}\int_{4m_\pi^2}^{\infty} [F^{B,0}_I(t') + \Delta F^0_I(t')]\mathrm{Im}\frac{1}{\Omega^0_I(t')}\frac{dt'}{t'^2(t'-t)} \\ &+ A^0_I + tB^0_I\Big]\Big\}. \end{aligned} \tag{210}$$

The expression in Eq. (210) is given for the s-wave amplitude where contributions going beyond the Born approximation have been taken into account. The leading term in (210) is a superposition of a Born term, $F^{B,0}_I(t)$, and a pion-structure dependent correction, $\Delta F^0_I(t)$. Since the reactions $\gamma\gamma \to \pi^+\pi^-, \pi^-\pi^+, \pi^0\pi^0$ show up with two components having isospin $I = 2$ and one component having $I = 0$ we have to take into account these two isospins with the appropriate weights (see e.g. [152]):

$$\begin{aligned} F_{I=0} &= F^C + \frac{1}{2}F^N \\ F_{I=2} &= F^C - F^N \end{aligned} \tag{211}$$

where F^C is the charged and F^N the neutral component.

For both isospin values, $I = 0$ and $I = 2$, the Born terms are

$$F^{B,0}_0(t) = F^{B,0}_2(t) = 2e^2\frac{1-v^2}{v}\frac{1}{2}\ln\frac{1+v}{1-v}, \tag{212}$$

where v is the pion velocity. At low energies, the pion-structure dependent corrections can be expressed through the electromagnetic polarizabilities of the pions in the form

$$\begin{aligned} \Delta F^0_0(t) &= 2\pi m_\pi t[(\alpha_{\pi^\pm} - \beta_{\pi^\pm}) + \frac{1}{2}(\alpha_{\pi^0} - \beta_{\pi^0})], \\ \Delta F^0_2(t) &= 2\pi m_\pi t[(\alpha_{\pi^\pm} - \beta_{\pi^\pm}) - (\alpha_{\pi^0} - \beta_{\pi^0})]. \end{aligned} \tag{213}$$

The last term $A^0_I + tB^0_I$ has been introduced to represent those contributions to $F^0_I(t)$ which go beyond the Born + pion-polarizability approximation. They are constructed in a way (i) that general constraints available for the amplitude $F^0_I(t)$ are fulfilled and (ii) that experimental data [153,154] on the total cross sections of the reactions $\gamma\gamma \to \pi^+\pi^-$ and $\gamma\gamma \to \pi^0\pi^0$ are fitted. The amplitude $F^2_0(t)$ is constructed analogously.

The amplitudes of interest for the prediction of $(\alpha - \beta)^t$ are the S-wave amplitude $F^0_0(t)$ and the D-wave amplitude $F^2_0(t)$ with the D-wave amplitude leading to only a small correction. It, therefore, is appropriate to restrict the discussion mainly to the amplitude $F^0_0(t)$. The essential property of this amplitude is provided by the Omnès function which introduces a zero crossing of the amplitude at about

570 MeV. This zero crossing may be considered as a manifestation of that part of the σ meson which shows up through phase-shift $\delta_0^0(t)$ of the correlated $\pi\pi$ pair.

If we restrict ourselves in the calculation of the t-channel absorptive part to intermediate states with two pions with angular momentum $J \leq 2$, the sum rule (202) takes the convenient form for calculations [66]:

$$(\alpha-\beta)^t = \frac{1}{16\pi^2}\int_{4m_\pi^2}^{\infty}\frac{dt}{t^2}\frac{16}{4M^2-t}\left(\frac{t-4m_\pi^2}{t}\right)^{1/2}\Big[f_+^0(t)F_0^{0*}(t) - \left(M^2-\frac{t}{4}\right)\left(\frac{t}{4}-m_\pi^2\right)f_+^2(t)F_0^{2*}(t)\Big], \quad (214)$$

where $f_+^{(0,2)}(t)$ and $F_0^{(0,2)}(t)$ are the partial-wave helicity amplitudes of the processes $N\bar{N} \to \pi\pi$ and $\pi\pi \to \gamma\gamma$ with angular momentum $J = 0$ and 2, respectively, and isospin $I = 0$.

6.4.3 Test of the BEFT sum rule

Though being the first who published the BEFT sum rule in its presently accepted form, Bernabeu and Tarrach [66] were not aware of the appropriate amplitudes to calculate this sum rule numerically. Also the first calculation of Guiasu and Radescu [139] remained incomplete because the amplitudes were used in the form of their Born approximation and, as the major drawback, the correlation of pions was not taken into account. Table 18 summarizes those results of tests of the BEFT sum rule where at least

Table 18: Numerical evaluation of the BEFT sum rule, with corrections a) and b) supplemented by the present author. The unit is 10^{-4}fm^3.

$(\alpha_p-\beta_p)^s$	$(\alpha_p-\beta_p)^t$	$(\alpha_p-\beta_p)^{\rm BEFT}$	authors
-4.92	$+9.28^{a)}$	$+4.36$	Guiasu, Radescu,1978 [140]
-4	$+10.4^{b)}$	$+6.4$	Budnev, Karnakov, 1979 [141]
-5.42	$+8.6$	$+(3.2^{+2.4}_{-3.6})$	Holstein,Nathan,1994 [142]
-5.56	$+16.46$	$+(10.7\pm0.2)^{c)}$	Drechsel,Pasquini, Vanderhaeghen,2003 [1]
$-(5.0\ \pm1.0)$	$+\ (14.0\ \pm\ 2.0)$	$+\ (9.0\pm2.2)$	Levchuk, et al. [52]

a) corrected for the D-wave contribution (-1.7) included. In an earlier work Guiasu and Radescu [139] used the Born approximation without $\pi\pi$ correlation for both amplitudes $N\bar{N} \to \pi\pi$ and $\pi\pi \to \gamma\gamma$ and arrived at $(\alpha-\beta)^t = +17.51$.
b) correction for the polarizability of the pion ($+3.0$) included.
c) best value from a range of results given by the authors [1].

the $\pi\pi$ correlation is taken into account. In the early works of Guiasu and Radescu [140] and Budnev and Karnakov [141] some missing pieces in the results were identified which are supplemented in Table 18 on the basis of the results given by Holstein and Nathan [142]. In case of the Holstein and Nathan result [142] we interpret the estimated upper and lower bounds as errors. In case of the Drechsel et al. result [1] we quote the s-channel and t-channel contributions calculated at $\theta = 180°$. The total result $(\alpha_p-\beta_p)^{\rm BEFT}$ is the best value for this quantity extracted by the authors from results obtained in the angular region $140° \leq \theta_{\rm lab} \leq 180°$. The result obtained in [147] (see Figure 20) confirmes the result of Holstein and Nathan [142] when using using a cut-off in the integration in (214) at $t = 30m_\pi^2$.

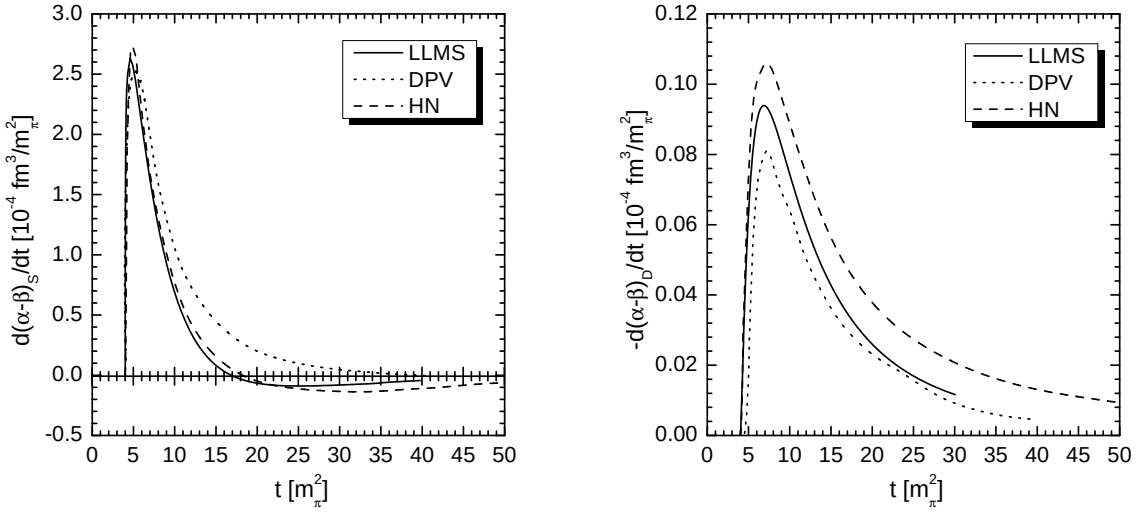

Figure 20: Left panel: The integrand for the t-channel S-wave contribution to $\alpha - \beta$ as given by a recent calculation [147] (solid: LLMS), Ref. [142] (dashed: HN), and Refs. [1,80] (dotted: DPV). Right panel: Same for the t-channel D-wave contribution. Units are $10^{-4}\text{fm}^3/m_\pi^2$. The dotted curve in the left panel may be considered as an upper limit the dashed curve as a lower limit of a band of possible results [52].

There is consistency between the five results as far as the s-channel contribution is concerned but an apparent discrepancy in case of the t-channel between the results of Holstein and Nathan [142] on the one hand and of Drechsel et al. [1] on the other. In order to find an explanation for this discrepancy we extended the calculation of [147] where a cut-off in the integration in (214) at $t = 30m_\pi^2$ was used by a more complete calculation. This investigation showed that the available data to be used as input are not very precise and lead to large differences in the predictions for $(\alpha - \beta)^t$. The curves obtained for $d(\alpha - \beta)_S/dt$ were located in a broad band between the dotted curve and the dashed curve shown in the left panal of Figure 20. Nevertheless, is appears possible to give a tentative result for the t channel part of the BEFT sum rule prediction in the form $(\alpha - \beta)^t = 14.0 \pm 2.0$. This result is in agreement with the result of Drechsel et al. [1] but has a considerably larger error. We will use the results given in line 6 of Table 18 in the further discussion.

6.4.4 Summary on predicted information on $\alpha - \beta$ compared with the experimental result

In the foregoing the BEFT sum rule has been discussed making predictions for the s-channel part, $(\alpha - \beta)^s$, and the t-channel part, $(\alpha - \beta)^t$, of the difference of electromagnetic polarizabilities. In fixed-t dispersion theory the s-channel part is replaced by the integral (along the ν axis) part, $(\alpha - \beta)^{\text{int}}$, and the t-channel part by the asymptotic (contour integral) part, $(\alpha - \beta)^{\text{as}}$, where the two versions are closely related to each other but are not completely identical. For illustration it is of interest to derive expressions for $(\alpha - \beta)^{\text{int}}$ in a similar form as those obtained for $(\alpha - \beta)^s$.

In fixed-t dispersion theory we may write

$$(\alpha - \beta)^{\text{int}} = -\frac{1}{2\pi} A_1^{\text{int}}(0,0) = -\frac{1}{\pi^2} \int_{\nu_{thr(0)}}^{\infty} \text{Im} A_1(\nu', 0) \frac{d\nu'}{\nu'}. \tag{215}$$

In (215) the finite upper limit $\nu_{\text{max}}(0)$ of the integral is replaced by ∞. From the general formula given

in (148) we may derive the relevant special case for $t = 0$

$$\mathrm{Im}A_1(s,0) = \frac{1}{(s-M^2)^2}\left[-\frac{s}{M}\mathrm{Im}\,\tau_4 - \frac{\sqrt{s}}{M}\mathrm{Im}\,\tau_5\right]. \tag{216}$$

with

$$\nu = \frac{s-M^2}{2M}. \tag{217}$$

Restricting the further discussion to the 1π channel we may write

$$\mathrm{Im}[\tau_4]^{1\pi}_{t=0} = 8\pi q\sqrt{s}\sum_{k\geqslant 1}\frac{k(k+1)^2(k+2)}{2}\left(A_{k+}B^*_{k+} - A_{(k+1)-}B^*_{(k+1)-}\right), \tag{218}$$

$$\mathrm{Im}[\tau_5]^{1\pi}_{t=0} = 8\pi q\sqrt{s}\sum_{k\geqslant 0}2(k+1)^2\left(|A_{k+}|^2 - |A_{(k+1)-}|^2\right) \tag{219}$$

with

$$\begin{aligned}
A_{k+}B^*_{k+} &= \frac{1}{2}\big[(k+2)|E_{k+}|^2 + kM_{k+}E^*_{k+} - (k+2)E_{k+}M^*_{k+} - k|M_{k+}|^2\big],\\
A_{(k+1)-}B^*_{(k+1)-} &= \frac{1}{2}\big[-k|E_{(k+1)-}|^2 + (k+2)M_{(k+1)-}E^*_{(k+1)-}\\
&\qquad -kE_{(k+1)-}M^*_{(k+1)-} + (k+2)|M_{(k+1)-}|^2\big],\\
|A_{k+}|^2 &= \frac{1}{4}\big[(k+2)^2|E_{k+}|^2 + (k+2)kE_{k+}M^*_{k+} + k(k+2)M_{k+}E^*_{k+} + k^2|M_{k+}|^2\big],\\
|A_{(k+1)-}|^2 &= \frac{1}{4}\big[k^2|E_{(k+1)-}|^2 - (k+2)kM_{(k+1)-}E^*_{(k+1)-}\\
&\qquad -k(k+2)E_{(k+1)-}M^*_{(k+1)-} + (k+2)^2|M_{(k+1)-}|^2\big].
\end{aligned} \tag{220}$$

This shows that the integrand entering into Eq. (215) has no such a simple decomposition into photoabsorption cross-sections of definite electromagnetic multipolarity as found for the corresponding integrand (203) valid in case of fixed-$\theta = \pi$ dispersion theory. For further illustration we simplify the expressions by taking only the multipoles $E_{0+}(E1)$ and $M_{1+}(M1)$ into account which are the most prominent ones at low energies. Then some algebra shows that in this approximation

$$(\alpha-\beta)^{\mathrm{int}} = \frac{1}{2\pi^2}\int_{\omega_0}^{\infty}\sqrt{1+\frac{2\omega}{M}}\left[\sigma_{E1}(\omega) - \left(\frac{3}{2}\sqrt{1+\frac{2\omega}{M}} - \frac{1}{2}\right)\sigma_{M1}(\omega)\right]\frac{d\omega}{\omega^2} \tag{221}$$

where ω is the photon energy in the lab system, to be compared with

$$(\alpha-\beta)^{s} = \frac{1}{2\pi^2}\int_{\omega_0}^{\infty}\sqrt{1+\frac{2\omega}{M}}\left[(\sigma_{E1}(\omega) - \sigma_{M1}(\omega)\right]\frac{d\omega}{\omega^2}. \tag{222}$$

For infinitely heavy particles both expressions converge against the well known relation

$$(\alpha-\beta)_{M\to\infty} = \frac{1}{2\pi^2}\int_{\omega_0}^{\infty}\left(\sigma_{E1}(\omega) - \sigma_{M1}(\omega)\right)\frac{d\omega}{\omega^2}. \tag{223}$$

For numerical predictions, calculations on the basis of the complete expressions are required. For fixed-t dispersion theory this has latest been carried out by Wissmann [2] leading to the result

$$(\alpha_p-\beta_p)^{\mathrm{int}} = +7.1(1\pi) + 2.0(2\pi) - 12.2(\Delta) = -3.1. \tag{224}$$

Table 19: Predicted information $(\alpha-\beta)_p^{\rm calc}$ on the polarizability difference compared with the experimental result $(\alpha-\beta)_p^{\rm exp} = 10.5 \pm 1.1$ (global average of [104]) or $(\alpha-\beta)_p^{\rm exp} = 10.1 \pm 0.9$ (adopted average including all existing data [17, 104]). In fixed-t dispersion theory the prediction $(\alpha-\beta)_p^{\rm calc}$ corresponds to the integral part $(\alpha-\beta)_p^{\rm int}$, in fixed-$\theta$ dispersion theory $(\alpha-\beta)_p^{\rm calc}$ is either chosen to be the s-channel contribution only (line 3) or the predicted s-channel contribution supplemented by the predicted $\gamma\gamma \to \pi\pi \to N\bar{N}$ t-channel contribution according to the BEFT sum rule (line 4). The unit is $10^{-4}{\rm fm}^3$.

disp. theory	$(\alpha-\beta)_p^{\rm calc}$	$(\alpha-\beta)_p^{\rm exp} - (\alpha-\beta)_p^{\rm calc}$
fixed-t	$(\alpha-\beta)_p^{\rm int} = -3.1$ [2]	$(\alpha-\beta)_p^{\rm as} = 13.2 \pm 1.3$
fixed-θ	$(\alpha-\beta)_p^{s} = -(5.0 \pm 1.0)$	$(\alpha-\beta)_p^{t\text{-exp}} = 15.1 \pm 1.3$
fixed-θ	$(\alpha-\beta)_p^{s+t} = +(9.0 \pm 2.2)$	$(\alpha-\beta)_p^{t\text{-miss}} = 1.1 \pm 2.4$

As a summary Table 19 shows differences between calculated values for $(\alpha-\beta)_p$ and the experimental value for this quantity obtained under conditions explained in the caption of the table. We see that in fixed-t dispersion theory we have to explain $(\alpha-\beta)_p^{\rm as} = 13.2 \pm 1.3$ through a contribution which has no interpretation in terms of the integral part in fixed-t dispersion theory. This value, therefore, may be interpreted as an empirical result for the asymptotic contribution to $(\alpha-\beta)$. In case of fixed-θ dispersion theory the quantity $(\alpha-\beta)_p^{t\text{-miss}}$ is compatible with zero. This means that the BEFT sum-rule is likely to be confirmed.

An interesting alternative for the prediction of $(\alpha-\beta)$ which deserves further consideration has been proposed and evaluated by Akhmedov and Fil'kov [155]. In this approach $(\alpha-\beta)$ is expressed through a dispersion relation at fixed $u = M^2$ in the point $t = 0$. Due to the different dispersion theory a different partition of $(\alpha-\beta)$ into s and t channel parts is obtained. Nevertheless, the conclusion is drawn that a σ meson in the intermediate state is responsible for the largest part of $(\alpha-\beta)$.

6.4.5 The effective σ pole and an outlook on an interpretation of $(\alpha-\beta)$

According to [51] we have reasons to assume that the σ meson has a composite structure of the type

$$|\sigma\rangle = \cos\theta_\sigma |\pi\pi\rangle + \sin\theta_\sigma |q\bar{q}\rangle, \tag{225}$$

implying that the σ meson has two possibilities to couple to two photons, i.e. via a π loop and via a quark loop. There is ongoing work [52] where this ansatz is used to make predictions on $\alpha-\beta$ and the relevant invariant amplitude. It is too early to refer to this ongoing work at the present stage of development. Instead we tentatively make use of an evaluation of the reaction $\gamma\gamma \to \pi^0\pi^0$ [81] which has led to a determination of the position of the σ pole as well as to a determination of the photon decay width $\Gamma_{\sigma\to\gamma\gamma}$ (Table 7). We start from Eq. (21) of [68]

$$\frac{g_{\sigma NN} F_{\sigma\gamma\gamma}}{2\pi m_\sigma^2} = (\alpha-\beta)^{\sigma\text{-pole}} \tag{226}$$

and first insert the nominal value of the σ mass $m_\sigma = 600$ MeV$\hat{=}$3.04 fm^{-1} which has been found to be consistent with experimental differential cross sections in the second resonance region [107, 108] (see also Section 3.8). The relation to the decay width is given by

$$g_{\sigma NN} F_{\sigma\gamma\gamma} = +16\pi \sqrt{\frac{g_{\sigma NN}^2}{4\pi} \frac{\Gamma_{\sigma\to 2\gamma}}{m_\sigma^3}} \tag{227}$$

where the approximate equality of the two coupling constants in (227)

$$\frac{g^2_{\sigma NN}}{4\pi} \simeq \frac{g^2_{\pi NN}}{4\pi} = 13.75 \tag{228}$$

may be justified through the linear σ model. Using

$$\Gamma_{\sigma\to\gamma\gamma} = 0.68 \pm 0.19 \text{ keV} \tag{229}$$

as evaluated by Fil'kov and Kashevarov [81], we arrive at

$$(\alpha-\beta)^{\sigma\text{-pole}} = 10.7 \pm 1.7. \tag{230}$$

The same calculation may be carried out using the experimental value $m_\sigma = (547\pm45)$ MeV as obtained by Fil'kov and Kashevarov [81]. Then we arrive at

$$(\alpha-\beta)^{\sigma\text{-pole}} = 14.8^{+2.1}_{-2.5}(\Delta\Gamma_{\sigma\to2\gamma})^{+5.2}_{-3.6}(\Delta m_\sigma). \tag{231}$$

It is satisfactory to see that the numbers obtained for $(\alpha-\beta)^{\sigma\text{-pole}}$ are compatible with $(\alpha-\beta)^{\text{as}} = 13.2 \pm 1.3$ given in the third row of Table 19.

In a quark-level linear σ model (LσM) [51] the decay widths of the $\sigma \to \gamma\gamma$ decay has been obtained in the form

$$\Gamma_{\sigma\to\gamma\gamma} = \frac{m^3_\sigma}{64\pi}\left[\frac{5}{3}\frac{\alpha_e}{\pi f_\pi} + \frac{1}{3}\frac{\alpha_e}{\pi f_\pi}\right]^2 \approx 3.5 \text{ keV} \tag{232}$$

for $m_\sigma = 650$ MeV. Here, the first term is due to the nonstrange quark triangle, while the second term stems from charged-kaon and -pion triangle graphs. This result was found to be compatible with the data estimate given in [156]. We cite this result as a possible guidance for future research in connection with attempts of including the physics of the scalar t channel of $(\alpha-\beta)$ into a model of the nucleon.

7 Summary and Discussion

It has been shown that Compton scattering by the nucleon at energies below 1 GeV provides insight into the structure of the nucleon which barely can be seen by other methods. It has been found advantageous to analyze the results of Compton scattering experiments in terms of four fundamental sum rules:

1. The Baldin or Baldin-Lapidus (BL) sum rule for the sum of electromagnetic polarizabilities $(\alpha+\beta)$, related to spin-independent forward scattering.

2. The Gerasimov-Drell-Hearn (GDH) sum rule for the square of the anomalous magnetic moment κ^2, related to spin-dependent forward scattering.

3. The Bernabeu-Ericson-FerroFontan-Tarrach (BEFT) sum rule for the difference of the electromagnetic polarizabilities $(\alpha-\beta)$, related to spin-independent backward scattering.

4. The L'vov-Nathan (LN) sum rule for the backward spin-polarizability γ_π, related to spin-dependent backward scattering.

The BL sum rule has been found to be fulfilled within rather small experimental errors. The largest part of the BL-integral is related to the conventional constituent-quark-meson structure of the nucleon. A smaller fraction of the BL integral is related to tensor-meson and pomeron exchanges. This part can be taken into account by making a Regge ansatz to describe the high-energy total photo-absorption cross section $\sigma_{\rm tot}(\omega)$.

The result for the GDH sum rule is very similar to the one for the BL sum rule. The largest part of the GDH-integral is related to the conventional constituent-quark-meson structure of the nucleon. For the mesonic part of the nucleon structure showing up in the energy range from 0.14 – 0.20 GeV, the cross section $\sigma_{1/2}$ is larger than the cross section $\sigma_{3/2}$ whereas for the resonant part due to the excitation of the constituent-quark structure the opposite is true. In the Regge range the cross section $\sigma_{1/2}$ is again larger than the cross section $\sigma_{3/2}$ thus making contributions to the GDH integral negative. Taking all these parts together we find the GDH sum rule likely to be fulfilled.

For backward scattering the conventional constituent-quark-meson structure is of minor importance. Instead, intermediate states of the scattering process are observed where the production and annihilation of mesons is essential. For the BEFT sum rule the relevant meson is the scalar-isoscalar σ meson, whereas for the LN sum rule the pseudoscalar π^0 is the most relevant one with minor contributions from the η and η' mesons. It has been shown that the LN sum rule is fulfilled whereas the BEFT sum rule is likely to be fulfilled. Furthermore, there are arguments that the σ meson has a composite structure with a $|\pi\pi\rangle$ and a $|q\bar{q}\rangle$ component. In order to arrive at a consistent description of the observations made so far for the t-channel part of the BEFT sum rule, this sum rule may be investigated in terms of a quark-level linear σ model where the coupling of the σ meson to two photons takes place via a pion loop as well as via a quark loop.

If we start from the reasonable supposition that the electromagnetic polarizabilities and spin polarizabilities are quantities which are related to the internal structure of the nucleon, we come to the conclusion that the π^0 and σ t-channel exchanges have to be considered as part of the nucleon structure. Since these intermediate states cannot be understood in terms of an excitation of the constituent-quark-meson structure of the nucleon they have to be considered as part of the constituent quarks or of the surrounding QCD vacuum. This view certainly provides a fascinating aspect for further investigations.

Acknowledgement:
The author is indebted to M.I. Levchuk, A.I. L'vov and A.I. Milstein for valuable discussions, for carefully reading the manuscript, and for providing results of their work prior to publication. He is indebted to F. Smend and F. Wissmann for carefully reading the manuscript and many valuable comments. He thanks T.R. Hemmert and an anonymous referee for clarifying information on chiral perturbation theory.

References

[1] D. Drechsel, B. Pasquini, M. Vanderhaeghen, *Phys. Rept.* 378 (2003) 99

[2] F. Wissmann, *Springer Tracts in Modern Physics* Volume 200 (2004)1

[3] A.I. L'vov, *Int. J. Mod. Phys.* A 8 (1993) 5267

[4] V.A. Petrun'kin, *Fiz. Elem. Chastits At. Yadra* 12 (1981) 692 [*Sov. J. Part. Nucl.* 12 (1981) 278]

[5] R.G. Sachs, L.L. Foldy, *Phys. Rev.* 80 (1950) 824

[6] Yu. A. Aleksandrov, P.I. Bondarenko, *Zh. Eksp. Teor. Fiz.* 31 (1956) 726 [*Sov. Phys. - JETP* 4 (1957) 612]

[7] F.E. Low, *Phys. Rev.* 96 (1954) 1428

[8] M. Gell-Mann, M.L. Goldberger, *Phys. Rev.* 96 (1954) 1433

[9] A.Klein, *Phys. Rev.* 99 (1955) 998

[10] A.M. Baldin, *Nucl. Phys.* 18 (1960) 310

[11] V.A. Petrun'kin, *Zh. Eksp. Teor. Fiz.* 40 (1961) 1148 [*Sov. Phys.-JETP* 13 (1961) 808]

[12] V.A. Petrun'kin, *Nucl. Phys. 55* (1964) 197

[13] V.A. Petrun'kin, *Tr. P.N. Lebedev Phys. Inst.* (in Russian) 41 (1968) 165

[14] V.M. Shekhter, *Yad. Fiz.* 7 (1968) 1272 [*Sov. J. Nucl. Phys.* 7 (1968) 756]

[15] V.I. Gol'danskii, O.A. Karpukhin, A.V. Kutsenko, V.V. Pavlovskaya, *Zh. Eksp Teor. Fiz* 38 (1960) 1695 [*Sov. Phys.-JETP* 11 (1960) 1223]; Nucl. Phys. 18 (1960) 473

[16] P.S. Baranov, L. Fil'kov, L.N. Shtarkov, *ZhETF Pis. Red.* 20 (1974) 762 [*JETP Lett.* 20 (1974) 353]; P.S. Baranov, et al., *Yad. Fiz.* 21 (1975) 689 [*Sov. J. Nucl. Phys.* 21 (1975) 355]; P.S. Baranov et al., *Phys. Lett.* B 52 (1974) 22; *Sov. J. Phys.* 21 (1975) 355

[17] P.S. Baranov, A.I. L'vov, V.A. Petrun'kin, L.N. Shtarkov, *9th International Seminar on Electromagnetic Interactions of Nuclei at Low and Medium Energies, Moscow, Russia, 20-22 Sep 2000*, *e-Print Archive:* nucl-ex/0011015, *Phys. Part. Nucl.* 32 (2001) 376

[18] Yu. A. Aleksandrov, *Fundamental Properties of the Neutron* (Clarendon Press, Oxford 1992)

[19] Y.A. Alexandrov, et al., *Sov. J. Nucl. Phys.* 44 (1986) 900

[20] L. Koester, et al., *Physika* B 137 (1986) 282

[21] J. Schmiedmayer, et al., *Phys. Rev. Lett.* 61 (1988) 1065

[22] L. Koester, et al., *Z. Phys.* A 329 (1988) 229

[23] K. Hagiwara, et al. (Particle Data Group), *Phys. Rev.* D 66 (2002) 010001 (URL:http://pdg.lbl.gov)

[24] S. Eidelman, et al. (Particle Data Group), *Phys. Lett.* B 592 (2004) 1; URL: http://pdg.lbl.gov

[25] L.D. Landau, E.M. Lifschitz, *Lehrbuch der Theoretischen Physik IV, Quantenelektrodynamik* (Akademieverlag, Berlin 1990); V.B. Berestetskii, E.M. Lifshitz, L.P. Pitaevskii, *Quantum Electrodynamics* (Pergamon, New York 1982)

[26] P.C. Hecking, G.F. Bertsch, *Phys. Lett.* B 99 (1981) 237; A. Schäfer, B. Müller, D. Vasak, W. Greiner, *Phys. Lett.* B 143 (1984) 323;

[27] G. Dattoli, G. Matone, D. Prosperi, *Lett. Nuovo Cim.* 19 (1977) 601; D. Drechsel, A. Russo, *Phys. Lett.* B 137 (1982) 295; M. De Sanctis, D. Prosperi, *Nuovo Cim.* A 103 (1990) 1301; S. Capstick, B. D. Keister, *Phys. Rev.* D 46 (1992) 84 ; H. Liebl, G.R. Goldstein, *Phys. Lett.* B 343 (1995) 363; M. Traini, R. Leonardi, *Phys. Lett.* B 334 (1994) 7

[28] R. Weiner, W. Weise, *Phys. Lett.* B 159 (1985) 85; N.N. Scocola, W. Weise, *Nucl. Phys.* A 517 (1990) 495

[29] N.N. Scocola, W. Weise, *Phys. Lett.* B 232 (1989) 287; W. Broniowski, M.K. Banerjee, T.D. Cohen, *Phys. Lett.* B 283 (1992) 22

[30] E.M. Nyman, *Phys. Lett.* B 142 (1984) 388; M. Chemtob, *Nucl. Phys.* A 473 (1987) 613; S. Scherer, P.J. Mulders, *Nucl. Phys.* A 549 (1992) 521

[31] V. Bernard, B. Hiller, W. Weise, *Phys. Lett.* B 205 (1988) 16; V. Bernard, D. Vautherin, *Phys. Rev.* D 40 (1989) 1615; B.R. Holstein, *Comment Nucl. Part. Phys.* 19 (1990) 221

[32] T.E.O. Ericson, J. Hüfner, *Nucl. Phys.* B 57 (1973) 604

[33] J.L. Friar, *Ann Phys. (N.Y.)* 95 (1975) 170

[34] R.N. Lee, A.I. Milstein, M. Schumacher, *Phys. Rev. Lett.* 87 (2001) 051601; R.N. Lee, A.I. Milstein, M. Schumacher, *Phys. Rev.* A 64 (2001) 032507; R.N. Lee, A.I. Milstein, M. Schumacher, *Phys. Lett.* B 541 (2002) 87

[35] M. Schumacher, et al., *Nucl. Phys.* A 576 (1994) 603

[36] M.-Th. Hütt, A.I. L'vov, A.I. Milstein, M. Schumacher, *Physics Reports* 323 (2000) 457

[37] H.M. Pilkuhn, *Relativistic Particle Physics* (Springer Verlag, New York, 1979)

[38] V. Bernard, N. Kaiser, U.-G. Meissner, *Phys. Rev. Lett.* 67 (1991) 1515; *Nucl. Phys.* B 373 (1992) 346

[39] A.I. L'vov, *Phys. Lett.* B 304 (1993) 29

[40] A.W. Thomas, W. Weise, *The Structure of the Nucleon* (WILEY-VCH Verlag Berlin GmbH 2001)

[41] V. Bernard, N. Kaiser, U.-G. Meissner, *Int. Journ. Mod. Phys.* E 4 (1995) 193

[42] V. Bernard, N. Kaiser, J. Kambor, U.G. Meissner, *Nucl. Phys.* B 388 (1992) 315

[43] V. Bernard, N. Kaiser, A. Schmidt, U.-G. Meissner, *Phys. Lett.* B. 319 (1993) 269; V. Bernard, N. Kaiser, U.-G. Meissner, A. Schmidt, *Z. Phys.* A 348 (1994) 317

[44] T.R. Hemmert, B.R. Holstein, J. Kambor, G. Knöchlein, *Phys. Rev.* D 57 (1998) 5746; T.R. Hemmert, B.R. Holstein, J. Kambor, *Phys. Rev.* D 55 (1997) 5598

[45] V. Pascalutsa, *e-Print Archive:* nucl-th/0412008

[46] R.P. Hildebrandt, H.W. Griesshammer, T. R. Hemmert, B. Pasquini, *Eur. Phys.* J. A 20 (2004) 293; *e-Print Archive:* nucl-th/0307070

[47] V. Pascalutsa, D.R. Phillips, *Phys. Rev.* 67 (2003) 055202; *e-Print Archive:* nucl-th/0212024; J.A. McGovern, *Phys. Rev.* C 63 (2001) 064608; *e-Print Archive:* nucl-th/0101057; S.R. Beane et al., *e-Print Archive:* nucl-th/0403088

[48] F.E. Low, Proc. 1958 *Ann. Intern. Conf. on High Energy Physics at CERN*, p.98

[49] A.C. Hearn, E. Leader, *Phys. Rev.* 126 (1962) 789

[50] R. Köberle, *Phys. Rev.* 166 (1968) 1588

[51] M.D. Scadron, et al., *Phys. Rev. D 69 (2004) 014010*; Erratum-ibid. D 69 (2004) 059901; *e-Print Archive:* hep-ph/0309109

[52] M.I. Levchuk, A.I. L'vov, A.I. Milstein, M. Schumacher (to be submitted)

[53] B. Holstein, et al., *Phys. Rev.* 61 (2000) 034316

[54] D. Babusci, G. Giordano, A.I. L'vov, G. Matone, A.M. Nathan, *Phys. Rev.* C 58 (1998) 1013

[55] R.L. Walker, *Phys. Rev.* 182 (1969) 1729

[56] F.J. Gilman, *Phys. Rep.* 4 (1972) 95

[57] P. Roman, *Advanced Quantum Theory* (Addison-Wesley Publishing Company, Inc. Reading, Massachusetts 1965)

[58] G. Höhler, in: *Landolt-Börnstein, New Series*, Group I, Vol. 9, Subvolume b: Pion Nucleon Scattering, Part 2: Methods and Results of Phenomenological Analysis.

[59] L.I. Lapidus, *Zh. Eksp. Teor. Fiz.* 43 (1962) 1358 [*Sov. Phys. JETP* 16 (1963) 964]

[60] S.B. Gerasimov, *Sov. J. Nucl. Phys.* 2 (1966) 430

[61] S.D. Drell and A.C. Hearn, *Phys. Rev. Lett.* 16 (1966) 908

[62] M. Hosada and K. Yamamoto, *Prog. Theor. Phys.* 36 (1966) 425

[63] M. Jacob, G.C. Wick, *Ann. Phys. (NY)* 7 (1959) 404

[64] Y. Hara, *Prog. Theor. Phys. Suppl.* 51 (1972) 96

[65] J. Bernabeu, T.E.O. Ericson, C. Ferro Fontan, *Phys. Lett.* 49B (1974) 381

[66] J. Bernabeu and B. Tarrach, *Phys. Lett.* 69B (1977) 484

[67] A.I. L'vov, A.M. Nathan, *Phys. Rev.* C 59 (1999) 1064

[68] A.I. L'vov, V.A. Petrun'kin, M. Schumacher, *Phys. Rev.* C 55 (1997) 359

[69] L.D. Landau, *Dokl. Akad. Nauk.*, USSR 60 (1948) 207

[70] C.N. Yang, *Phys. Rev.* 77 (1950) 242

[71] J. Schwinger, *Ann. Phys.* 2 (1957) 407

[72] M. Gell-Mann and M. Levy, *Nuovo Cim.* 16 (1960) 705

[73] M. Taketani, et al., *Prog. Theor. Phys. Suppl.* No. 39 (1967) 1; K. Erkelenz, *Phys. Rep.* 5 (1974) 191; R. Machleidt, K. Holinde, Ch. Elster, *Phys. Rep.* 149 (1987) 1

[74] Y. Nambu, G. Jona-Lasinio, *Phys. Rev.* 122 (1961) 345; R. Delbourgo, M.D. Scadron, *Phys. Rev. Lett.* 48 (1982) 379; T. Hatsuda, T. Kunihiro, *Phys. Lett.* B 145 (1984) 7; *Prog. Theor. Phys.* 74 (1985) 765; *Phys. Rep.* 247 (1994) 221; V. Elias, M.D. Scadron, *Phys. Rev. Lett.* 53 (1984) 1129; S. Klimt, M. Lutz, U. Vogl, W. Weise, *Nucl. Phys.* A 516 (1990) 429

[75] K.L. Au, D. Morgan, M.R. Pennington, *Phys. Rev.* D 35 (1987) 1633; D. Morgan, M.R. Pennington, *Phys. Rev.* D 48 (1993) 1185

[76] M. Ishida, *Prog. Theor. Phys.* 96 (1996) 853; *e-Print Archive:* hep-ph/9905261

[77] N.N. Achasov, G.N. Schestakov, *Phys. Rev.* D 49 (1994) 5779; R. Kaminski, L. Lesniak, J.-P. Maillet, *Phys. Rev.* D 50 (1994) 3145; N.A. Tornqvist, M. Roos, *Phys. Rev. Lett.* 76 (1996) 1575; M. Svec, *Phys. Rev.* D 53 (1996) 2343; M. Harada, F. Sannio, J. Schechter, *Phys. Rev.* D 54 (1996) 1991; S. Ishida, M. Ishida, H. Takahashi, T. Ishida, K. Takamatsu, T. Tsuru, *Prog. Theor. Phys.* 95 (1996) 745; 98 (1997) 1005; I.G. Alekseev, et al., *Phys. At. Nucl.* 61 (1998) 174

[78] G. Colangelo, J. Gasser, H. Leutwyler, *Nucl. Phys.* B 603 (2001) 125

[79] M. Ishida, *Prog. Theor. Phys. Suppl.* 149 (2003) 190; *e-Print Archive:* hep-ph/0212383

[80] D. Drechsel, M. Gorchtein, B. Pasquini, M. Vanderhaeghen, *Phys. Rev.* C 61 (1999) 015204

[81] L.V. Fil'kov, V. L. Kashevarov, *Eur. Phys.* J A 5 (1999) 285

[82] H. Marsiske, et al., *Phys. Rev.* D 41 (1990) 3324

[83] J. Ahrens, et al., *e-Print Archive:* nucl.-ex/0407011

[84] A. Rostovtsev, *Surveys High Energy Phys.* 16 (2001) 209; *e-Print Archive:* hep-ph/0108019; C.W. Akerlof, et al., *Phys. Rev.* D 14 (1976) 2864; V. N. Bolotov, et al., Nucl. Phys. B 73 (1974) 365

[85] A. Donnachie, P.V. Landshoff, *Phys. Lett.* B 296 (1992) 227

[86] W.P. Hesse, et al., *Phys. Rev. Lett.* 25 (1970) 613

[87] N. Bianchi and E. Thomas, *Phys. Lett.* B 450 (1999) 439

[88] R.E. Prange, *Phys. Rev.* 110 (1958) 240

[89] W.A. Bardeen and W.K. Tung, *Phys. Rev.* 173 (1968) 1423

[90] A.I. L'vov, *Sov. J. Nucl. Phys.* 34 (1981) 597

[91] A.I. L'vov, private communication (2004)

[92] A.I. Milstein, private communication (2003)

[93] G.F. Chew, M.L. Goldberger, F.E. Low, Y Nambu, *Phys. Rev.* 106 (1957) 1345

[94] I. Karliner, Phys. Rev. D 7 (1973) 2717

[95] R.A. Arndt, I.I. Strakovsky, R.L. Workman, *Phys. Rev.* C 53 (1996) 430

[96] Computer code SAID, solution SM95 (1995)

[97] J. Peise, et al., *Phys. Lett.* B 384 (1996) 37; A. Hünger, et al., Nucl. Instr. Meth. A 372 (1996) 135; A. Hünger, et al., *Nucl. Phys.* A 620 (1997) 385

[98] http://www.kph.uni-mainz.de/MAID/; S.S. Kamalov, S.N. Yang, D. Drechsel, O. Hanstein, L. Tiator, *Phys. Rev.* C 64 (2001) 032201; http://gwdac.phys.gwu.edu; R.A. Arndt, W.J. Briscoe, I.I. Strakovsky, R.L. Workman, *Phys. Rev.* C 66 (2002) 055213

[99] F.J. Federspiel, et al., *Phys. Rev. Lett.* 67 (1991) 1551

[100] A.I. L'vov, V.A. Petrun'kin, S.A. Startsev, *Sov. J. Nucl. Phys.* 29 (1979) 651

[101] A. Zieger, et al., *Phys. Lett.* B 278 (1992) 34

[102] E.L. Hallin, et al., *Phys. Rev.* C 48 (1993) 1497

[103] B.E. MacGibbon, et al., *Phys. Rev.* C 52 (1995) 2097

[104] V. Olmos de León, et al., *Eur. Phys. J.* A 10 (2001) 207

[105] J. Tonnison, et al., *Phys. Rev. Lett.* 80 (1998) 4382

[106] F. Wissmann, et al., *Nucl. Phys.* A 660 (1999) 232

[107] G. Galler, et al., *Phys. Lett.* B 501 (2001) 245

[108] S. Wolf, et al., *Eur. Phys. J.* A 12 (2001) 231

[109] D. Drehsel, O. Hanstein, S.S. Kamalov, L. Tiator, *Nucl. Phys.* A 645 (1999) 145

[110] M. Camen, et al., *Phys. Rev.* C 65 (2002) 032202

[111] G. Blanpied, et al., *Phys. Rev.* C 64 (2001) 025203

[112] J. Schmiedmayer, et al., *Phys. Rev. Lett.* 66 (1991) 1015

[113] L. Koester, et al., *Phys. Rev.* C 51 (1995) 3363

[114] T.L. Enik, et al., *Sov. J. Nucl. Phys.* 60 (1997) 567

[115] F. Wissmann, M.I. Levchuk, M. Schumacher, *Eur. Phys. J.* A 1 (1998) 193

[116] M.I. Levchuk, A.I. L'vov, V.A. Petrun'kin, *Lebedev Physical Institute Preprint FIAN* No. 86; *Few-Body Syst.* 16 (1994) 101

[117] K.W. Rose et al., *Phys. Lett.* B 234 (1990) 460; *Nucl. Phys.* A 514 (1990) 621

[118] K. Kossert et al., *Phys. Rev. Lett.* 88 (2002) 162301; *Eur. Phys. J.* A 16 (2003) 259, *e-Print Archive:* nucl-ex/0210020

[119] M.I. Levchuk, A.I. L'vov, *Nucl. Phys.* A 674 (2000) 449; A 684 (2001) 490

[120] N.R. Kolb, et al., *Phys. Rev. Lett.* 85 (2000)1388

[121] M. Lundin, et al., *Phys. Rev. Lett.* 90 (2003) 192501-1

[122] R.P. Hildebrandt, H.W. Griesshammer, T.R. Hemmert, D.R. Phillips, *e-Print Archive:* nucl-th/0405077; Accepted for publication in *Eur. Phys. J.* A

[123] S.R. Beane, M. Malheiro, J.A. McGovern, D.R. Phillips, U. van Kolck, *e-Print Archive:* nucl-th/0403088

[124] C. Molinari, et al., Phys. Lett. B 371 (1996) 181

[125] P.S. Baranov, et al., *JETP* 23 (1966) 242 ; *Sov. J. Nucl. Phys.* 3 (1966) 3791

[126] E.R. Gray, A.O. Hanson, *Phys. Rev.* 160 (1967) 121

[127] H. Genzel, M. Jung, R. Wedemeyer, H.J. Weyer, *Z. Phys.* A 279 (1976) 399

[128] T. Ishii, et al., *Nucl. Phys.* B 165 (1980) 189

[129] M. Damashek, F.J. Gilman, *Phys. Rev.* D 1 (1970) 1319

[130] R.L. Workman, R.A. Arndt, *Phys. Rev.* D 45 (1992) 1789; A.M. Sandorfi, C.S. Whisnant, M. Khandaker, *Phys. Rev.* D 50 (1994) R6681; R.A, Arndt, I.I. Strakovsky, R. Workman, *Phys. Rev.* C 53 (1996) 430; D. Drechsel, G. Krein, *Phys. Rev.* D 58 (1998) 116009

[131] G.C. Fox, D.Z. Freedman, *Phys. Rev.* 182 (1969) 1628; S. B. Gerasimov, *Yad. Fiz.* 5 (1967) 1263 [*Sov. J. Nucl. Phys.* 5 (1969) 902]; H.D. Abarbanel, M.L. Goldberger, *Phys. Rev.* 165 (1968) 1594; J.B. Bronzan, I.S. Gerstein, B.W. Lee, F.E. Low, *Phys. Rev. Lett.* 18 (1967) 32; *Phys. Rev.* 157 (1967) 1448; K. Kawarabayashi, M. Suzuki, *Phys. Rev.* 150 (1966) 1362; 152 (1966) 1383; K. Kawarabayashi, W. Wada, *Phys. Rev.* 152 (1966) 1286; L.N. Chang, Y. Liang, *Phys. Lett.* B 268 (1991) 64; *Phys. Rev.* D 45 (1992) 2121; L. N. Chang, Y. Liang, R.L. Workman, *Phys. Lett.* B 329 (1994) 514

[132] J. Ahrens, et al., *Phys. Rev. Lett.* 84 (2000) 5950

[133] J. Ahrens, et al., *Phys. Rev. Lett.* 87 (2001) 022003

[134] J. Ahrens, et al., *Phys. Rev. Lett.* 88 (2002) 232002

[135] H. Dutz, et al., *Phys. Rev. Lett.* 91 (2003) 192001

[136] H. Dutz, et al., *Phys. Rev. Lett.* (to be published)

[137] L. Tiator, Proc. GDH2002, p. 27, M. Anghinolfi, M. Battaglieri, R. De Vita Eds. (World Scientific, New Jersey 2002)

[138] S. Simula, et al., *Phys. Rev.* D 65 (2002) 034017

[139] I. Guiasu and E.E. Radescu, *Phys. Rev.* D14 (1976) 1335; *Phys. Lett.* 62B (1976) 193

[140] I. Guiasu and E.E. Radescu, *Phys. Rev.* D 18 (1978) 1728

[141] V.M. Budnev, V.A. Karnakov, *Yad. Fiz.* 30 (1979) 440 [*Sov. J. Nucl. Phys.* 30 (1979) 228]

[142] B.R. Holstein, A.M. Nathan, *Phys. Rev.* D 49 (1994) 6101

[143] R. Omnès, *Nuovo Cimento* 8 (1958) 316

[144] G.E. Bohannon, *Phys. Rev.* D 14 (1976) 126

[145] W.R. Frazer and Fulco, *Phys. Rev.* 117 (1960) 1603

[146] D. Morgan, M.R. Pennington, *Z. Phys.* C 37 (1988) 431

[147] M.I. Levchuk, private communication (2004)

[148] A.E. Kaloshin, V.V. Serebryakov, *Z. Phys.* C 64 (1994) 691

[149] M.R. Pennington, *Nucl. Phys.* A 623 (1994) 189c

[150] B. Hyams, et al., *Nucl. Phys.* B 64 (1973) 134

[151] C.D. Froggatt, J.L. Peterson, *Nucl. Phys.* B 129 (1977) 89

[152] M. Gourdin, A. Martin, Nuovo. Cim. 17 (1960) 224

[153] J. Boyer, et al., *Phys. Rev.* D 42 (1990) 1350

[154] H.J. Behrend, et al., *Z. Phys.* C 56 (1992) 381

[155] D.M. Akhmedov, L.V. Fil'kov, *Yad. Fiz.* 33 (1981) 1083 [*Sov. J. Nucl. Phys.* 33 (1981) 573]

[156] M. Boglione and M.R. Pennington, *Eur. Phys. J.* C 9 (1999) 11; *e-Print Archive:* hep-ph/9812258